Bilal Mustafa

Field Weakening Control of Interior Permanent Magnet Synchronous Motor Employing Model Order Reduction

School of Electrical Engineering

Thesis submitted for examination for the degree of Master of Science in Technology.

Espoo 13.05.2018

Thesis supervisor:

Prof. Anouar Belahcen

Thesis advisor:

Mehrnaz Farzam Far (M.Sc.)

Aalto University
School of Electrical
Engineering

AALTO UNIVERSITY
SCHOOL OF ELECTRICAL ENGINEERING

ABSTRACT OF THE
MASTER'S THESIS

Author: Bilal Mustafa

Title: Field Weakening Control of Interior Permanent Magnet Synchronous Motor Employing Model Order Reduction

Date: 13.05.2018 Language: English Number of pages:7+75

Department of electrical engineering and automation

Professorship: Electromechanics Code: S-17

Supervisor: Prof. Anouar Belahcen

Advisor: Mehrnaz Farzam Far (M.Sc.)

Various control strategies have been adopted for the field weakening control of the interior permanent magnet synchronous motors. Most of these either use the magnetic model parameters or utilize the approaches like the look up tables to minimize the effects of parametric sensitivity. The variation of the inductance values due to the magnetic saturation or the cross-coupling and fluctuation in the stator resistance and the permanent magnet flux due to the temperature difference can significantly affect the control performance especially at high speeds.
In this thesis, the field weakening algorithm has been proposed that employs one of the model order reduction technique, i.e. orthogonal interpolation method. This technique obtained from reducing the order of the finite element model of the machine takes the stator current components as input and outputs the corresponding flux linkage components. At first, the control design was implemented utilizing the reduction technique that contained the motor parameters to test the validity of the orthogonal interpolation method in the field weakening operation. Thereupon, the technique was designed operating independent of any machine parameter that put into place the orthogonal interpolation method and its inversion for the references calculation. The simulink feature, 'algebraic constraint', was used in combination with the reduction technique to produce the required current components. The control techniques were implemented in the field oriented control scheme. The methods were at first tested through simulations in the MATLAB/Simulink environment and then the experiments were performed in the dSPACE laboratory for validity of the results. The results provided in the end confirm the feasibility of the approach used. The motor operates well in the field weakening region and can operate in the wide speed range. The results also confirm that the approach operating independent of the machine parameters exibit better control performance.

Keywords: Field oriented control (FOC), field weakening (FW), interior permanent magnet synchronous motors (IPMSM), model order reduction (MOR), orthogonal interpolation method (OIM)

Preface

I would like to express the gratitude to my supervisor Prof. Anouar Belahcen for giving me the awesome opportunity to work on this thesis. His valuable insight helped me a lot in improving the quality of this work. I am also obliged to my instructor Mehrnaz Farzam Far for her kind cooperation and counselling. Her guidance in understanding the experimental setup and performing simulations was of great help. Moreover, her detailed review assisted me a lot in producing a good thesis work.

I would like to make a special thanks to Dr. Ahmed Hemeida for his worthy ideas and well needed motivation. I am grateful to Hafiz Asad Ali Awan, Victor Mukherjee, Dr. Seppo Saarakkala and Ari Haavisto for their precious suggestions and time at various points. I definitely would like to thank all of my colleagues at Research group of Electromechanics for creating a healthy and cheerful working environment.

I would also like to acknowledge the support and sincerity of my friends before and during my stay in Finland, especially Mahar Riaz, Tayyab Farooq, Muhammad Sajjad Awan, Abid Saleem sheikh, Usama Riaz, Faisal usman sheikh, Zia ur rehman, Adnan Syed, Rana jehanzeb jabbar and all those I am not able to mention due to the space limitation.

Finally, not merely the words, I am absolutely incapable of expressing my deepest love and indebtedness for my parents, Mr. and Mrs. Iftikhar Hussain, for their endless support and uplifting through out my life. I am beholden to my beloved siblings Asad Ullah, Abdul Mannan, Ali Iftikhar and my dearest sister for being there with me at every difficult step of my life. I also won't forget some of my very close relatives, especially my grandparents and aunt, whose kind prayers and unequivocal support always stay with me.

Espoo, 13.05.2018

Bilal Mustafa

Contents

Symbols and abbreviations

Symbols

Boldface letters represent the matrices and the vectors. Reference values are shown with subscript ref.

$\boldsymbol{A}$	Magnetic vector potential
$\boldsymbol{B}_r$	Remanance flux density
$\boldsymbol{B}_{rotor}$	Rotor flux density
$\boldsymbol{B}_{stator}$	Stator flux density
d_a, d_b, d_c	Switching states of a, b and c phases
dq	Synchronous coordinates
$\boldsymbol{E}$	Taylor series expansion term
$\boldsymbol{F}$	Source vector
$\boldsymbol{H}_c$	Coercitive field strength
$\boldsymbol{H}_{ci}$	Intrinsic coercive force
$\boldsymbol{H(s)}$	Closed-loop transfer function in s-plane
I_{ch}	Characteristic current
i_d	Direct-axis component of the stator current
i_{dq}	Direct and quadrature-axis components of the stator current
I_{max}	Maximum current
i_q	Quadrature-axis component of the stator current
$\boldsymbol{i}_s$	Stator current space vector
i_s	Magnitude of stator current space vector
j	Size of stiffness matrix and source vector
k	Number of solutions for the system under study
$\boldsymbol{K}_i$	Discrete-time integral gain matrix
$\boldsymbol{K}_t$	Discrete-time feedforward gain matrix
$\boldsymbol{K}_1$	Discrete-time state feedback gain matrix
$\boldsymbol{K}_2$	Discrete-time voltage state feedback gain matrix
L_d	Direct-axis inductance
L_q	Quadrature-axis inductance
p	Number of pole pair
P_{out}	Output power
R_s	Stator resistance

$\boldsymbol{S}$	Stiffness matrix
S_1, S_2, S_3	Switches on phase a, b and c
T	Electromagnetic torque
T_s	Sampling period
$\boldsymbol{U}$	Orthogonal matrix of left singular vectors
u_d	Direct-axis component of the stator voltage
U_{dc}	DC bus voltage
U_{max}	Maximum voltage
u_q	Quadrature-axis component of the stator voltage
$\boldsymbol{u_s}$	Stator voltage space vector in synchronous coordinates
$\boldsymbol{u_s^s}$	Stator voltage space vector in stator coordinates
$\boldsymbol{V}$	Orthogonal matrix of right singular vectors
$\boldsymbol{x}_i$	Integral state of the current controller
$\boldsymbol{X}_0$, $\boldsymbol{X}_1$, $\boldsymbol{X}_2$, $\boldsymbol{Y}_1$	Coefficient matrices for a discrete-time reference-following transfer function
$\alpha\beta$	Stator coordinates
θ_r	Angle between the stator phase A axis and the d axis
ω_m	Mechanical angular speed
$\boldsymbol{\psi_s}$	Stator flux linkage space vector
ψ_s	Magnitude of stator flux linkage space vector
ψ_f	Permanent magnet flux
ψ_d	Direct-axis component of the stator flux linkage
ψ_q	Quadrature-axis component of the stator flux linkage
ξ	Saliency ratio
$\boldsymbol{\Sigma}$	Rectangular diagonal matrix used in the singular value decomposition
σ	Singular values defining energy of the system

Abbreviations

AC	Alternating Current
DTC	Direct torque control
FEM	Finite element method
FOC	Field oriented control
FW	Field weakening
IM	Induction machine
IPMSM	Interior permanent manget synchronous motors
LUT	Look up table
MMF	Magnetomotive force
MOR	Model order reduction
MTPA	Maximum torque per ampere
OIM	Orthogonal interpolation method
PI	Proportional integral
PM	Permanent mangets
PMSM	Permanent magnet synchronous motors
p.u.	Per unit
SPM	Surface mounted permanent magnet synchronous motor
SPWM	Sinusoidal pulse width modulation
SVPWM	Space vector pulse width modulation
SyRM	Synchronous reluctance motor

1 Introduction

1.1 Background

For a proper conversion of energy sources to a useful form, electrical machines have become a mandatory part of our daily lives. Most of the times the machines used are AC machines. For many years, the induction motors (IM) are in use for the industrial purposes. Two main factors contributing to their significance is the self-starting behaviour and low costs. Synchronous generators are also used all over for the production of electricity. DC machines are, however, outdated nowadays and used on a very small scale, particularly in the industries.

Energy efficiency has become a matter of importance in the recent years to save cost and energy and improve the climatic conditions. For this purpose, not only the measures for upgrading the industrial and commercial solutions have been focused but also the efforts for the pollutants free environment have been enhanced quite much. It can also relate the advent of the permanent magnet synchronous motors (PMSM) in the present-day era. PMSM are much more efficient than IM because of elimination of the rotor windings causing the copper losses (Jahns, Kliman and Neumann, 1986). In addition, high power density, small size and high torque production capability increase the demand for this class of machines.

The rotor structure plays an important part in the working of PMSM. These are usually categorized into the two types. One of these is the surface mounted permanent magnet (SPM) motors and other one is the interior permanent magnet synchronous motors (IPMSM). As the name suggests, in the former type, permanent magnets (PM) are visible at the rotor surface. However, in IPMSM, PM cannot be seen on the rotor rather these are set inside it. IPMSM, however, provide more torque per unit volume of the rotor as compared to the SPMs due to the presence of the magnetic saliency feature. It arises due to the inductances values of the synchronous coordinates, L_d and L_q, that differ in the IPMSM but are same in the SPM. These inductance values, L_d and L_q, are stated for the synchronous coordinates that are represented as dq axis in this thesis.

Electric Vehicles are replacing the conventional internal combustion engine (ICE) vehicles quite rapidly to maintain the good atmospheric conditions and avoid shortage of the fossil fuels. Regenerative braking is another advantage which circumvents wastage of electric energy. Most of the electric vehicles use the IPMSM due to the constant power range and the high torque to current ratio characteristics and also providing good acceleration rate due to the presence of the PM.

In the vector control techniques, the two main schemes used are the direct torque control (DTC) and the field oriented control (FOC). In DTC, the rotor position measurement and a separate pulse width modulation (PWM) modulator are not required since the stator flux and torque act as controlled variables (Foo and Zhang, 2016). The angle of the stator flux with respect to the rotor axis is controlled that regulates the torque accordingly. In FOC, torque and the rotor flux are governed by d and q-components of the stator current respectively. FOC makes both these quantities, the torque and the flux independent of each other and makes the control easier. In this work, FOC control has been utilized for the control purpose of the prototype IPMSM machine.

Various control techniques are applied to operate a machine below and above the base speed as well. Depending upon the application and motor characterisitics, it is determined to follow one method or the other. In case of IPMSM, to speed up the machine upto the base limit, either i_d zero principle or maximum torque per ampere (MTPA) principle is followed. Depending on the saliency level, if its higher, MTPA principle is followed to achieve better efficiency. However, the IPMSM with low saliency or PMSM with non-salient strucuture can operate on the zero i_d principle as well.

For the salient machines like IPMSM and SyRM, it is recommended to make these machines operate at higher speeds than the rated one in order to fully utilize their capabilities. In IPMSM, it becomes particularly a difficult task due to the presence of the PM flux that needs to be controlled. However, the FW has become today the essential part of the control algorithms. Especially, for the traction applications, the need for the extended speed range is a must demand.

Once, a machine reaches the base speed, the inverter limits should be considered. Both the current and voltage limits should be maintained during the whole operation of the machine. It is definite to operate within these limits ensuring the safety of a system in general. Virtually there is no possible way to increase the speed further wihtout increase in the voltage, that is in turn, not feasible. The only way to speed up the machine forward is to weaken the flux. This objective is achieved by the increase in the stator current towards the negative direction that opposes the ideally constant flux produced by PM. It becomes possible by introducing the negative d-component of the stator current that causes the FW and make IPMSM go much higher speeds than they are otherwise capable of. In some of the machines, in which the maximum current surpass the center of ellipse formed by the voltage limit, the infinite speed can be reached in theoretical terms and the FW doesn't allow the machine to reach the maximum speed. In these kind of the machines, another

principle known as maximum torque per volt (MTPV) is applied and it works taking into account the voltage limit only. However, due to the practical limitations, these machines can also operate upto the finite speed but their maximum speed is much higher than the finite speed drives.

It is also to be noticed that the parameters of the machine such as d and q-axis inductances L_d and L_q , the stator resistance R_s and the PM flux ψ_f do not remain constant. Ferro-magnetic materials used in the construction of electrical machines have the instrinsic property of saturation when the flux passing through these machines reaches upto a certain limit. At this stage, the relationship between the flux and current becomes non-linear. Further increase in the current will not help in the flux crossing, therefore, the inductance drop during the machine operations is evident. The inductances, therefore, if assumed constant throughout the operation may degrade the performance of the control system. Furthermore, the temperature changes may also affect the machine parameters. R_s and ψ_f increase and decrease respectively with the increase in the temperature. Therefore, any machine parameter included in the control algorithm may affect the overall control performance.

Many numerical techniques have been adopted to perform the design and anlaysis of electrical machines. One of those finite element method (FEM) remains the basic tool of researchers for long. It doesn't only help to obtain the optimized design solution but also improve the perfomance characteristics of electrical machines. It is easier to solve simpler cases effectively but when it comes to the complex geometries and the non-linear materials, especially when the order of the model is large, the FEM solutions beome quite intensive and computationally demanding. Model order reduction (MOR) provides the superior alternative in this ragard and makes it possible to have faster and still accurate solutions for electrical machines. Various methods have been adopted for this purpose and their validity has been proven.

OIM is one of those methods that calculates the magnetic vector potential for IPMSM very well. This method is proficient in the fast and even accurate estimation as compared to some other methods like proper orthogonal decomposition (POD) and standard interpolation method (Farzamfar et al., 2018). It is possible to utilize the property of this particular MOR technique to exploit for the control purposes in the real-time.

This thesis aims to implement control of the prototype IPMSM in the FW region. To make the control indepedent of the the machine parameters, the OIM technique needs to be utilized in the control method. Below the base speed, the control has already been implemented in the lab taking into account the i_d zero method. Using this approach, the reluctance term in the torque expression vanishes that makes the control independent of the L_d and L_q terms, avoiding the effect of the magnetic saturation.

1.2 Literature review

Field weakening has become the essential part of IPMSM control structure especially for the traction applications. As the name suggests, the air-gap flux is decreased to enable machines operate at much higher than the rated speeds. For this purpose, the demagnetizing field is generated by introduction of the negative d-component of current since otherwise the field of PM remains fixed except with the change of temperature.

From the early 90s, various efforts has been made to implement and improve the FW methods for both synchronous and asynchronous machines. However, the high efficiency of the former class due to the absence of the rotor cage or the windings and the magnetizing current makes it more applicable for the control goals.

(Blaschke, 1971) proposed the methodology for the field oriented control that he applied for the control purpose of asynchronous machines.

(Sebastian, Slemon and Rahman, 1986) presented the equivalent circuit models for PM motors connected with the supply and the rotor position being sensed. And the results were compared with the experimental work on two motors.

(Jahns, Kliman and Neumann, 1986) exploited the benefits of IPMSM for the applications where variable and adaptable speed are the demand. The low magnet cost of IPMSM and the presence of the reluctance torque term due to the rotor saliency were manifested. The feed forward current vector control was illustrated. The simulation and experimental results were also shown.

(Jahns, 1987) again presented a paper stating that the FW in IPMSM can be achieved similarly as in the separately excited DC motors. He proposed the new flux weakening technique that was modification of the previously available feed forward algorithm. It took into account the effect of the degenerated torque and power characteristics at high speeds and the change of the DC bus voltage during the operation.

(Bose, 1988) presented the control scheme for IPMSM based on the six step voltage control utilizing maximum availability of the DC bus voltage. And the machine in this kind of scheme was operated in all the four quadrants. FW was implemented by controlling the direction of the torque angle.

(Pillay and Krishnan, 1989) studied the modeling and simulation of the PMSM drive incorporating the vector control scheme. Also the difference between the PWM and the hysteresis controller were presented along with the experimental results.

(Morimoto, Takeda, Hirasa and Taniguchi, 1990) in their paper presented a technique for the vector control of IPMSM, focusing the high speed applications. In this paper, their aim was to expand the operating limits of the operation keeping inside the inverter limits. They chose to divide the drive operation in the three different regions and have the current vector according to that. The optimum operation point

for the current components were stored in the LUTs for corresponding speed and torque values.

The same authors (Morimoto, Sanada and Takeda, 1994) again presented a technique to improve the FW control of a IPMSM without the use of look up tables. They studied the current behavior in the FW region and proposed the method to compensate the current transients in case of low availability of the maximum voltage in the FW regions. The current regulator with improved performance was tested with the experimental results as well.

(Kim and Sul, 1997) proposed the FW technique for IPMSM that also took care of the current regulation particularly in the FW region. Smooth transition into the FW region and independence from the machine parameters was another significance of the control highlighted in this paper.

(Zelaya De La Parra, 1999) made a control strategy that employed the FW approach by using a feedback method. The purpose of this feedback was to monitor the voltage and make it capable to approach its limit. The reference values for the currents in this technique were calculated by the values at the previous step. The voltage controller was set to provide the additional negative d-component of current in the deep FW region.

(Soong and Ertugrul, 2002) compared the performance of various machines including IM, SyRM and IPMSM for the FW region. The load tests were performed at the 50 Hz and it was concluded that the IPMSM was more suitable in terms of output power in the FW region as compared to considered machines.

(Kim and Lorenz, 2002) suggested the on-line parameter estimation method through the usage of LUT but it was limited to the maximum torque per ampere region.

(Meyer and Bocker, 2006) proposed a method for the off-line calculation to attain the optimum operating points through the usage of LUT as well.

(Kwon, Choi, Kwak and Sul, 2008) implemented the FW control through the look up tables and utilized the difference of output and reference voltage generated by the current regulator. The experimental results were shown that the torque obtained through this approach remained close to the maximum available torque of the machine.

(Awan, Song, Saarakkala and Hinkkanen, 2017) suggested the recognition of the magnetic model once during the life start-up of drives and the look-up table computations for the appropriate region of operations.

There are various techniques that had been employed to implement the model order reduction. Some of the details and classifications of these methods was given in work by (Antoulas and Sorensen, 2001) .

Another very commonly used method known as proper orthogonal decomposition was introduced by (Kerschen, G., F. Vakakis and A. Bergman, 2005) though he developed it to study the dynamics of structures.

For any MOR technique, the amount of data for any variable or quantity to be included in the mehtod itself plays an important role in the accuracy. The method was introduced known as 'method of snapshots' for this purpose by (Sirovich, 1987).

(Farzamfar et al., 2018) developed the OIM and showed that this procedure produced faster and accurate results in comparison to the alike MOR methods. Moreover, this particular technique is employed in this work to design the control for the real-time.

In the research literature mentioned above and others as well, various techniques have been proposed to develop and improve the FW algortihms and numerical solutions for electrical machines. But none of these explores the plausibility and productivity of any order reduction technique in the control systems of IPMSM, specifically in the real-time.

1.3 Objective of the thesis

The thesis deals with the design and implementation of the field weakening control for a prototype IPMSM. The main objective is to utilize the MOR technique, i.e. OIM to make the control independent of the parametric senstivity.

For this purpose, it is necessary to acquire understanding of the different FW algorithms for IPMSM and concurrently the essentials of OIM. Firstly, the field weakening control through the conventional methods using the machine parameters needs to be designed and implemented in the lab to confirm the validity of the OIM in the FW operation. Afterwards, an approach needs to be implemented that makes no use of the machine parameters, especially the inductances values, i.e. L_d and L_q, to avoid the effects of the magnetic saturation and the cross-coupling. In addition, it is also aimed not to use any other parameter like the stator resistance and the PM flux that may vary with temperature in the control design.

The simulations are performed in the MATLAB/Simulink environment for testing the methodologies through the field oriented control scheme. Then, the experiments are conducted on the prototype 2.2 KW IPMSM in the real-time utilizing the dSPACE setup to test the validity of the results.

1.4 Structure of the thesis

This thesis is organized as follows.

Section 2 discusses about the description of IPMSM and the methods used for the control purpose. It briefs about the construction and different rotor topologies for IPMSM. The modeling of IPMSM is also presented and then the transformations needed to make the control easier. Afterwards, various principles have been discussed to operate the machine either below or above the base speed. It also discusses about the limits to be cared for, while operating in these regions. The operation and algorithm of the field oriented control scheme is also presented. Section 3 highlights the main methodology adopted in this thesis. MOR technique, orthogonal interpolation method has been explained in detail. The property of the OIM to convert the current components into the flux linkage components, which enables it to be used in the control, has been discussed. Then, the three different methodologies have been explained that make the references generation for the FW operation. Experimental setup and its operation has been explained subsequently. Section 4 emphasizes on the simulation and the experimental results obtained from the designed approaches. The discussion and comparison of these results have also been given here. Lastly, Section 5 concludes the whole work of this thesis and make some recommendations for the future work and suggestions to improve the results.

2 Description and control of IPMSM

Synopsis This secton at firts briefs about the assembly of IPMSM. The different IPMSM types are given based on the geometry of PM inside the rotor surface. Afterwards, modeling of IPMSM is given to obtain the equations to be used for the control purpose. The transformations necessary for the modeling in the synchronous dq axis is also provided in subsection 2.2.2 that makes the control easier. In subsection 2.3, various control principles are defined that are needed to operate the machines below and above the rated speed. Subsection 2.3.3 briefs about the capabilites of the machine based on the short cicuit current to operate either only through the FW technique or also extend to the MTPV operation. The prototype machine operates in accordance to the FW approach at higher than the base speeds. After these techniques are explained, the field oriented conntrol (FOC) scheme is introduced in subsection 2.4 that is used in this thesis to implement the overall control structure. The main idea of the FOC and two of its main constituents, the speed and flux controllers are also discussed in subsection 2.4.3.

2.1 Construction of IPMSM

PMSMs are the type of the synchronous machines in which the excitation is provided by PM instead of the conventional windings in the rotor frame. Depending upon the location of the PM mounted at rotor surface, PMSM can be divided into the two basic categories as SPMs and IPMSM. SPM have uniform air-gap with the magnets on the rotor surface, therefore, behave as non-salient machines. We will mainly focus on IPMSM in this thesis. However, depending on the type of back emf voltage induced in stator windings and the salient nature, PMSMs are categorized in Figure 2.1.

Except the rotor configurations, both types of PMSM, IPMSM and SPM resemble in their overall construction. In the similar fashion to the asynchronous motors, PMSM have the three phase windings in the stator frame that are connected with an ac supply. These windings are distributed in a sinusoidal manner separated by the phase shift of 120 deg. It helps to avoid the harmonic components of a higher order

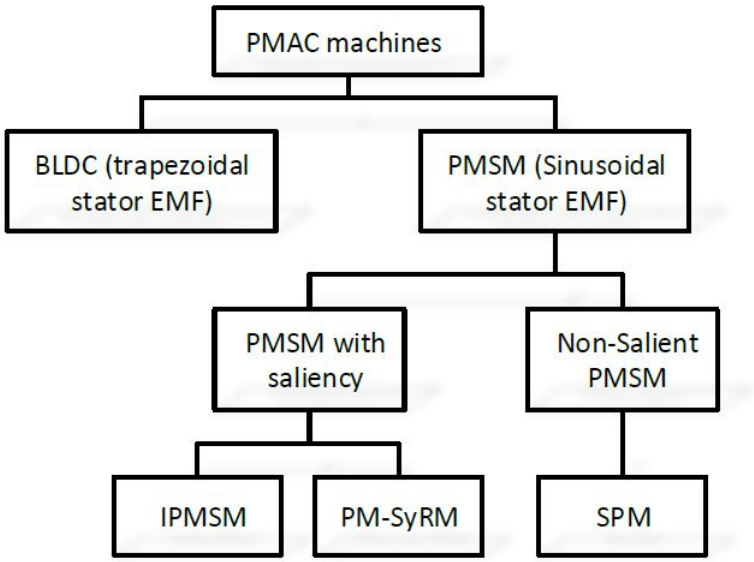

Figure 2.1: PMSM types

and also enables the machine to generate the air-gap field that typically contains the fundamental sinusoidal component. As synchronous motors are doubly-excited, the other source of excitation, PM in the rotor play an important role in the evolution of these machines. Indeed, the discovery of new magnetic materials became the source of development for PMSM. The absence of windings in the rotor arrangement make PM machines more efficient and reliable. The copper losses in the machine are reduced to a great extent and there remains no requirement of either the slip rings or brushes. Therefore, the PM machines are compact and light as compared to other synchronous machines. In contrary, one cannot control the field produced by the rotor directly as in case of other doubly excited machines since the PM generate a constant magnetic field (Perera, 2002). In these brushless PM motors, the supply frequency is adjusted according to the rotor speed in a way that the stator and rotor magnetic fields remain in synchronism with each other. Therefore, these kind of the drives are preferred in constant speed applications.

2.1.1 IPMSM rotor topologies

IPMSM are preferred usually for high speed applications due to their salient nature. The PMs are hidden inside the core of the rotor in these machines. Broadly speaking, IPMSM can be categorized based on the flux crossing through its air-gap in the following types, axial flux, transversal flux and radial flux machines. The most common types of IPMSM are the radial flux machines (Dutta and Telecommunications, 2007). Focusing on the placement of PMs inside the rotor surface, the main classes of IPMSM are given in Figure 2.2.

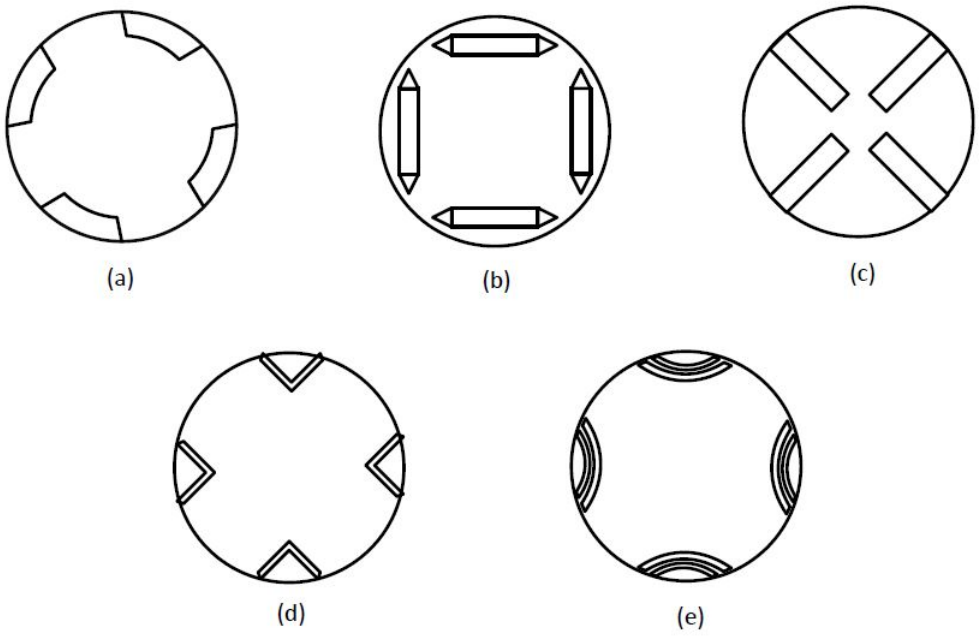

Figure 2.2: IPMSM types

Figure 2.2 (a) shows the inset type in which the PMs are located along with the inside surface of the rotor. NdFeB magnets are the appropriate option for these kind of the machines and less PM material is needed as compared to other types (Schiferl and Lipo, 1988). Figure 2.2 (b) shows the buried magnet type. The magnets are not embedded fully on the rotor surface, rather they are placed within the rotor core. The centrifugal forces do not damage the magnets in this type (Jahns, Kliman and Neumann, 1986). Radial magnet IPMS in Figure 2.2 (c) exhibit high magnetic torque but relatively less reluctance torque (Soong, Han and Jahns, 2007) and difficult to manufacture. Figure 2.2 (d) shows the V-shape magnet configuration that is very well suitable for high speed applications due to the presence of high saliency ratio that causes the additional reluctance torque (Lindh et al., 2011). Figure 2.2 (e) illustrates the multiple barrier configuration which consists of multiple barriers that give rise to the increased saliency as compared to other mentioned types (Soong, Han and Jahns, 2007) but they possess more complex design as well. The magnets are more protected in IPMSM as compared to non-salient configuration and the demagnetization risk is also lowered significantly.

Figure 2.3 shows the placement of PM in IPMSM (Dutta and Telecommunications, 2007). Very small iron bridges are provided at the end of magnet poles in the IPMSM that usually saturate because of the leakage flux. The flux barriers between these iron bridges and magnetic poles are made of non-magnetic materials to avoid short circuit with the adjacent magnetic poles.

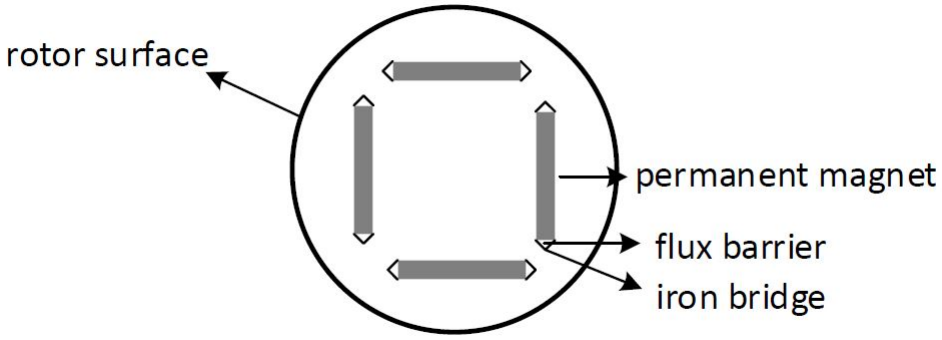

Figure 2.3: PM in IPMSM

2.1.2 Saliency

Saliency is the characteritic of PMSM, that affect significantly on the FW properties. Infact, a maximum speed achievable in these machines depends on saliency ratio as well. It arises due to the difference in L_d and L_q and is interpreted as the ratio of the two, i.e.

$$\xi = \frac{L_q}{L_d} \tag{2.1}$$

where ξ is the saliency ratio. SPMs provide with no saliency since the L_d and L_q in these type of machines possess the same values or with minor difference. In contrary, the synchronous reluctance machines (SyRM) have high saliency ratios, since these are made to operate through this reluctance term present in the torque equation with no presence of the PM flux. IPMSM, in particular, are conventionally designed with the saliency ratio of 2 to 3. However, the machines with very low or high saliency ratio exhibit the disadvantage of not being able to achieve very high speeds in the FW region. The prototype machine used for the experimental purpose in this work exhibit, however, the low saliency ratio of 1.05 that can be known from Table 3.2 . It means that the salient characteristics in the case of this protoype machine cannot be most effectively exhibited in terms of torque or speed. Figure 2.4 from (Dutta and Telecommunications, 2007) shows the torque characteristics for the IPMSM. It can be seen that with no or little saliency, the machines are much less efficient in terms of the torque and power.

2.1.3 PM materials in IPMSM

The magnetic materials used for the construction of IPMSM or other PM machines significantly affect their performance. The presence of PMs in place of the winding itself diminishes the intrinsic factor of losses. The application for which the PMSM is to be used determines the design for PMs deployed in it.

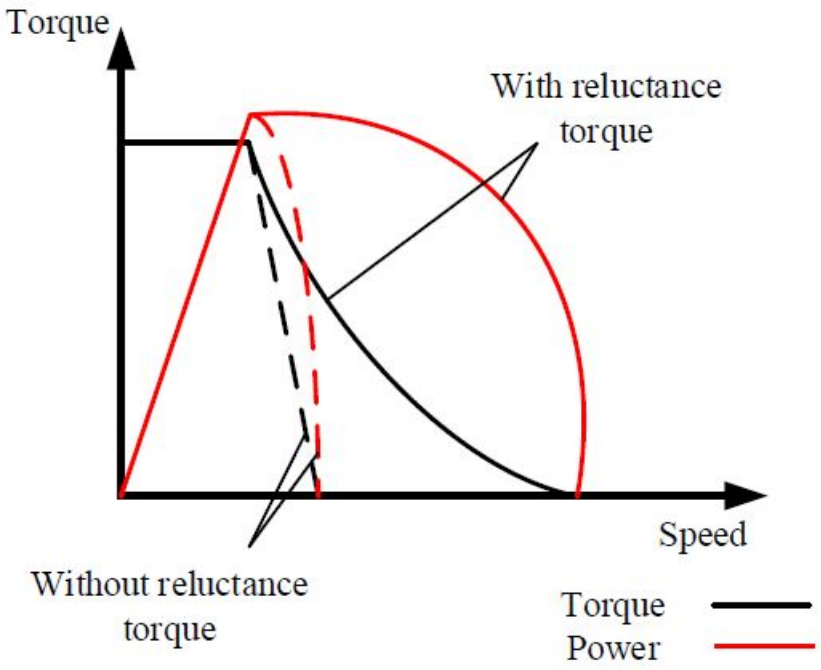

Figure 2.4: Saliency effect on power and torque

The *BH* loop can well explain the characteristics of a PM as in case of other ferromagnetic materials as shown in Figure 2.5. The remanance flux density and coercitive field strength of a magnet are its features of paramount importance that determine its behaviour during the operation of the machine. The remanance flux density or residual induction denoted by $\boldsymbol{B}_r$ describes the property of a PM that tells about the amount or value of the magnetic flux that resides inside the magnet even in the absence of magnetic field ($\boldsymbol{H}$) around it. Other property known as coercitive field strength ($\boldsymbol{H}_c$) is the negative or demagnetizing force required to bring the flux density to zero after magnetizing the material to the saturation level. Another relevant property known as the intrinsic coercive force of a material, denoted by ($\boldsymbol{H}_{ci}$) specifies the resistance of the material to the demagnetization effect.

The demagnetizing curve occurring in the second quadrant of the hard materials is most of the times sufficient to describe the behaviour of the magnet itself. While operating the PMSM, the care has to be taken to be within the temperature range feasible for the magnetic materials. Curie temperature refers to the temperature point at which the magnetization of the material reduces to zero and it loses its magnetic properties. The negative value of the d-component of the stator current should not go much high that it cause the risk of demagnetization of a PM.

Different types of magnetic materials have been discovered and employed in the past for various applications. In the last century, PMs were started to be used in motors. Alnico (Aluminum Nickel and Cobalt) alloys discovered in the 1930s

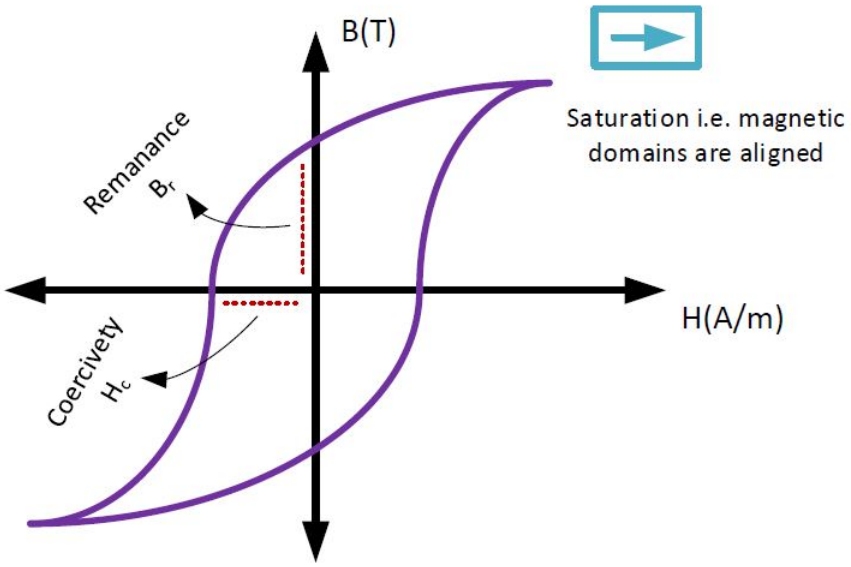

Figure 2.5: BH loop of a PM material

have very high remanance and has been used in the PMDC brush commutated motors and other applications widely (Ruoho, 2011). However, the low coercive force makes its magnetization and demagnetization very easily, therefore, it cannot be used extensively in machine applications.

The Barium Ferrite and other ferrite magnets have high coercitive field strength and low costs but these bear low remanance flux density that does not make it feasible to use in the high power applications. Some other rare earth magnets like $SmCo_5$ and Sm_2Co_{17} were also introduced that have high remanance flux density, coercitive field strength and the maximum operating temperatures. Though they are expensive, still they are used in machines because of their very high temperature durability of up to around 350 deg.

Nowadays, the most widely used PM in PMSM are NdFeB (Pyrhonen, Jokinen and Hrabovcova, 2009). These magnets have higher remanance flux density than any other existing magnet and they have high coercitive field strength as well. But the demerit of these kind of magnets is their vulnerability to corrosion and the low temperature endurance, as compared to the SmCo or AlNiCo. However, due to their superior overall magnetic properties, they are preferred over all the other permanent magnets to be used in PM machines.

2.2 Modeling of IPMSM

The presence of PM inside the core of the rotor provides IPMSM, an intrinsic property of the magnetic saliency that enhances the torque production capability. The

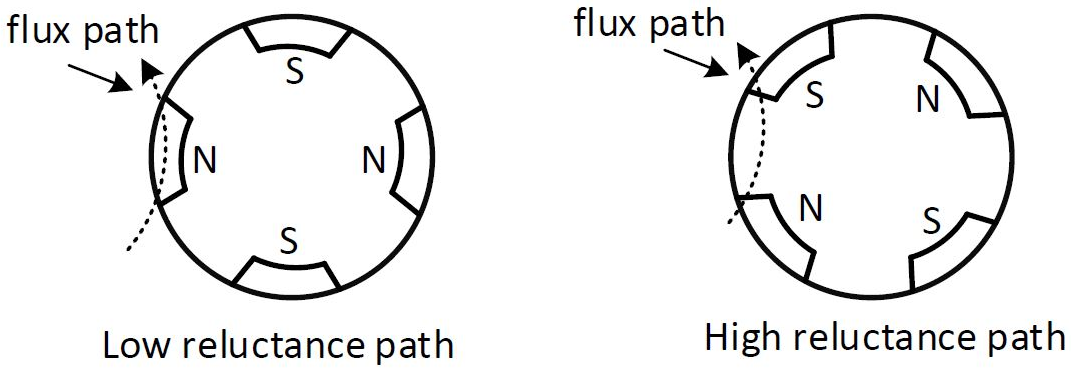

Figure 2.6: Inductance variation in IPMSM

inductances in IPMSM are the function of the rotor angle and become time-variant. It can be well understood from the fact that the reluctance of magnets is more than the iron in the structure of the stator or the rotor. Therefore, the reluctance path for the flux differ with the change in the rotor position that, in turn, causes the change in inductances. The flux path encountering the magnets at a particular time will cause the reduction of inductance value due to higher reluctance. The pictorial representation of this phenomenon is given in Figure 2.6. To avoid the complexity caused by this variation of inductances, the IPMSM are usually modeled in the two axis frame of references as dq axis.

Figure 2.7 illustrates IPMSM cross-sectional view in three frame of references, i.e. ABC, $\alpha\beta$ and dq. The magnetic axis of phase windings A, B and C are pointed towards their respective phases and the angles between these axis is 120 *deg*. The magnetic axis for the phase A directs towards the maximum magneto motive force (MMF) available when the peak positive current is provided to a motor. The $\alpha\beta$ reference frame is also fixed according to the stator reference. The α axis is in the direction of phase A whereas β axis resides in the perpendicular direction to the α axis. It is a stationary reference frame, therefore, modeling in this $\alpha\beta$ axis is also not suitable because of varying inductances. Most widely adopted reference frame for the modeling purpose is the dq axis frame of reference. It rotates along with the rotation of the rotor at the same speed and makes the angle θ_r with A or α axis. The direct-axis is directed towards the direction of the PM flux and the quadrature-axis lies orthogonal to the d-axis in the direction of induced EMF.

2.2.1 Three phase modeling

The modeling of IPMSM can be well understood from (Pillay and Krishnan, 1989). The supply voltage to the stator winding is the summation of the voltage drop across the stator windings and the induced voltage regarded as back EMF. Hence, in the form of phase variables, the voltage equations for the three phase model can be

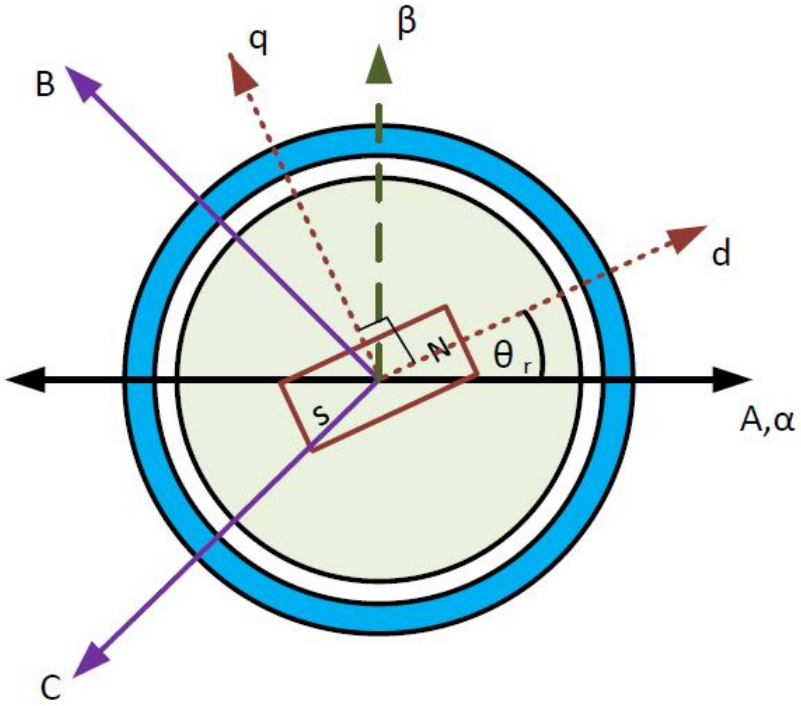

Figure 2.7: Transformation of axis

written as

$$u_a = R_s i_a + \frac{\partial \psi_a}{\partial t} \tag{2.2}$$

$$u_b = R_s i_b + \frac{\partial \psi_b}{\partial t} \tag{2.3}$$

$$u_c = R_s i_c + \frac{\partial \psi_c}{\partial t} \tag{2.4}$$

where u_a, u_b and u_c are the phases voltages, i_a, i_b and i_c are the phase currents and R_s is the stator resistance that remains same for all the phases. Similarly ψ_a, ψ_b and ψ_c are the flux linkages for the stator windings. The equations for the flux linkages are

$$\psi_a = L_{aa} i_a + M_{ab} i_b + M_{ac} i_c + \psi_{fa} \tag{2.5}$$

$$\psi_b = M_{ba} i_a + L_{bb} i_b + M_{bc} i_c + \psi_{fb} \tag{2.6}$$

$$\psi_c = M_{ca} i_a + M_{cb} i_b + L_{cc} i_c + \psi_{fc} \tag{2.7}$$

where L_{aa}, L_{bb} and L_{cc} are the stator self-inductances and M_{ab}, M_{ac} and M_{bc} are the mutual inductances for all the phases. Due to the symmetrical nature of stator

structure, the relation for the mutual inductances will be such that $M_{ab} = M_{ba}$. In (2.5), (2.6) and (2.7), either the stator self-inductances or the mutual inductances and the flux produced by PM depend on the position of the rotor. The PM flux can be expressed as a function of the rotor position as

$$\psi_{fa} = \psi_f \cos\theta_r \tag{2.8}$$

$$\psi_{fb} = \psi_f \cos\theta_r - 120deg \tag{2.9}$$

$$\psi_{fc} = \psi_f \cos\theta_r + 120deg \tag{2.10}$$

Since the q-axis offers less reluctance path, the self-inductance for a particular phase will be maximum when the q-axis is in the direction of that phase. Similarly, for any two phases, the mutual inductance will be maximum when q-axis lies in between these two phases. The saliency effect for the stator inductances can be specified by $2\theta_r$. The equations for the stator self and mutual inductances can be written as (Lyshevski, 2018).

$$L_{aa} = L_l + L_m - L_{hm}\cos 2\theta_r \tag{2.11}$$

$$L_{bb} = L_l + L_m - L_{hm}\cos 2(\theta_r - 120deg) \tag{2.12}$$

$$L_{cc} = L_l + L_m - L_{hm}\cos 2(\theta_r + 120deg) \tag{2.13}$$

$$M_{ab} = -\frac{1}{2}L_m - L_{hm}\cos 2(\theta_r - 120deg) \tag{2.14}$$

$$M_{ac} = -\frac{1}{2}L_m - L_{hm}\cos 2(\theta_r + 120deg) \tag{2.15}$$

$$M_{bc} = -\frac{1}{2}L_m - L_{hm}\cos 2(\theta_r) \tag{2.16}$$

where, L_l is the stator self-leakage inductance, L_m and L_{hm} are the average and half of the magnetizing inductances. The value of L_l remains same for all the three phases, since all phases winding are uniform. L_m and L_{hm} can be given as

$$L_m = \frac{1}{2}(L_q + L_d) \tag{2.17}$$

$$L_{hm} = \frac{1}{2}(L_q - L_d) \tag{2.18}$$

Also, in (2.14) , (2.15) and (2.16), -1/2 appears since all the phases are phase shifted by 120 deg and cos ($\pm$ 120 deg) = -1/2.

The stator resistance and the PM flux also change with the change in the temperature. According to (Nalepa and O. Kowalska, 2012), the variation in the PM flux occurs as

$$\psi = \psi_{25deg}(1 - \alpha_{\psi} \triangle T) \tag{2.19}$$

Here, ψ_{25deg} is the flux at room temperature which is 25 deg, $\triangle T$ is the difference between the actual temperature and room temperature and α_{ψ} is the reversible temperature coefficient.

The change in the stator resistance due to temperature variation can also be given by the similar equation as

$$R = R_{25deg}(1 + \alpha_{Cu} \triangle T) \tag{2.20}$$

Here, α_{Cu} is the temperature coefficient for the copper material.

2.2.2 Transformations

The mathematical modeling and control schemes for the IPMSM utilize two main transformations. These transformations are named as the Clarke and Park transformations. The former changes the three axis coordinate system into the two axis stationary and orthogonal coordinate system known as $\alpha\beta$ having the stator as the reference. The later then changes these two axis stator referenced coordinate system into the two axis orthogonal system with reference to the rotor termed as dq axis.

Clarke transformation The three phases currents i_a, i_b and i_c can be considered as the components of the stator current vector $\boldsymbol{i}_s$ that now needs to be represented in the two axis frame α and β. Edith Clarke provided the solution with the set of equations that can be used for the conversion purpose keeping the whole information intact. This set of equation can be shown as (Akin, Bhardwaj and Warriner, 2013)

$$i_{\alpha} = i_a \tag{2.21}$$

$$i_{\beta} = \frac{1}{\sqrt{3}} i_a + \frac{2}{\sqrt{3}} i_b \tag{2.22}$$

These equations can also be termed as $\alpha\beta\gamma$ transformation. (2.21) and (2.22) point towards the existence of any common-mode currents but since the outcome for the addition of i_a, i_b and i_c remain 0, therefore it is not usually considered in FOC calculations. Ultimately, we get the current vector $\boldsymbol{i}_s$ in the $\alpha\beta$ axis.

The Clarke transformation can also be considered as the process which takes the three coils evenly distributed at 120 deg and set them into the two coil formations orthogonal to each other. The output of these equations appear to be two phase waveforms that possess the same amplitude as that of the original three phase waveforms.

If the control is done taking into account these two waveforms, the controller has to be modified in such a way that the measured and reference values are time-variant which makes the situation much more complex.

Park transformation For the convenience of the control purpose, the current vector is then modified so that it can be represented on the dq axis that will be synchronized with the rotation of the rotor. The sinusoidal currents obtained at the two axis behave as the steady state DC values. The transformation is done taking into account the rotor flux angle θ_r that is measured with respect to any arbitrary stationary stator axis usually along phase A. The set of equations proposed by Robert Park (Akin, Bhardwaj and Warriner, 2013) are as follows:

$$i_d = i_\alpha \cos\theta_r + i_\beta \sin\theta_r \tag{2.23}$$

$$i_q = -i_\alpha \sin\theta_r + i_\beta \cos\theta_r \tag{2.24}$$

Both these components of current do not vary with the change in time, as dq axis frame is rotating along with the reference frame of rotor and the limitation of controller at high speeds does not exist.

Since the requirement of FOC is to have the rotor flux and d-axis in the same direction with q-axis being orthogonal, independent control of both these quantities become possible. The rotor flux can be simply controlled by the i_d whereas the torque can be controlled by the manipulation of i_q accordingly. Figure 2.8 shows the transformation process from abc to dq axis.

2.2.3 *dq*-axis modeling

The complex phasor models are only confined to the steady state conditions, whereas the phase variable models become too complex. The space vectors can be used effectively to model IPMSM as these are easier for modeling and control purposes. The phase variables can also be easily transformed to the space vector models. In addition, the space vectors do not include the zero sequence components because the stator winding is delta connected or even if the winding is connected in the star, the neutral point is open.

Since in a three phase machine, there's a difference of 120 deg between the phases that can be represented by α as

$$\alpha = e^{\frac{j2\pi}{3}} \tag{2.25}$$

The space vectors equations for the current and voltage are expressed in the following forms

$$\boldsymbol{i}_s(t) = \frac{2}{3}[i_{sa}(t) + \alpha i_{sb}(t) + \alpha^2 i_{sc}(t)] \tag{2.26}$$

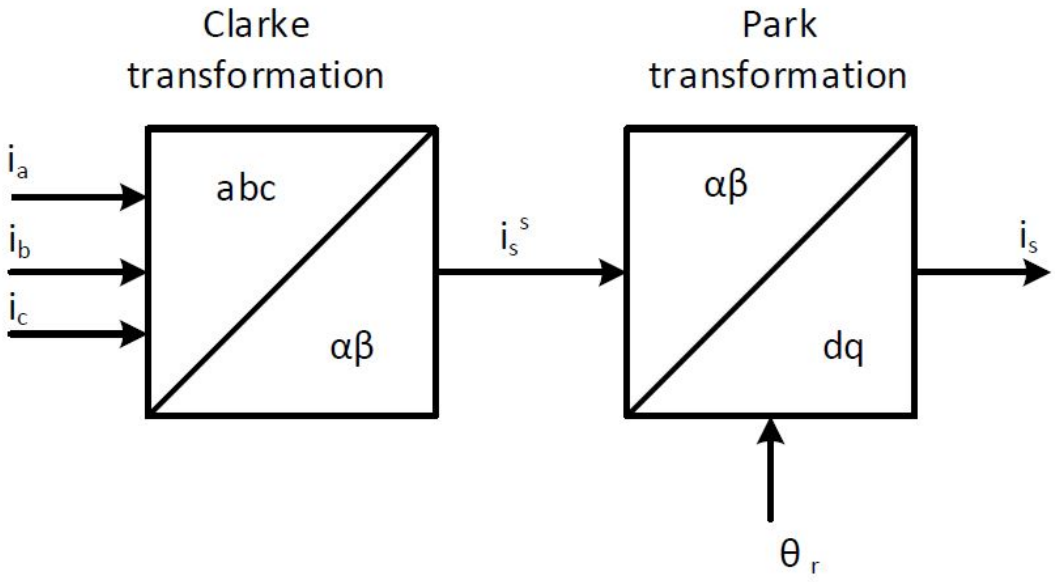

Figure 2.8: abc to dq axis

$$\boldsymbol{u}_s(t) = \frac{2}{3}[u_{sa}(t) + \alpha u_{sb}(t) + \alpha^2 u_{sc}(t)] \tag{2.27}$$

The reduction of the vector with the factor of 2/3 gives the corresponding actual length of that variable in the sinusoidal form.

The voltage equation for the reference frame fixed with the stator is as

$$\boldsymbol{u}_s^s = R_s \boldsymbol{i}_s^s + \frac{\partial \boldsymbol{\psi}_s^s}{\partial t} \tag{2.28}$$

Similarly, for the reference frame, that rotates alongwith the rotor itself, the voltage equation can be obtained by the multiplying (2.28) with $e^{-j\theta_r}$ as

$$\boldsymbol{u}_s = R_s \boldsymbol{i}_s + \frac{\partial \boldsymbol{\psi}_s}{\partial t} + j\omega_m \boldsymbol{\psi}_s \tag{2.29}$$

The last term in the above equation represents the back emf and it increases with the increase in the speed of a machine. As in case of the salient pole machines, all the quantities including the voltage, currents and flux are dealt in dq coordinates. For operating in these coordinates, it is must to know the voltage along both the axis given as

$$u_d = R_s i_d - \omega_m L_q i_q + \frac{\partial \psi_d}{\partial t} \tag{2.30}$$

$$u_q = R_s i_q + \omega_m (L_d i_d + \psi_f) + \frac{\partial \psi_q}{\partial t} \tag{2.31}$$

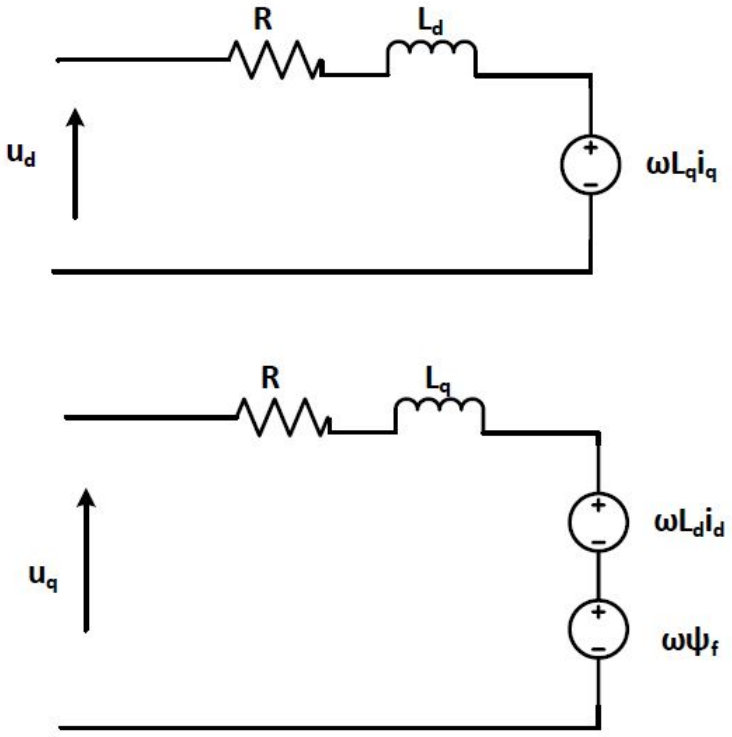

Figure 2.9: Equivalent model in dq frame

The motor model in the rotor reference frame is shown in the Figure 2.9. Similar to the other basic quantities, the stator flux linkages, ψ_d and ψ_q also vary for the dq axis and depends on the corresponding current components as well.

$$\psi_d = L_d i_d + \psi_f \tag{2.32}$$

$$\psi_q = L_q i_q \tag{2.33}$$

Since the d-axis is aligned with the PM flux, it adds to the current produced in the d-axis direction that needs to be weakened in order to go high speeds. The total stator flux linkage can also be calculated if the flux components along both the axis are known, as

$$\psi_s = \sqrt{\psi_d^2 + \psi_q^2} \tag{2.34}$$

The power of a three phase machine can be known from the dq component values of the voltages and currents . As considered for ideal conditions that output power is the same as an input power, it can be obtained as

$$P_{out} = \frac{3}{2}(u_d i_d + u_q i_q) \tag{2.35}$$

Knowing the value of the currents in the dq axis and putting the voltage values from the previous equations, it can be given as

$$P_{el} = \frac{3}{2}\omega_m(\psi_f i_q + (L_d - L_q)i_d i_q) \tag{2.36}$$

In the steady state, the electromagnetic power P_{el} can be considered well by taking into account (2.36). Another term needs to be included for more accurate study in case of losses and transients (Harnefors, Hinkkanen, Wallmark and Yepes, 2014).

$$P_{out} = P_{el} + \frac{3}{2}(R_s i_d^2 + \frac{\partial \psi_d}{\partial t} i_d + R_s i_q^2 + \frac{\partial \psi_q}{\partial t} i_q) \tag{2.37}$$

The presence of PM and difference in the inductance values of d and q-axis simultaneously provide IPMSM with a very attractive feature in terms of torque. The torque expression for IPMSM is most commonly found in the literature as

$$T = \frac{3p}{2}(\psi_f i_q + (L_d - L_q)i_d i_q) \tag{2.38}$$

that can be derived from the (2.36). The component of the torque arising from PM is known as the field torque or the reactance torque and can be represented as

$$T_f = \frac{3p}{2}(\psi_f i_q) \tag{2.39}$$

The other component representing the reluctance torque can be written as

$$T_{rel} = \frac{3p}{2}((L_d - L_q)i_d i_q) \tag{2.40}$$

As is evident from (2.40), the negative value of i_d will make an addition to the torque expression when L_d is less than L_q. It means if there would be no field torque because of ψ_f=0; reluctance torque can still be used to produce the toqrue in the SyRM.

The torque expression can, however, be given as in many other forms as the cross product of the flux linkages or the current linkages. The control of angles between these currents or flux linkages can also help in controlling the torque. An expression for the torque can be obtained depending on the angle between the stator flux and the PM flux is known, lets say δ. The d and q-components of flux can then be written as

$$\psi_q = \psi_s sin\delta \tag{2.41}$$

$$\psi_d = \psi_s cos\delta \tag{2.42}$$

Substituting these values in the torque equation (2.43),

$$T = \frac{3p}{2}(\psi_d i_q - \psi_q i_d) \tag{2.43}$$

one can easily get the new form of torque (Perera, 2002) as

$$T = \frac{3p}{2}\left(\frac{\psi_s \psi_f \sin\delta}{L_d} + \frac{\psi_s^2 (L_d - L_q)\sin 2\delta}{2L_d L_q}\right) \tag{2.44}$$

2.3 Control principles

There are different principles applied for the control purpose. For operating machines upto the rated or base speed, either i_d can be kept zero or maximum torque per ampere (MTPA) method is utilized. At higher speeds, the FW control is implemented. Maximum torque per volt (MTPV) is also included with the FW control in some cases as explained later in this subsection. Furthermore, there are certain practical limitations that the machine has to follow either below or above the base speed.

2.3.1 Current and voltage limits

The maximum current limit of a motor depends on the inverter limit and machine thermal limits and can be represented in the form of equation

$$\sqrt{i_d^2 + i_q^2} \leqslant I_{max} \tag{2.45}$$

It is to be noted that in the i_d-i_q plane, a circle can be formed of the radius I_{max} representing the maximum phase current of the motor as shown in Figure 2.10 that represents current limit and is independent of the speed of the machine.

The voltage limit U_{max} for the inverter depends on the DC link voltage U_{dc} and the machine insulation. In the linear modulation region, this voltage is limited to the range $U_{dc}/\sqrt{3}$ (Sarkar and Bhunia, 2017), which ensures the presence of voltage vector inside the limit. The voltage limit can be represented by the set of ellipses and the sizes of these ellipses vary inversely with angular speed of the machine. The center of these ellipses can be represented by the point $(-\psi_f/L_d, 0)$ in the i_d-i_q plane, Figure 2.10. The voltage limit equation can be shown as

$$\sqrt{u_d^2 + u_q^2} \leqslant U_{max} \tag{2.46}$$

where u_d and u_q are the dq axis components for the voltage, respectively. All the points in the i_d-i_q plane that point inwards to the current limit circle from its intersection point with ellipses form the feasible operating points area.

In the steady sate and neglecting losses, the equation for the maximum flux linkage in the form of stator currents is given in (2.47)

$$\psi_s = \sqrt{(\psi_f + L_d i_d)^2 + (L_q i_q)^2} \leqslant \frac{U_{max}}{|w_m|} \tag{2.47}$$

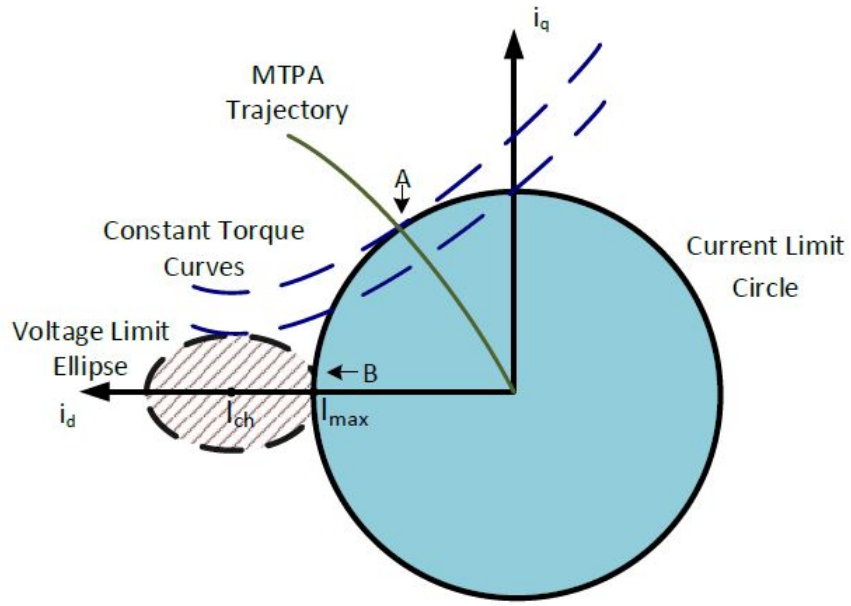

Figure 2.10: IPMSM operation

2.3.2 Control principles below the base speed

For the operation of machine below the base speed, two methods are usually adopted. One keeps the value of i_d to zero that makes the control easier. While the other method, maximum torque per ampere (MTPA) generates the minimum stator current to obtain the maximum torque.

Keeping i_d zero For the PMSM with the PM mounted on the rotor surface such as SPM, there is no or minute saliency, since the d and q-axis inductances do not really differ in their values. The absence of the reluctance torque in these kind of machines is the cause of limited FW region and these cannot be used for very high speed applications. Furthermore, the salient pole machines with low saliency or possessing almost equal values of L_d and L_q reside in the same category. Hence, in these kind of machines, the torque is mainly governed by one component of current (q component). i_d plays no significant role in the torque production. But employing this control, the FW cannot be achieved and different techniques have to be used to go above the rated speed of the machine. However, the advantage of this method is that it makes the control process much easier and give good results up to the base speed. The prototype IPMSM in this thesis operates on this principle below the base speed.

Maximum torque per ampere In IPMSM, the presence of reluctance torque makes it quite possible to enable the contribution of both the current components i_d and i_q in the total torque production. The q-axis inductance is most often greater than the d-axis inductance, therefore, the negative i_d will be needed to produce the positive torque. With this negative i_d value available, the lesser i_q will be needed to achieve the desired torque as well. The positive i_d value is always avoided since it resists the field torque to be produced.

A specific torque can be obtained by utilizing the innumerable combinations of i_d and i_q sets but there exists only a single pair that gives the torque with the minimum stator current. The copper losses for the stator depend on the stator current vector, therefore it is desirable to operate at the current pairs which result in the minimum current. This will lead to the maximum torque in response to the minimum current or indirectly minimum losses. Hence, this approach is usually named as maximum toque per ampere or MTPA.

The torque term in (2.38) can be stated considering only i_d (Li and Li, 2012) as

$$T = \frac{3p}{2}(\psi_f + (L_d - L_q)i_d)(\sqrt{i_s^2 - i_d^2}) \tag{2.48}$$

The optimum minimum value of i_d for maximizing the torque can be deduced by equating the derivative of the torque taken with respect to the i_d as zero. It can be obtained as following:

$$i_d = \frac{\psi_f}{2(L_q - L_d)} - \sqrt{\frac{\psi_f^2}{4(L_q - L_d)^2} + i_q^2} \tag{2.49}$$

The above equation will lead to the result as in the form where i_s can replace i_q as

$$i_d = \frac{\psi_f + \sqrt{\psi_f^2 + 8(L_q - L_d^2){i_s}^2}}{4(L_q - L_d)} \tag{2.50}$$

In addition, the i_d reference point can also be calculated by the angle between the d-axis towards PM flux and the phase current vector of the stator. This angle is known as the torque or current angle (β). Hence, $\boldsymbol{i_s}$ can be decomposed into its component currents as

$$i_d = i_s \cos\beta \tag{2.51}$$

$$i_q = i_s \sin\beta \tag{2.52}$$

In the above equations, i_s represents the magnitude of the stator phase current vector and β varies from 0 deg to 180 deg . Similar to the i_d, if the derivative of β with respect to the torque is taken, the i_d value can be obtained within the MTPA

region. By putting the (2.51) and (2.52) in torque equation (2.38), we can obtain the equation as

$$T = \frac{3p}{2}(\psi_f i_s \sin\beta + \frac{1}{2}(L_d - L_q) i_s^2 \sin 2\beta) \tag{2.53}$$

By taking the derivative of above equation in respect of the current angle and equating it as zero, one can get the following quadratic equation (Khan, 2016) that will give the same expression for i_d as given in equation (2.49) and (2.50)

$$(L_d - L_q) i_d^2 + \psi_f i_d + (L_d - L_q) i_d^2 = 0 \tag{2.54}$$

In the Figure 2.10, the MTPA trajectory can be seen on the synchronously rotating dq reference frame. This trajectory consist of the i_d and i_q pairs which produce the desired torques with the minimum current amplitude. The constant torque curves consist of all the i_d and i_q pairs which are capable of producing same amount of the torque. But the intersection of these torque curves with the MTPA curve indicate the optimum points to be operated on. The voltage limit does not need to be bothered in the MTPA region rather it is the current limit that needs to observed strictly. Furthermore, the supply current is the main motor parameter affecting the torque production. The stator current is controlled in a way so that the reluctance torque could be utilized fully to maximize the efficiency.

2.3.3 Control principles above the base speed

The methods described above cannot operate machines high above the base speed. The FW control has to be implemented for this purpose.

Field weakening The FW control needs to be implemented efficiently to obtain wide constant power speed range. The increase in speed of IPMSM also causes the proportional increase in the back emf, i.e. electromotive force. At the beginning of the operation, the voltage applied exceeds the total of the stator voltage drop and also the back electromotive force (EMF). To increase the speed, the voltage is increased accordingly and the behaviour of voltage and speed are alike upto base values. As the rated value of the voltage is met, the speed then corresponds to the base speed as well. However, above the base speed, the speed cannot be increased further by extension of the voltage. It is quite evident because of the voltage bound that inverter cannot overreach and the voltage limit of the motor insulation system. At this stage, the back EMF and the voltage drop become significant and exceed the applied voltage. To go above this speed, either the voltage needs to be increased or the flux needs to be decreased. It is quite evident from the steady state voltage equation (2.55)

$$\psi_s = \frac{U_{max}}{w_m} \tag{2.55}$$

The voltage can be increased if the extra power stage is added on the inverter, keeping in view the voltage limit of the motor. However, it will be costly and quite troublesome. The only feasible option left behind is to weaken the flux of the air-gap. Since the PM produce their own flux which cannot be controlled directly, the most widely used technique is to introduce the demagnetizing magneto motive force (MMF) from the stator to decrease the flux present in the air-gap (Jahns, 1987). The MMF of the PM flux is encountered by this induced MMF. The demagnetizing MMF from the stator can be originated with the instigation of the negative i_d current from the stator. Hence in the FW area, the stator current is partially or even sometimes completely utilized for the curtailment of the stator flux.

The FW operation of a machine can be well explained by the torque-speed curve. In the Figure 2.4, the area in which the torque remains constant indicates constant torque zone and the area beyond that represents the FW region. In the former region, the voltage increases along with the power. However, the flux has to be kept constant in this region for the increase in the speed according to the (2.55) therefore it is referred to as a constant flux. The current commands can be produced through i_d zero principle or MTPA operation in this region. Above the base speed, the voltage cannot be increased further therefore the flux has to be decreased in this case and hence, the torque will also be decreased in turn. This represents the FW area of the machine. However, the power will remain constant in this region since the flux or torque will decrease proportionally to the increase in the speed of machine. In addition, the current also retains its value close to the nominal value which indicates the constant electrical power in the FW region. In case, the MTPA region is followed below the base speed, the FW happens to start from point A shown in Figure 2.10.

Finite and infinite speed drives The short circuit or characteristic current is the main factor which decides the operation of the machine above the base speed. It specifies the center of the voltage ellipses formed in the i_d-i_q plane. Moreover, it can be correlated with the PM flux linkage and d-axis inductance taking their ratio as

$$I_{ch} = \frac{\psi_f}{L_d} \tag{2.56}$$

For the two cases that either the characteristic current is greater than the I_{max} or not, the following operations will occur:

If $I_{ch} > I_{max}$ the maximum speed of the machine is limited, it can be regarded as the finite speed drive. For these kind of machines, the maximum torque occurs at the point where the current limit circle cuts the voltage limit ellipse. Furthermore, the voltage and current limits both will be considered while operating in FW operation (Soong and Miller, 1994). The machine will not enter into the MTPV operation since the ellipse lies outside the circle as shown in Figure 2.10.

The prototype IPMSM used for the validation of the results in this thesis has the characteristic current of almost 9 A, which is more than twice of the maximum

current of the machine. Therefore, the operation is feasible at higher speeds by applying the FW approach and MTPV mehtod cannot be utilized.

If $I_{max} > I_{ch}$, then this category lies under the infinite speed drives. The characteristic current point in these machines resides in the circle of current limit and to achieve the maximum torque, the current starts to follow the voltage limit ellipse instead of the current limit circle. Now the voltage limit will only be cared. MTPV operation will be utilized to gain very high speeds in these kind of machines.

Maximum torque per voltage (MTPV) The infinite drives have been growing these days to be used in EV or HEV. Maximum torque per voltage can also be referred to as maximum torque per flux (MTPF) as well since the voltage and the flux are correlated with each other in the control of IPMSM. MTPV allows a machine to extend its constant power speed range beyond the FW operation, if the point representing the characteristic current lies inside the current limit circle (Soong and Miller, 1994). If the machine is not able to operate in the MTPV operation as in the case of the finite drives, the flux cannot be minimized above a certain limit for gaining the maximum torque and hence the theoretical limit of the machine speed is also limited to a definite range rather than the infinity.

While working in the MTPV range, the voltage limit is considered only since the current follows the voltage limit trajectory instead of the current limit circle when it enters into this region of operation. The current in this case gets lower than the rated current and hence, the power falls inversely with the increase in speed. The current references for MTPV operation can also be obtained in the similar way as were obtained for MTPA in (2.49) and (2.50). Since the current limit was the only limiting parameter in the MTPA operation, therefore, the partial derivative of torque for i_d was gained. In the MTPV operation, the torque derivative will be taken with respect to d-component of the stator flux linkage, ψ_d which will result in the equation

$$(\psi_f + L_d i_d)^2 + (L_q/L_d - L_q)(\psi_f + L_d i_d) - (L_q i_q)^2 = 0 \tag{2.57}$$

(2.57) gives the current references to be implemented in the i_d-i_q plane within the MTPV operation. This equation is legitimate only when the short circuit current is less than the maximum current I_{max}. However, still most of the machines today operate as the finite speed drives. MTPV operation occurs keeping the voltage to its maximum limit U_{max}.

Suitable region of operation As discussed previously, the i_d zero or MTPA operation is limited by the current only, whereas the MTPV region cares merely for the voltage. In the case of the finite speed drives, where the current trajectory is not able to enter the MTPV region, the limiting point is the intersection point that presests just outside or at the current limit cirlce.

It is recommended to have the combination of either the i_d zero or MTPA, FW and MTPV during the whole range of operation of the drives to attain the best performance depending upon its specifications. In this work of thesis, i_d zero principle is followed in the constant flux region, whereas, FW starts as soon as the speed crosses its normal base point. The points present at the intersection of the current limit circle and the torque, depicted by Figure 2.10, represents the production of nominal torque at the rated voltage and current values. For further increasing the speed, the more negative i_d current is needed obtained as the trajectory follows the current limit circle towards the intersection of MTPV limit with the current limiting circle. Up to this point B in Figure 2.10, the finite speed drives and infinite speed drives behave exactly in the same manner.

After this point, in the case of infinite drives, since the trajectory has already approached the MTPV limit, the current trajectory move towards the short circuit current that lies within the circle formed by current limit. Hence, the speed of these drives can be considered to approach infinity in theory.

2.4 Field oriented control scheme

In order to obtain a good performance in all the four quadrants, the torque of an electric machine needs to be controlled efficiently. For this purpose, the control techniques have been defined and improved significantly with time to achieve best results. The basics for the control of the synchronous and asynchronous motors remain the same with some definite changes due to the differences in the working principles. The scalar control and vector control have been employed over the years to apply variable frequency drives.

The torque can be well defined and produced by the regulation of the stator and rotor magnetic fields. Moreover, the stator field can be divided into two components, the orthogonal component (to the rotor flux) for producing the torque and then the parallel component that only causes heating and is undesirable, therefore, it is required to minimize this component of the stator flux. As the d and q current components correlate with the parallel and the orthogonal components of the stator flux respectively, it is advantageous to reduce the d-component to ensure the minimization of the copper losses. Nevertheless, in the case of the FW operation, where machines have to be operated above the base speeds, the d-component i_d is manipulated to go negative direction for reducing the stator flux and hence increasing the speed. Consequently, whatever the control method is employed, the ultimate goal is to maximize the torque and minimize the losses of the machine.

2.4.1 Scalar control

An easy way to control the machines is the scalar control or voltage per Hertz control. In this method, the flux is regulated by the voltage, whereas, the torque is governed

by the frequency. As is depicted from the name, the magnitude of the variables take part only in the control process while the phase is not the focus. Scalar control involves the open loop control without using any feedback in which the voltage and frequency do vary but their ratio is kept constant. The frequency corresponds to the desired rotor speed. To attain the constant ratio, the voltage is then adjusted consistently.

The cost of the overall system becomes low in this kind of system since no position sensor is required and simultaneously simple to implement. But this technique has become obsolete (Kumar and Samyuktha, 2013) as it cannot be used in the high precision control applications though still found in the fans, pumps and air condition. Some of the other downsides of this mechanism are the instability after a certain frequency and low dynamic performance due to the absence of feedback.

2.4.2 Vector control

It was imperative that a better kind of control could be obtained by reckoning the magnitude and phase of the control variables as well. Vector control or FOC was introduced in 1970s that can be used for the control of the synchronous and asynchronous machines as well. It is named so since the three phase stator currents expressed as the two orthogonal components imagined as a vector are used to control the machine where one component controls the flux while the other is responsible for the torque. The realization that the AC and separately excited DC machines can have same controlling principle brought a new epoch of the industrial progress. The development in the PE equipment and microcontrollers time by time assisted the process.

The emergence of the vector control occurred from the fact that the AC motors could be controlled in a similar way as the separately excited DC motors that led to the industrial evolution significantly. The design of the DC machine is made so that the field and armature flux remain orthogonal to each other. The stator and the rotor are excited separately, that in turn, allows the control of the flux and torque independently. The rotor current controls the torque, whereas, the flux is directed by the field excitation. The commutator connected with the brushes acts in a way that aligns the windings to have optimal torque throughout the operation.

However, the case of AC is not that straight forward as DC machines. It is because of the fact that the direction of the rotor and the stator flux keep changing during the operation and these do not stay orthogonal always (Cheles, 2009). To obtain the analogous control, the rotor flux should be observed continuously and accordingly the stator current should be adapted; in a way that allows independent control of the flux and torque. This puts the basis for the vector control.

The brushless motors can be typically categorized into two types, brushless DC Motors and PMSM. They both possess the PM as a rotor and the stator windings, however, the stator windings are symmetrically wounded in PMSM in contrast to

BLDC which has evenly distributed windings in the stator, thus the shape of the back EMF differs for both.

Various kinds of controls are practiced for brushless motors that include the sinusoidal control, trapezoidal control and certainly field oriented control. Trapezoidal control is a simple and good option at high speeds but unfortunately, it originates the ripples in the torque, at low speeds (Controls, 2011). The sinusoidal control, on the other hand, circumvents the ripples and operates quite well at low speeds. Due to the limited bandwidth of PI controllers, however, there may be problems operating at elevated speeds.

Since the sinusoidal control deals with the currents whose magnitude and phase vary with time, the PI controllers at high speed get saturated and do not perform well. The remedy of this issue can be provided if the currents vector can be decomposed into such quantities that remain constant with reference to the rotor position. FOC offers with the solution utilizing the current transformation in to dq axis. In this way the frame of reference is fixed and the controllers work appropriately irrespective of the motor speed.

2.4.3 Main theory of FOC

The procedure of the field oriented control basically can be well understood taking into account the fact that the field has to be controlled in such a way to attain the desired outcomes. And the field, in turn, can be controlled via the current or the flux manipulation. The methodology of the FOC can be well explained by mentioning a few steps as follows:

- Measure the currents flowing through the motor
- The reference fluxes set according to the control region is compared to the actual flux and the difference is then measured
- The difference in the flux controller then applied to attain the reference voltage
- Regulate the voltage accordingly to apply to the motor terminals through PWM

The main motive of the FOC is to gain individualistic control for both the quantities of the torque and flux which enables the operation of a machine in the more efficient manner. For this purpose, the i_d and i_q are set to obtain the desired flux and torque, respectively. To understand the main operation of IPMSM under FOC, let's consider the three phase currents flowing through the windings of the machine. Since this is a time variant phenomenon, the three phase current is converted into two referenced frame i_d and i_q making the use of Clark and Park transformations as explained in section 2.

The block diagram showing the working of FOC is given in Figure 2.11. These two components of the current are dc in nature and do not change with time that make the control much easier. These two current components are compared with their references such as $i_{d,ref}$ and $i_{q,ref}$ obtained and the difference is made to be the lowest possible. These references tend the machine to achieve the desired torque

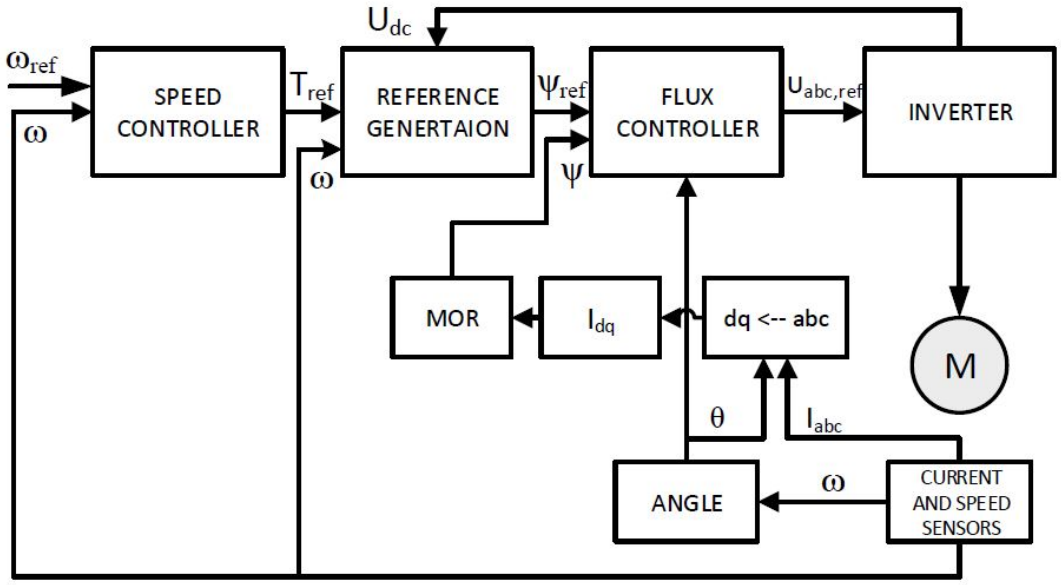

Figure 2.11: FOC scheme

commanded by the speed controller. These currents are converted through MOR to generate the flux references. The difference between the ψ_d, $\psi_{d,ref}$ and ψ_q, $\psi_{q,ref}$ are then fed into the flux controller which ensures the actual current and flux follow its references. The flux controller operates on the fluxes and produce the corresponding voltages as the output. Before giving the output, the voltages have to be converted back into three phase reference frame with the help of inverse Park transformation. The final voltages are then obtained by implementing the SVPWM technique that applies the duty ratios to produce the appropriate voltage output that is fed to operate the inverter. And then the speed controller operates in a way that actual speed follow the reference speed commanded to the system. The main components of the FOC scheme, the speed controller and the flux controller are explained below. The 'Reference generation' block in Figure 2.11 is explained in the section 3.

PI speed controller In most of the applications exercising the control of PMSM like the traction, the ultimate goal is the speed control. A desired speed can be obtained or adjusted accordingly. The parametric variation or any other kind of interruption does not really affect the operation of a well-designed system. A good system works in a way that it readily approaches the commanded speed without any kind of overshoots or abnormalities in the system.

According to the applied algorithm for FOC, the speed controller design can vary in its complexity. Generally, the reference torque is produced form the speed controller. The references generation is then obtained according to the directed torque. The torque remains constant until the machines operate under base speed, the torque

reduces its value according to the increase in speed moving forward from this region.

The actual speed of the machine is monitored throughout the operation through the incremental encoder and its difference with the speed reference is applied to the speed controller. It tries to eliminate this error and produce the output accordingly. Two loops are usually implemented in the whole system. The control loop for the current needs to be much faster at least ten times than the outer loop, i.e. the speed control loop to have fast response and avoid malfunction of the system as a whole.

Flux controller The flux or current controller used in the FOC scheme forms the base for the control. In this thesis, the discrete time current controller used in (Hinkkanen et al., 2015) has been transformed into the flux controller employing OIM. The current from the motor terminals are changed into the fluxes through OIM for the processing of the flux controller. The conversion process has been explained in the section 3.

Different methods are used to employ the flux controller. For the continous-time domain, the state controller can be made with the inclusion of the reference feedorward $\boldsymbol{K}_{tc}$, the state feedback $\boldsymbol{K}_{1c}$ and the integral $\boldsymbol{K}_{ic}$ as well. This control law in laplace domain can be represented as

$$\boldsymbol{u}_{s,ref} = \boldsymbol{K}_{tc}\boldsymbol{\psi}_{\boldsymbol{s,ref}} + \frac{\boldsymbol{K}_{ic}}{s}(\boldsymbol{\psi}_{\boldsymbol{s,ref}} - \boldsymbol{\psi}_{\boldsymbol{s}}) - \boldsymbol{K}_{1c}\boldsymbol{\psi}_{\boldsymbol{s}} \tag{2.58}$$

The above equation holds for the rotor coordinates and the gains are the real 2×2 matrices . The closed loop transfer function for this control law can be given as

$$\boldsymbol{H(s)} = \frac{\boldsymbol{\psi}_{\boldsymbol{s}}(s)}{\boldsymbol{\psi}_{\boldsymbol{s,ref}}(s)} = \frac{\alpha}{s+\alpha} \tag{2.59}$$

where α is the bandwidth of current controller. However, one step delay in the discrete-time domain modeled as $\frac{1}{z}$ is always there while the conversion from the continous-time domain. Hence, the closed loop transfer function moving form the s-plane to the z-plane is represented as

$$\boldsymbol{H(z)} = \frac{\boldsymbol{\psi}_{\boldsymbol{s}}(z)}{\boldsymbol{\psi}_{\boldsymbol{s,ref}}(z)} = \frac{1-p}{z(z-p)} \tag{2.60}$$

Here p represents the real pole of system equivalent to

$$p = e^{-\alpha T_s} \tag{2.61}$$

The flux linkages involved in the scheme are operated in the synchronous coordinate system. The state feedback method in which the output voltage is given as a delayed input to the controller operates the scheme in the discrete time domain. Looking at the Figure 2.12, the control law for this scheme can be given as

$$\boldsymbol{x}_i(k+1) = \boldsymbol{x}_i(k) + \boldsymbol{\psi}_{\boldsymbol{s,ref}}(k) - \boldsymbol{\psi}_{\boldsymbol{s}}(k) \tag{2.62}$$

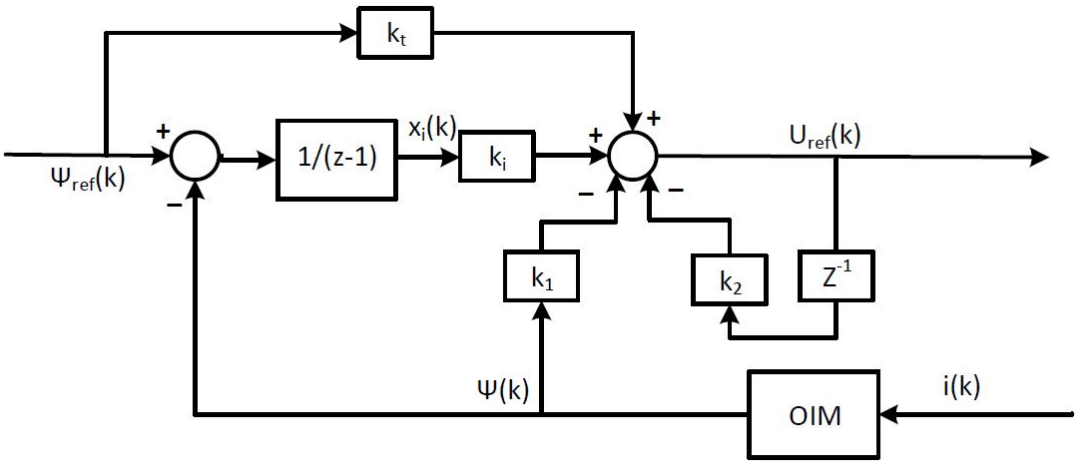

Figure 2.12: Flux controller structure

Similarly the value of u_{ref} that will enter towards the plant model is

$$\boldsymbol{u}_{s,ref}(k) = \boldsymbol{K}_t\boldsymbol{\psi}_{\boldsymbol{s,ref}}(k) + \boldsymbol{K}_i\boldsymbol{x}_i(k) - \boldsymbol{K}_1\boldsymbol{\psi}_{\boldsymbol{s}}(k) - \boldsymbol{K}_2\boldsymbol{u}_s(k) \tag{2.63}$$

Finally, the control law for IPMSM in the z-domain can be presented in the form (Kataja et al., 2016)

$$\boldsymbol{u}_{s,ref}(z) = \boldsymbol{K}_t\boldsymbol{\psi}_{\boldsymbol{s,ref}}(z) + \frac{\boldsymbol{K}_i}{z-1}[\boldsymbol{\psi}_{\boldsymbol{s,ref}}(z) - \boldsymbol{\psi}_{\boldsymbol{s}}(z)] - \boldsymbol{K}_1\boldsymbol{\psi}_{\boldsymbol{s}}(z) - \frac{\boldsymbol{K}_2}{z}\boldsymbol{u}_{s,ref}(z) \tag{2.64}$$

In this equation, $\boldsymbol{K}_t$, $\boldsymbol{K}_i$, $\boldsymbol{K}_1$, $\boldsymbol{K}_2$ are the gain matrices of dimension 2×2. The method for finding the original formulations of these matrices will be off the subject, however, it can be well understood from (Awan, 2015).

Nevertheless, the discretization of the plant model is necessary for the designing the control law. So, lets consider a matrix $\boldsymbol{X}_c$ from the motor parameters in the continous-time domain

$$\boldsymbol{X_c} = \begin{bmatrix} \frac{-R_s}{L_d} & \omega_m \\ -\omega_m & \frac{-R_s}{L_q} \end{bmatrix} \tag{2.65}$$

Here, $\boldsymbol{X}_c$ represents the system matrix for IPMSM in the continous-time domain. The discretization of this matrix can be obtained with the series expansion method. In the discrete-time domain, the system matrix represented by $\boldsymbol{X}$ can be given as

$$\boldsymbol{X} = \boldsymbol{I} + T_s\boldsymbol{X}_c\boldsymbol{E} \tag{2.66}$$

where $\boldsymbol{I}$ is the unity matrix written as

$$\boldsymbol{I} = \begin{bmatrix} 1 & 0 \\ 0 & 1 \end{bmatrix} \tag{2.67}$$

and $\boldsymbol{E}$ becomes the expansion terms

$$\boldsymbol{E} = \boldsymbol{I} + \frac{T_s \boldsymbol{X}_c}{2!} + \frac{T_s^2 \boldsymbol{X}_c^2}{3!} \tag{2.68}$$

Most of the times, only first two terms suffice to give the correct approximate results. The goals of the flux controller either in the continuous-time domain or the discrete-time domain are similar. One is to evade cross-coupling of dq axis itself which requires all entries of $\boldsymbol{H(z)}$ to be zero except the diagonal ones that should remain same to have similar closed-loop dynamics for dq axis (Hinkkanen et al., 2015).

Different kinds of approaches are applied for the implementation of the controller. Internal model control has been widely used technique in this regard. It acts very well for the IM or synchrnonous machines without saliency, however, it is not appropriate to use in the machines with magnetic saliency like IPMSM at high speeds becasue of exisiting substantial cross-coupling effect at high speeds. The design technique adopted while producing the coefficient matrices to generate gain matrices $\boldsymbol{K}_t$, $\boldsymbol{K}_i$, $\boldsymbol{K}_1$ and $\boldsymbol{K}_2$ is complex vector design. First coefficient, $\boldsymbol{X}_0$ is taken as $\boldsymbol{O}$ because of the inevitable time delay in the discrete-time domain where $\boldsymbol{O}$ is the zero matrix as

$$\boldsymbol{O} = \begin{bmatrix} 0 & 0 \\ 0 & 0 \end{bmatrix} \tag{2.69}$$

Equations for the other coefficients are given as

$$\boldsymbol{X}_1 = p^2 * \boldsymbol{X} \tag{2.70}$$

$$\boldsymbol{X}_2 = -p(\boldsymbol{I} + \boldsymbol{X}) \tag{2.71}$$

$$\boldsymbol{Y}_1 = (1-p)\boldsymbol{I} \tag{2.72}$$

Conclusion In this section, the modeling of IPMSM in the dq axis is acquired that provides the equations for the control purpose. Furthermore, it is manifested that the FW opeation needs to be designed and implemented to operate a prototype IPMSM at higher than the base speed. The limits to be considered for the FW opeartion are also highlighted. The field oriented control scheme is demonstrated and its algortithm is explained to implement the control structure in the simulations and experiments.

3 Methodology

Synopsis Once the necessary equations for the IPMSM are establised and the FOC scheme is presented, the FW algorithm can be deveploped utilizing MOR. In the beginning, the OIM being employed in this thesis is explained in subsection 3.1.1. Thereupon, the property of OIM to convert the current components in the corresponding flux linkage components is discussed in the subsection 3.3.1. Afterwards, the three approaches adopted in this thesis to implement the FW control are discussed in the subsection 3.2. All these three apporaches utilize OIM in their implementation. The subsections 3.2.1 and 3.2.2 disuss the methods using the L_d and L_q in the contrlol model. Subsequently, the approach that operates independent of any machine paramter is presented in subsection 3.2.3. The Simulink model and mechanism to implement OIM in the Simulink is explained in subsection 3.3. After that, the experimental setup used in the laboratory to validate the simulation results of all the three approaches is given in the subsection 3.4. Lastly, the connection scheme for the prototype IPMSM is described in subsection 3.5. Its effects on the experimental results are described as well.

3.1 Model order reduction

It is not impossible to have very accurate and precise field and parameter design solutions with the help of the already existing numerical methods like the finite element method (FEM) but the main challenge is that utilizing such methodologies demand exhaustive computational time and efforts (Farzamfar et al., 2017). In addition, the capacity needed in the PC to store the data is enormous enough to affect the other usual programs. One of the best well-known solutions to overcome this problem is called the MOR. For the decades, the engineering problems have been solved by the MOR. However, in the computational field for electrical machines, this method has emerged quite recently. Its main task is to reduce the size and complexity of electrical machines keeping intact the accuracy of the results. Different types of MOR techniques exist among which OIM has been discussed below.

3.1.1 System of equations for electrical machines

The electromagnetic problems occur due to the fact that the time varying electric fields give rise to the magnetic fields and vice versa holds true as well. These kind of problems can be described by the well-known differential form of the Maxwell equations as (Moyer and Schroeder, 1991):

$$\nabla \times \boldsymbol{E} = -\frac{\partial \boldsymbol{B}}{\partial t} \tag{3.1}$$

$$\nabla \times \boldsymbol{H} = \boldsymbol{J} \tag{3.2}$$

$$\nabla \cdot \boldsymbol{B} = 0 \tag{3.3}$$

The material properties for $\boldsymbol{B}$ and $\boldsymbol{J}$ in the above equations are expressed as

$$\boldsymbol{B} = \mu \boldsymbol{H} \tag{3.4}$$

$$\boldsymbol{J} = \sigma \boldsymbol{E} \tag{3.5}$$

In the above equations, $\boldsymbol{E}$ is the electric field strength, $\boldsymbol{B}$ is the magnetic flux density, $\boldsymbol{H}$ is the magnetic field strength, $\boldsymbol{J}$ is the electric current density, μ is the magnetic permeability and σ is the electrical conductivity.

Using the definition of the magnetic vector potential,

$$\boldsymbol{B} = \nabla \times \boldsymbol{A} \tag{3.6}$$

and substituting it back into Maxwell equations, one can obtain the solutions for magnetic problems as (Belahcen et al., 2016)

$$\nabla \times (\nu \nabla \times \boldsymbol{A}) = \boldsymbol{J} + \nabla \times \boldsymbol{M} \tag{3.7}$$

Here, $\boldsymbol{M}$ represents the magnetization of PM and ν is the reluctivity of a material, which is reciprocal of μ.

The FEM can be employed to solve (3.7) by its discretization. This solution can be obtained through Galerkin method which gives the equation (Farzamfar et al., 2017)

$$\boldsymbol{S}\boldsymbol{A} = \boldsymbol{F} \tag{3.8}$$

where $\boldsymbol{S}$ is the stiffness matrix of size $m \times m$, $\boldsymbol{A}$ is a vector of size m containing the nodal values of the magnetic vector potentials, and $\boldsymbol{F}$ is the source vector of size m. The stiffness matrix $\boldsymbol{S}$ depends on $\boldsymbol{A}$, which makes the system non-linear.

MOR techniques can be used to reduce the complexity, computational time and the order of (3.8), irrespective of its non-linearity. There are different kinds of methods implemented to perform this task that include the Lauguerre methods, Arnoldi and PRIMA method and proper orthogonal decomposition method (Antoulas and Sorensen, 2001). The method, however, used in this thesis to apply the MOR is orthogonal interpolation method (OIM) (Farzamfar et al., 2018).

Orthogonal interpolation method Like some other MOR techniques, the set of data to be involved in constructing the OIM based reduced model plays a vital role in the accuracy of the results. The methodology adopted in this technique to appropriately attain the reduced model is the method of snapshots. Snapshots refer to the output data of the system that can be obtained through the experiments or the numerical method, in frequency domain, time domain, or any other configuration. These solutions, nodal values of the magnetic vector potential in our case, are saved in a matrix called the snapshot matrix $\boldsymbol{A}_n$ of the size $m \times n$, where n refers to the number of solutions for the system under study. The snapshot matrix can be

decomposed into a smaller orthogonal basis by using singular value decomposition (SVD).

$$\boldsymbol{A}_n = \boldsymbol{U}\boldsymbol{\Sigma}\,\boldsymbol{V}^{\mathrm{T}} \tag{3.9}$$

SVD is a factorization process involving the three transformations, first of which is performed by the right singular vectors in $\boldsymbol{V}^{\mathrm{T}}$, followed by the extension along the coordinate axis by $\boldsymbol{\Sigma}$ and the final rotation with the left singular vectors in $\boldsymbol{U}$. $\boldsymbol{U}$ and $\boldsymbol{V}$ are the orthogonal matrices of the size $m \times m$ and $n \times n$, respectively. $\boldsymbol{\Sigma}$ is a rectangular diagonal matrix with size $m \times n$ and its diagonal entries represent the non-negative singular values σ_i that are arranged as $\sigma_1 > \sigma_2 > \ldots > 0$. The energy of the matrix is defined as the square sum of the singular values. The first r singular values *($r << m$)* capture most of the energy of the system. Therefore, the first r singular values and the corresponding left and right singular vectors are sufficient to reconstruct the snapshot matrix. In this way, we replace the matrices $\boldsymbol{U}$, $\boldsymbol{\Sigma}$, and $\boldsymbol{V}^{\mathrm{T}}$ by $\boldsymbol{U}_{\mathrm{r}}$, $\boldsymbol{\Sigma}_{\mathrm{r}}$ and $\boldsymbol{V}_{\mathrm{r}}^{\mathrm{T}}$ with the size of $m \times r$, $r \times r$, and $r \times n$, respectively.

The main difference between the OIM and some other projection-based methods like the proper orthogonal interpolation is that we mainly focus on the right singular vectors that refer to columns of $\boldsymbol{V}_{\mathrm{r}}$ instead of the left singular vectors, columns of $\boldsymbol{U}_{\mathrm{r}}$. The product of the two matrices $\boldsymbol{U}_{\mathrm{r}}$ and $\boldsymbol{\Sigma}_{\mathrm{r}}$ remains the same for any input variable within the domain of the snapshot matrix. However, the columns of $\boldsymbol{V}_{\mathrm{r}}^{\mathrm{T}}$ vary depending on the input set f from which the snapshot matrix is built, as expressed in (3.10). The input set can be the time, frequency, voltage, current, rotation angle, etc.

$$\boldsymbol{V}_{\mathrm{r}}^{\mathrm{T}} = \begin{bmatrix} v_{11} & v_{12} & \cdots & v_{1n} \\ v_{21} & v_{22} & \cdots & v_{2n} \\ \vdots & \vdots & \ddots & \vdots \\ v_{r1} & v_{n2} & \cdots & v_{rn} \\ \uparrow & \uparrow & & \uparrow \\ f_1 & f_2 & & f_n \end{bmatrix} \tag{3.10}$$

For any new input set within the snapshot range, each component of the new vector $\hat{\boldsymbol{V}}_{\mathrm{r}}^{\mathrm{T}} = [\hat{v_{11}} \cdots \hat{v_{r1}}]^{\mathrm{T}}$ is obtained by interpolating the corresponding right singular vector of $\boldsymbol{V}_{\mathrm{r}}$. The nodal values of the magnetic vector potential for this new input set can be given as

$$\hat{\boldsymbol{A}} = \boldsymbol{U}_{\mathrm{r}}\boldsymbol{\Sigma}_{\mathrm{r}}\hat{\boldsymbol{V}}_{\mathrm{r}}^{\mathrm{T}} \tag{3.11}$$

Thereafter, the magnetic flux linkage for each phase winding of the machine can be expressed as an integral of the magnetic vector potential over the whole problem

region Ω as

$$\psi_x = \frac{Nl}{C_T} \sum_{j=1}^{n} \int_{\Omega} \beta N_j \, d\Omega a_j \tag{3.12}$$

Here, x represents any one of the phases A, B or C. N and l represent the number of coil turns and the core length of the machine, respectively. C_T is the total cross-section area of the coils in series. β depends on the direction of the coil sides. β is 1 if the nodes are located within the positive coil sides, -1 if the nodes are located within the negative coil sides, and zero elsewhere. N_j and a_j are the FE shape function and nodal value of the vector potential of node j, respectively. The coefficients of a_j in (3.12) are constant for a given machine design, therefore, these coefficients are computed once and in advance the flux computation.

3.2 References generation for FW control

In the FW mode, the flux of the d-axis has to be reduced in IPMSM that will counter the field produced by PM and enable the machine to go much higher than its nominal value. In the base speed region, the ratio of the induced emf and the frequency, $\frac{U}{f}$ corresponding to the flux linkage is retained at the same level, the rated one. However, as the frequency reaches the base frequency, the voltage corresponds to its base value, the voltage limit of the inverter that demands the decrease in $\frac{U}{f}$ ratio to achieve higher speeds.

Furthermore, as described above, space vector PWM has been utilized to implement the control scheme. In the linear modulation region, it is possible to produce maximum of $U_{dc}/\sqrt{3}$ of the phase voltage in sinusoidal form. Hence, the flux has to be decreased once the inverter reaches its voltage limit. The reduction of the flux should be proportional to increment in the speed from the (2.55). It can be well undertood from the example that if the speed to approach double of the base speed, 2 $p.u.$, the flux linkage has to reduced two times, 0.5 $p.u.$ as well so that the voltage remains at its limit $(2 * 0.5 = 1 p.u.)$.

There has been three approaches used to generate the flux references for the FW region. One of those takes into account the current and volage limit equations and derives for the current references. In other approach, one component of the flux that is the d-component of the flux is obtained taking into account the volage equation. The current references are procured from flux-current relationships and current limit is applied. In both methods, the machine parameters are used for the reference calculation. The currents are then converted into the flux references employing OIM. The flux references thus generated are then passed to the flux controller described above that gives the voltage references accordingly given to the inverter. In the last approach described, a simulink feature works in combination with OIM and no machine parameter is involved in the calculation process.

3.2.1 Current approach

The procedure to calculate these references for IPMSM resemble to that of SPM as well with minor difference due to the presence of saliency in the formerly stated machines. As mentioned earlier, the FW control has to be designed keeping in view both the current and voltage limits. The current limit given in (2.45) can be written for i_q in terms of I_{max} as

$$i_q = \sqrt{I_{max}^2 - i_d^2} \tag{3.13}$$

Here, I_{max} corresponds to the current limit to be followed. Putting this value of i_q into the expanded form of (2.47) given as the voltage limit,

$$L_q{}^2 i_q{}^2 + L_d{}^2 i_d{}^2 + 2\psi_f L_d i_d + \psi_f^2 - \frac{U_{max}{}^2}{|w_m|^2} = 0 \tag{3.14}$$

one can get the final form of this equation to deduce the expression for i_d. The form hence obtained is

$$(L_d{}^2 - L_q{}^2) i_d{}^2 + 2\psi_f L_d i_d + (\psi_f^2 + L_q{}^2 I_{max}^2 - \frac{U_{max}{}^2}{|w_m|^2}) = 0 \tag{3.15}$$

In the above equations, the term U_{max} refers to the maximum available DC bus voltage which is equal to $U_{dc}/\sqrt{3}$. Lets assume that

$$a = L_d{}^2 - L_q{}^2 \tag{3.16}$$

$$b = 2\psi_f L_d \tag{3.17}$$

$$c = \psi_f^2 + L_q{}^2 I_{max}^2 - \frac{U_{max}{}^2}{|w_m|^2} \tag{3.18}$$

By using now simply the quadratic formula for the solution x,

$$x = -b + \frac{\sqrt{b^2 - 4ac}}{2a} \tag{3.19}$$

the solution for the d-component of the current can be obtained. It is obvious that the i_d must be negative in the FW region to oppose the magnetizig effect of the PM, therefore, negative root of the solution can be taken into consideration that gives the expression for the i_d as

$$i_d = \frac{-\psi_f L_d - \sqrt{\psi_f^2 L_d^2 - (L_d{}^2 - L_q{}^2)(\psi_f^2 + L_q{}^2 I_{max}^2 - \frac{U_{max}{}^2}{|w_m|^2})}}{L_d{}^2 - L_q{}^2} \tag{3.20}$$

(3.20) can be used to originate the current reference for d-axis of IPMSM. Similary, the reference currents to be induced for the q-axis can be obtained depending upon the refrence torque obtained from the speed controller and the negative value of i_d obtained from the above equation. When the current components are obtained,

the flux components can be produced through the OIM and passed to the flux controller. The negative value of the i_d should be taken care of that it should not risk the demagnetization of the PM. Moreover, the current control lost should be considered, that may cause the voltage high momentarily which should be endured by the DC link capacitors.

3.2.2 Flux-current approach

The other approach that used to operate in the FW region functions by getting the value of d-component of the stator flux and then getting the relevant current components. The voltage components thus obtained as a result of these current components approximate the maximum available voltage. The d-component of the stator flux can be obtained from the similar voltage limit equation

$$\psi_d = \sqrt{(\frac{U_{max}}{w_m})^2 - (L_q i_q)^2} \tag{3.21}$$

Here, the q-component of the current is obtained through the measured current. The *abc* current has been converted into *dq* current through the Clarke and Park transformation described above. The equation above gives the real value for i_d if the following condition satisfies

$$i_q \leqslant \frac{U_{max}}{w_m L_q} \tag{3.22}$$

It ensures that the flux generated by the q-component of the stator flux does not exceed the total stator flux that should not be the case in any situation. Once the value of ψ_d has been obtained, the currents for *dq* axis can be easily obtained from the current-flux relationship

$$i_d = \frac{\psi_d - \psi_f}{L_d} \tag{3.23}$$

The PM flux retains its value throughout the operation of a machine, however, the change in the temperature have some effect on the value of the PM flux. The value of the i_q can also be obtained through the torque equation as in previous approach. Once the values for i_d and i_q are obtained, the currents enter the data of the OIM and then the flux references are given to the flux controller. A term α is multiplied with the maximum flux relation in (2.47) as

$$\psi_{max} = \alpha \frac{U_{max}}{w_m} \tag{3.24}$$

Here, α denotes the voltage margin ensured to avoid the saturation of either the current or flux regulators in the control blocks. It represents a constant that is equal or almost equal to unity.

Furthermore, since the main role in the FW operation is played by the instigation of the negative i_d current, the maximum speed can be achieved by getting i_q as zero

and letting i_d to approach the maximum negative current. Hence, the equation for the maximum achievable speed can be known by putting these values in (2.46)

$$\omega_{max} = \frac{U_{max}}{\psi_f - L_d I_{max}} \tag{3.25}$$

The values for all the parameters in the above equation can be known and hence the maximum speed of the machine can be estimated. In case of the infinite speed drives, the theoretical speed can go upto the infinity, however, the practical limitations confine the speed upto a certain range.

3.2.3 Algebraic constraint approach

This approach is designed to acquire the d-component flux linkage ψ_d according to the FW conditions. It then generates the current component in the same axis that supports the required flux to establish the FW region. The conditions to be applied during the control procedures for a region depend on the constraints that need to be followed. For the flux weakening, in particular, both the voltage and current limits need to be considered as mentioned in section 2. It is also to be noticed that as the machine reaches its base speed, the voltage touches its ceiling point. Thereafter, it is not possible to further increase the voltage. Hence, applying (3.24), one can get ψ_s, the maximum stator flux linkage in the FW condition. This equation also clarifies that when the voltage reaches the limit of the inverter, the machine must enter the flux weakening area by reducing the flux.

From (2.34), the equation for ψ_d can be obtained as

$$\psi_d = \sqrt{\psi_s^2 - \psi_q^2} \tag{3.26}$$

From the above equation, ψ_s is known in the flux weakening region since U_{max} is restricted by limitation of the inverter.

The reference d-component of flux linkage $\psi_{d,ref}$, required for flux weakening region, is obtained from $\psi_{q,est}$ and (3.26) . To know the value of $\psi_{q,est}$ momentarily, OIM block is deployed in 'Reference generation' block of Figure 2.11 ; with the measured current components obtained through the I_{dq} block as the inputs.

Subsequently, reference currents are to be produced to proceed towards the current controller. For this purpose, a simuink feature known as 'algebraic constraint' is availed aptly in conjunction with the OIM block. In the representation of this block, *f(z)* and *z* hint at the input and output, respectively. The algebraic constraint block operates in a manner to curb the *f(z)* to zero and generates the *z* accordingly. To maintain this sequence of operation, it must have a feedback path that keeps the input at 0. Another key parameter for this block is the 'Initial guess', that will be set according to the required solution value that is 0 in our case, to upgrade the solver efficieny.

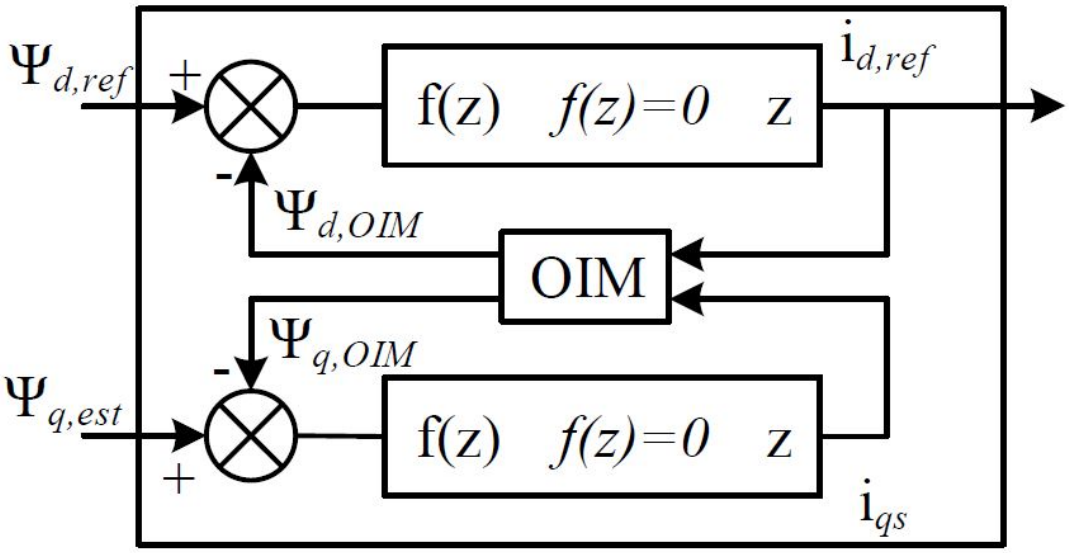

Figure 3.1: Computation for $i_{d,ref}$

Figure 3.1 shows the incorporation of this combination in the control algorithm for generating $i_{d,ref}$. Here, $\psi_{d,ref}$ behaves as $f(z)$, whereas $i_{d,ref}$ relates with z state. A secondary algebraic constraint block is also used to provide the input i_{qs} for the OIM block. The input of this block is the difference between the q-component flux $\psi_{q,est}$, previously obtained from measured i_q, and the q-component flux $\psi_{q,OIM}$ from OIM block. The resulting i_{qs} obtained through this block acts as the other input of the OIM, in addition to the $i_{d,ref}$. One can simply compute the q-component of the reference current by knowing the values of the $\psi_{d,ref}$, $\psi_{q,est}$, $i_{d,ref}$, and reference torque from:

$$T = \frac{3p}{2}(\psi_d i_q - \psi_q i_d) \tag{3.27}$$

However, the value of $i_{q,ref}$ to be passed to the current controller depends on the current limit as well. If the resultant magnitude of $i_{d,ref}$ and $i_{q,ref}$ exceed the current limit, the $i_{q,ref}$ is limited by (2.45).

3.3 Simulink model

The simulink model shown in the Figure 3.2 is executing in such a way that the plant model, model of the machine named as 'PMSM and Mechanics', operates in the continous-time domain. The control model, i.e. the subsytem 'Vector Control' functions in the discrete-time domain. The black and red wires in the simulink block represent these domains respectively. The zero order hold 'ZOH' blocks are employed

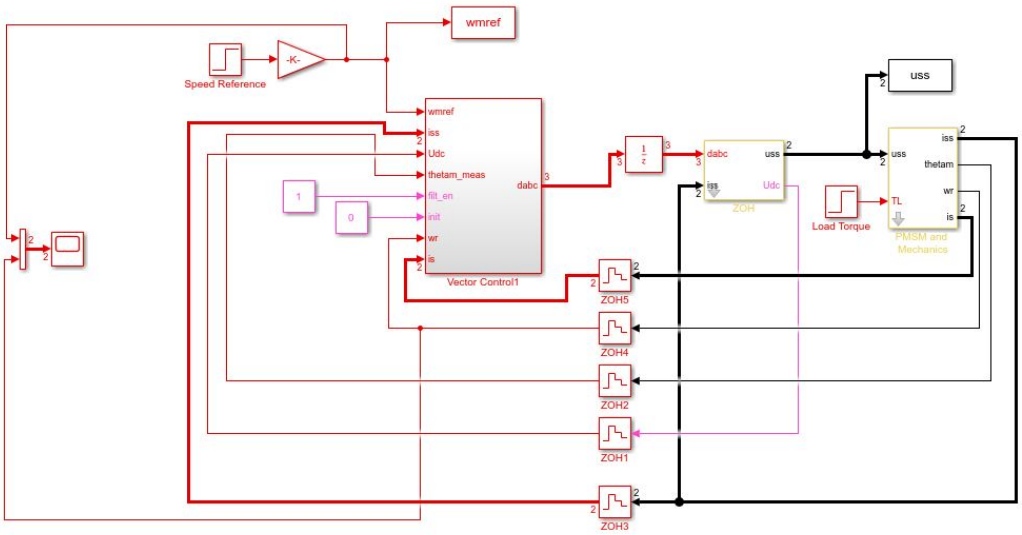

Figure 3.2: Simulink Model

to move between the two domains. The rating and paramters of the machine are given in Table 3.1 and Table 3.2 repsectively.

3.3.1 Implementation of reduced model in simulink

As mentioned in the section 3.1.1, the first step in building the reduced model via the OIM is to build the snapshot matrix. The FE model is solved for the 40 different operating points of the current components. These operating points are all the possible combinations of the 5 values of the i_d, equally distributed in [-I_N, 0], and the 8 values of i_q, equally distributed in [-I_N, I_N]. The ranges of i_d and i_q are chosen according to the values that of these components can take while the machine is working in the FW region.

The FE results are stored in the snapshot matrix and then decomposed via SVD. The first five singular values capture more than 95 % of the whole energy of the system. The corresponding right singular vectors [v_1, ..., v_5] of these five singular values are selected in constructing the reduced model, by introducing each of the right singular vectors as a function of the two variables i_d and i_q. Figure 3.3 is an example of the functions for the fourth singular vector for different values of i_d and i_q. Thereafter, for any values of the current components, the nodal values of the magnetic vector potential and the flux components are computed using (3.11) and (3.12).

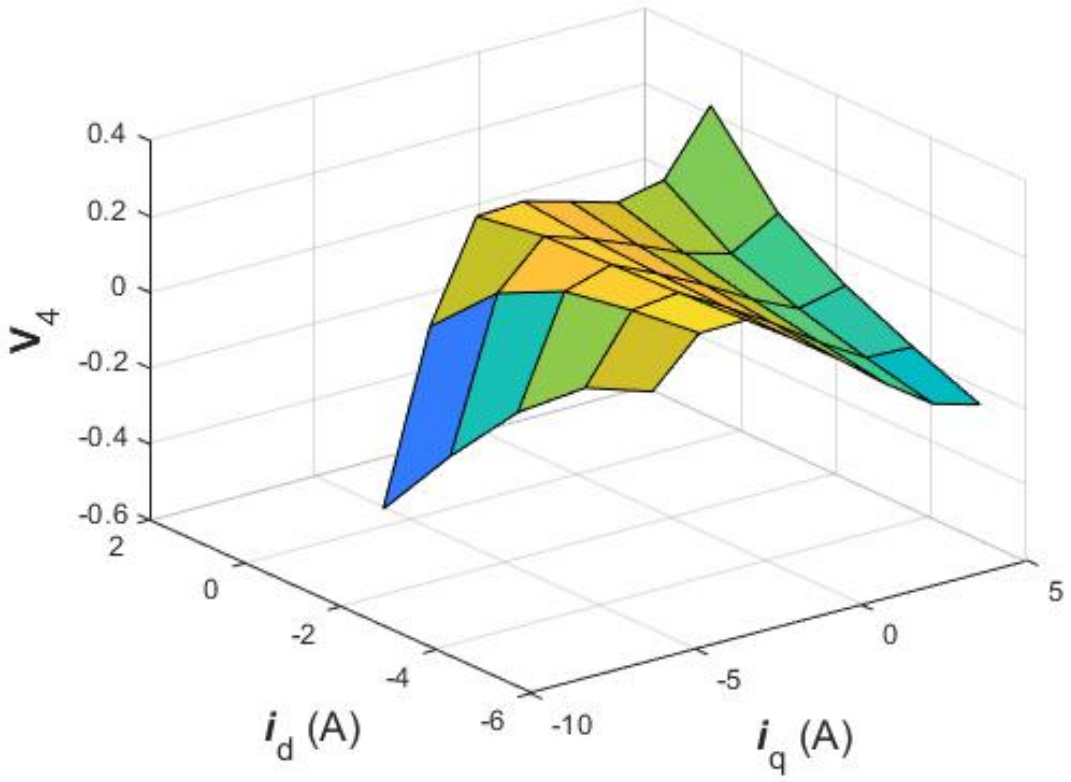

Figure 3.3: The fourth right singular vector presented as function of current components i_d and i_q.

3.4 Experimental setup

The block diagram is manifested in Figure 3.4 for the setup used in the experiments. The experiments were performed in the laboratory after the simulation have been done to validate the results thorougly. The results for these experiments have been shown in the figures in section 4.

The similar experimental setup being shown in Figure 3.4 was used in (Piippo et al., 2008). The stator of the IPMSM is taken from an induction machine and PM are buried inside the rotor surface. The simulink model was interfaced with the dSPACE DS1103 processor board fed by VLT5004 frequency converter. The simulink model after compilation for real-time execution was uploaded in the dSPACE processing board. A software for the dSPACE, 'Control desk' was used for the real-time processing of the data. For the measurement of the rotor position and speed, an incremental encoder was used with the specification of 600 pulses/revolution. The DC link voltage and phase currents being measured are fed to the dSPACE board that accordingly generates the switching sequence for the IGBTs of the inverter.

3.4.1 Real-time interface

The simulink model in the lab is a bit different from the one shown in Figure 3.2. It contains two main blocks that act as a real-time interface (RTI) model to be linked with the dSPACE. One of these blocks is the 'Measure and Control' block that measures the actual measurements occuring in the real-time. A protection block is also the part of this 'Measure and Control' block that ensures the protection of over all system and contains various protections like the overcurrent, overvoltage and short circuit protection. The other main block is the 'Vector Control' block that includes the main alogirthm to be implemented for the control purpose.

3.4.2 dSPACE

The model of the simulink contains some blocks that help in interfacing with the DS1103 processing board. Two processors are run by DS1103 board at the same time. The control algortihms are embedded in the master processor, PowerPC 604e RISC processor, whereas, the control signals for the inverter switching are generated by a Texas Instruments TMS320F240 that acts as a slave processor. To have the proper interface between DS1103 board and the other hardware components of the system, DS1103 board is linked with the signal conditioning unit (SCU). The fixed dead time for the inverter interface with other components is 1.5 μs. The DC link voltage measurement and the position of the rotor shaft through encoder is obtained

Parameter	Value
Power	2,2 kW
Rated Current (rms)	2,48 A
Rated Voltage	640 V
Rated Frequency	75 Hz
Number of pole pairs	3
Winding Connection	Star

Table 3.1: Prototype machine rated value

Parameter	Value
d-axis inductance	0.1085 H
q-axis inductance	0.161 H
Permanent magnet flux	0.96 Vs
Stator resistance	10.5877 Ω
Total moment of inertia	0.045 kgm^2

Table 3.2: Prototype machine parameters

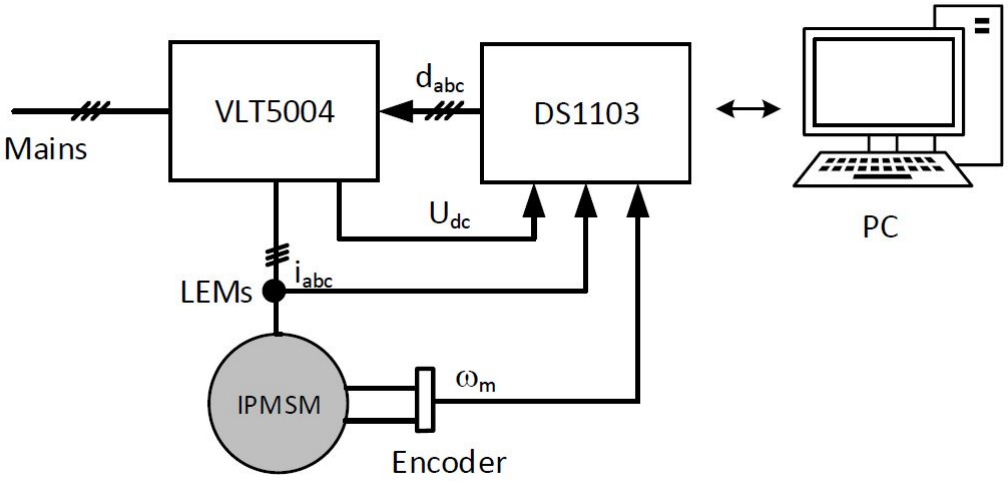

Figure 3.4: Experimental Setup

through SCU.

The phase currents of the motor are needed to be measured accurately for the good performance of IPMSM. For this purpose, the two LEM module current sensors measuring the phase currents of A and B phases are utilized. These currents are converted into voltage signals that are fed to the A/D converters of DS1103 processing board.

3.4.3 Position sensor

For the transformations from one reference frame to the other, that makes the modeling and control less complicated, the position of the rotor needs to be known. If there is some kind of the sensor mounted on the rotor shaft informing about its position during the real-time control, the control is referred to as the sensored control. There are different kinds of position sensors that include linear variable differential transformer, potentiometer, resolvers and encoders.

In optical encoders, the position of the rotor is measured with the light. There are three components that constitute the working of the encoder. A disc installed on the rotor shaft have adjacent opaque and transparent sectors that rotate with the rotation of the rotor. On one side is the light source and the other side of the disc there presents a light receiver (Kumar and Samyuktha, 2013). The light sent from the light source is received by the receiver when it passes through the transparent zones present in the disc that generate digital pulses, in turn. The counting of these pulses informs about the rotor position. Depending on the working principle, the optical encoders can be categorized as incremental encoder and the absolute encoder.

We will discuss incremental encoder as being used in our system. These are the most common type of encoders used in the control of electrical machines due to the precision and simplicity. It operates on the principle that two output channels called A and B give the information regarding the position. The code tracks on both of the outputs are shifted from each other with the angle of 90 *deg* thus giving both the information of the direction and position of the rotor. If one channel leads the other, it indicates one direction e.g. counter-clockwise and vice versa. The number of pulses give the data for the position, whereas, the phase shift indicates the direction of the rotor.

3.4.4 Pulse width modulation

PWM involves the control or modulation of the pulses width to attain the desired output waveform. The train of the pulses is applied to the gates of the switching power converters e.g. IGBTs in order to adjust the frequency and voltage of the signal from the source. Hence through alteration of the duty cycle, the output voltage or current can be changed appropriately. In addition, the motive is also to diminish harmonic distortion and the switching losses.

There are three types of PWM that include Sinusoidal PWM, Space Vector PWM and the Hysteresis PWM. We will be discussing SVPWM technique being used in the control.

Implementation of SVPWM The objective of applying this approach is to acquire the desired phase voltage waveforms. Furthermore, it also reduces the harmonic contents significantly which are responsible for the copper losses (Sarkar and Bhunia, 2017).

Figure 3.6 shows the inverter connected with the DC source and linked with the motor. Each phase can be considered as a switch forming S_1, S_2 and S_3 switches for the three phases. SVPWM entirely depends on the state of the above three switches. The three output terminals of the inverter are connected with either the positive or negative bus forming 8 combinations in total. Two of these eight combinations can be regarded as the null vectors, the state at which all the above three switches either remain ON or OFF. If for the upper switches, the ON state is represented as 1 and OFF state is represented as 0, the null vectors can be shown as U(0,0,0) and U(1,1,1). (3.28) shows the space vectors equation that represnt the output voltage for inverter applying this technique

$$\boldsymbol{u}_s = \frac{2}{3} U_{dc}(d_a + d_b\alpha + d_c\alpha^2) \tag{3.28}$$

Here, U_{dc} represents the DC bus voltage of inverter and the α shows the angle $1\angle 120$ deg. The magnitude for the other six vectors except the null vectors can be represented by $2/3\ U_{dc}$. These eight vectors can be shown in the figure as Figure 2.11.

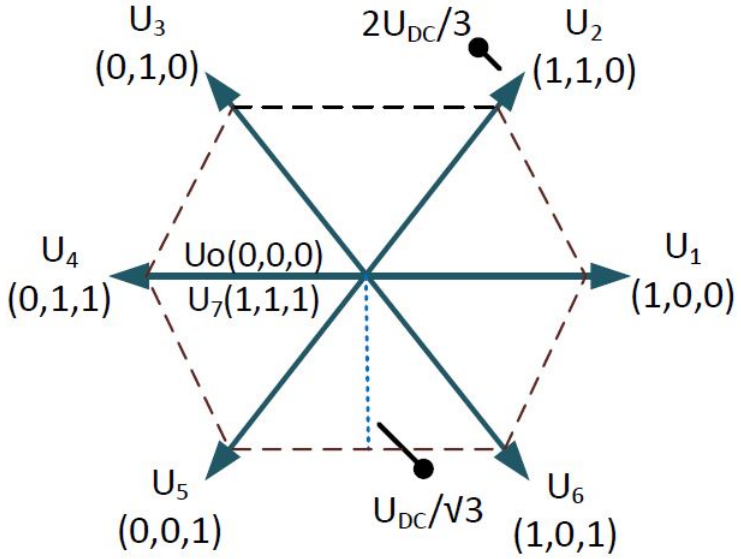

Figure 3.5: SVPWM vectors

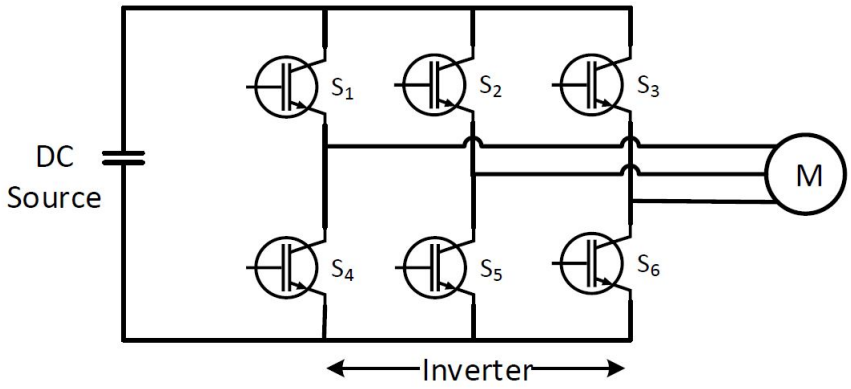

Figure 3.6: Inverter switching

Briefly, the SVPWM can be regarded as a technique which takes desired voltage vector components as the input and it outputs the time required to implement the relevant adjacent sector vectors.

SVPWM takes some dominance over sinusoidal pulse width modulation (SPWM) due to the following reasons:

- Harmonic distortion for the currents is minimum
- Voltage source is more effectively utilized
- In SVPWM length of each vector is $2/3\ U_{dc}$ while it is $1/2\ U_{dc}$ in case of SPWM
- SVPWM is $2/\sqrt{3}$ times more maximum output voltages in comparison with SPWM

3.5 Connection scheme

The prototype IPMSM mahcine has been designed particularly for the lab tests. Various experiments have been performed on this machine before the designing of its FW control. Usually the machines are available in two types of main windings, delta and star. Each has its merits and demerits. With the delta winding, the voltage can be exploited $\sqrt{3}$ times more than the star winding and the high power machines for the industrial applications are generally operated in the delta mode. However, one definite disadvantage while operating in the delta sequence is the loss caused by the circulating currents. In the three phase windings, the triple order harmoncis for EMF tend to produce these currents that circulate in the delta winding causing the copper losses to increase. Special designs have been made to avoid the third, fifth and seventh order harmonics as studied in (Ni et al., 2014). However to avoid these kind of additional losses, it was decided to operate the machine in star winding.

Another reason for the opreation in star winding is that a DC machine of 12 KW is attached to the prototype machine of 2.2 kW. The nominal rpm for this heavy DC machine attached is 2000 rpm, whereas, the nominal rpm for IPMSM in delta mode is 1500 rpm. If the machine is tried to operate at the high speeds of above 2000 rpm, there generates a weird noise due to the mechanical coupling of the two that may cause damage to the machines. And hence, the FW region confines to a very low range. Due to these two reasons, it was ultimately decided to operate the machine in the star mode so that the losses can be avoided and machine characterisitcs can be observed in a good field weakening range.

It is to be noticed that to operate the machine in the star mode, the voltage source needs to be available that should provide $\sqrt{3}$ times the phase voltage while operation in the delta mode. Since, in star connection

$$U_{line} = \sqrt{3}U_{phase} \tag{3.29}$$

So, it means that while operating with 370 V in the delta mode, the same kind of operation can be maintained utilizing the voltage source with the capacity of $\sqrt{3} * 370$. Unfortunately, no such source was available in the laborartory. Hence, the machine has to be operated in the star mode with 370 V. It reduced the base speed of the mahine approximately by a factor of $\sqrt{3}$.

Conclusion This section details about the methodologies used in this thesis. The OIM technique employed in the FW algorithms is explained and the procedure adopted to incorporate the OIM in the control algortihms is also defined. The three techniques to be applied for the FW operation of IPMSM have been developed. And the mechanism to be followed to implement these techniques in the laboratory through experimental apparatus is also signified.

4 Results and discussion

Synopsis Once the mehodologies to be utilized for operating the machine in the FW region are established, the simulations and experiments are needed to be performed to validate the feasibility of these approaches. The results for the FW operation of the prototype IPMSM are shown in this section. The findings of these results are discussed as well.

4.1 Results

The IPMSM machine has been tested through simulations and experiments for the control design. The simulations are performed in the MATLAB/Simulink. The tests are performed for the constant torque and in the FW region as well.

Below the base speed, the i_d has been kept zero and the FW control has been utilized to go high above the base speed. The base speed for the simulations and experiments has been kept the same i.e 800 rpm. The reason for that as explained in the previous section is the unavailability of the voltage source in the laboratory to provide the required voltage for the operation of the machine in the star mode. Thus approximately $1/\sqrt{3}$ times rated speed of the machine, around 800 rpm becomes the base speed of the machine. The reference speed is set according to the maximum speed that each approach can reach.

The simulations and experiments are performed for all the three techniques described in the subsection 3.2. The results are presented in such a way that the simulation and experimental results are shown for one approach and then the results for the other approaches are shown in a similar way. It is to be recalled that the first two approaches, current approach and flux-current approach use the inductance values, the stator resistance and the PM flux (L_d, L_q, R_s, ψ_f) in the calculations whereas the last one, 'algebraic constraint approach' works independent of any machine parameter. The results hence obtained confirm the feasibility of these approaches. Furthermore, as discussed later, the algebebraic constraint approach gives superior results than the other two approaches. The sequence of the results according to the approaches is as followed:

Approach I: Current approach

Approach II: Flux-current approach

Approach III: Algebraic constraint approach

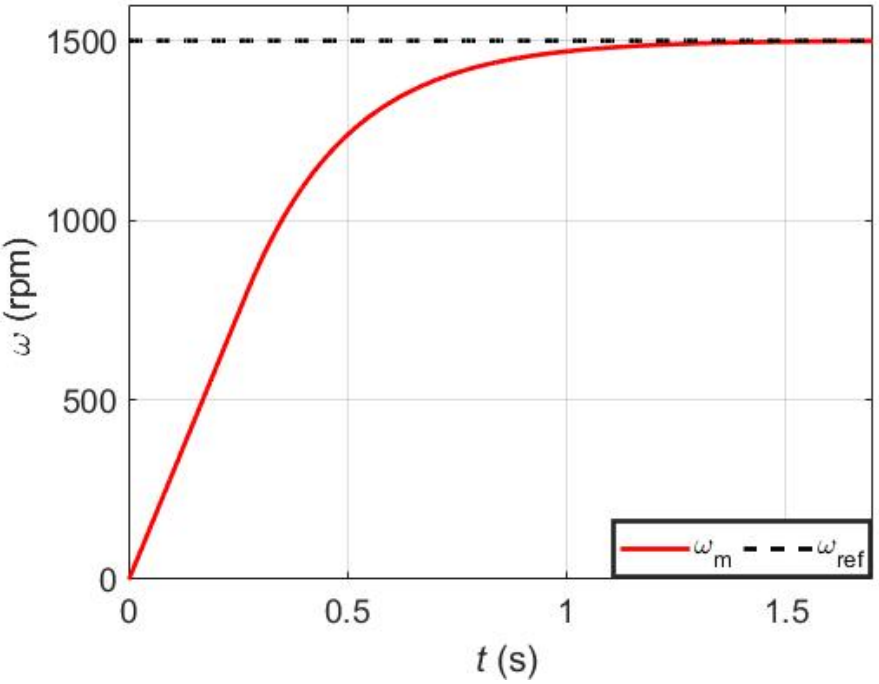

Figure 4.1: **Approach I** – *Simulated result*: Speed reference, i.e. ω_{ref} and speed measured, i.e. ω_m upto 1500 rpm

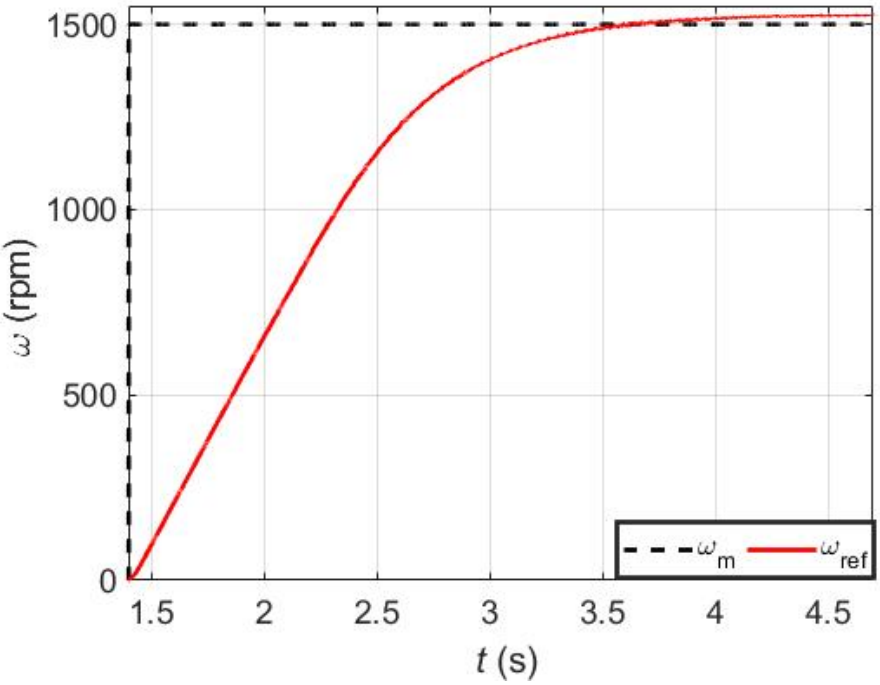

Figure 4.2: **Approach I** – *Experimental result*: Speed reference, i.e. ω_{ref} and speed measured, i.e. ω_m upto 1500 rpm

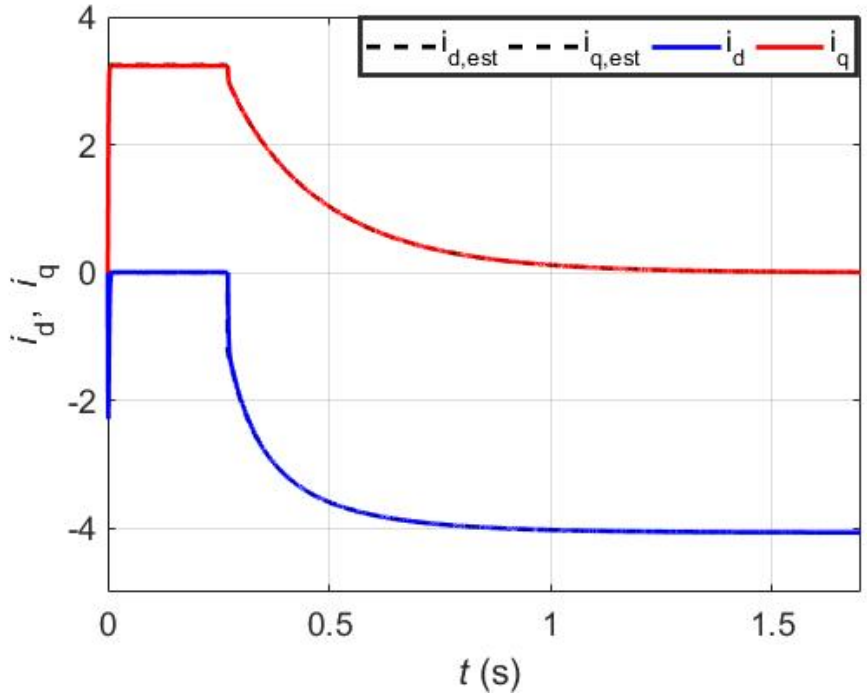

Figure 4.3: **Approach I** – *Simulated result*: Current components generated by the controller, i.e. $i_{d,cref}$, $i_{q,cref}$ and the actual ones, i.e. i_d and i_q upto 1500 rpm

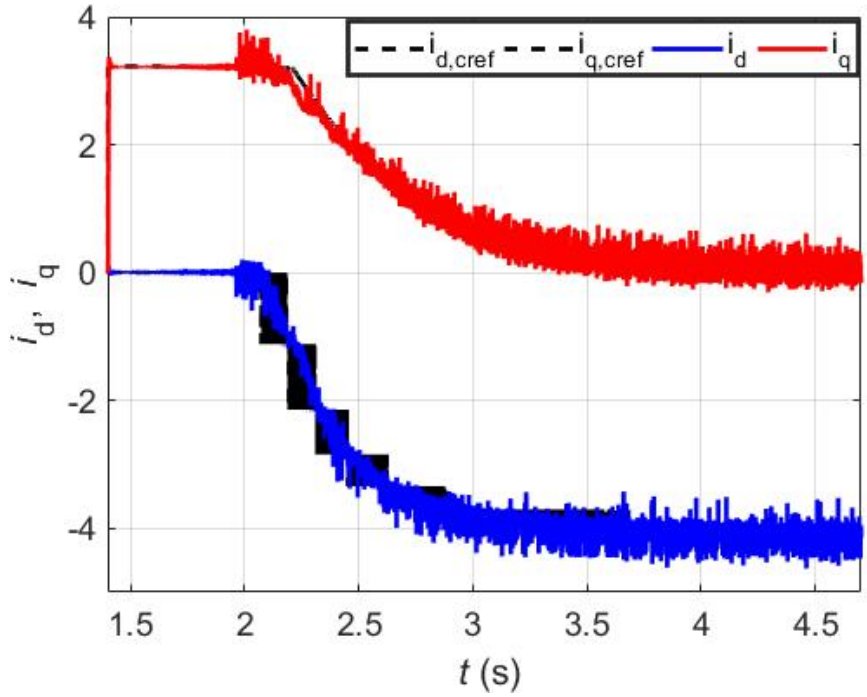

Figure 4.4: **Approach I** – *Experimental result*: Current components generated by the controller, i.e. $i_{d,cref}$, $i_{q,cref}$ and the actual ones, i.e. i_d and i_q upto 1500 rpm

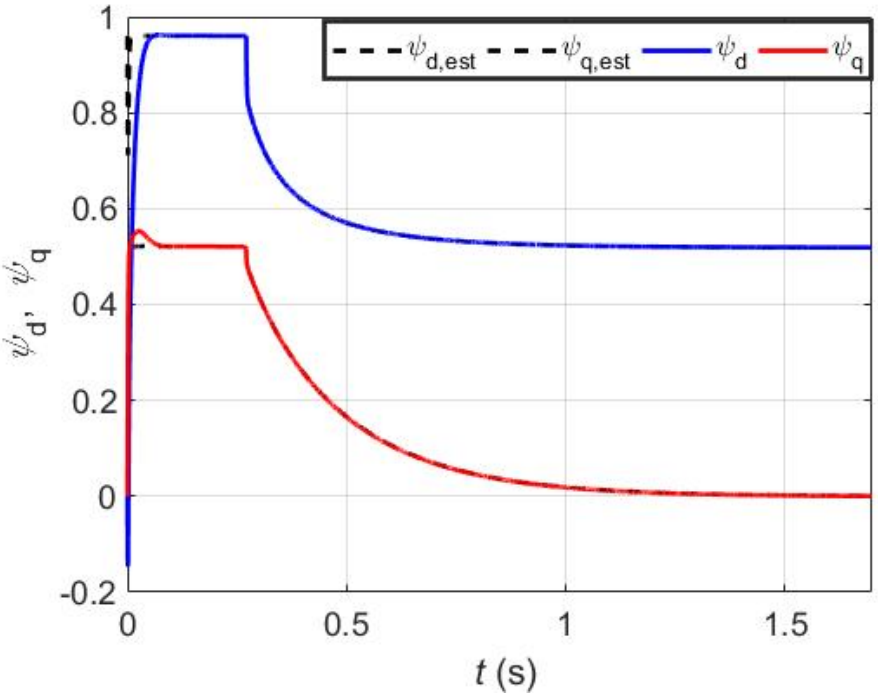

Figure 4.5: **Approach I** – *Simulated result*: Flux components generated, i.e. $\psi_{d,cref}$, $\psi_{q,cref}$ and estimated, i.e. $\psi_{d,est}$, $\psi_{q,est}$ by the controllers upto 1500 rpm

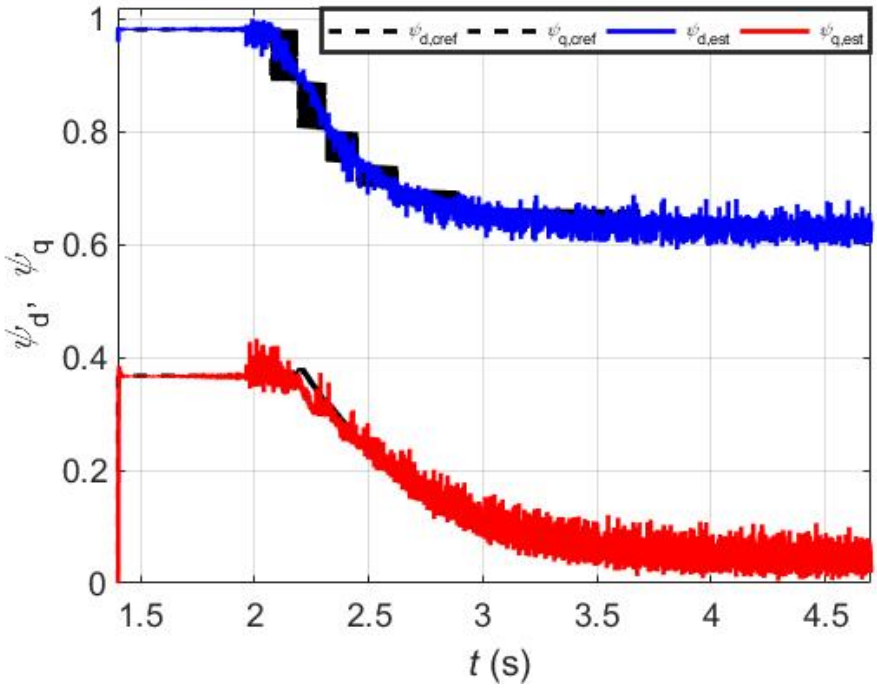

Figure 4.6: **Approach I** – *Experimental result*: Flux components generated, i.e. $\psi_{d,cref}$, $\psi_{q,cref}$ and estimated, i.e. $\psi_{d,est}$, $\psi_{q,est}$ by the controllers upto 1500 rpm

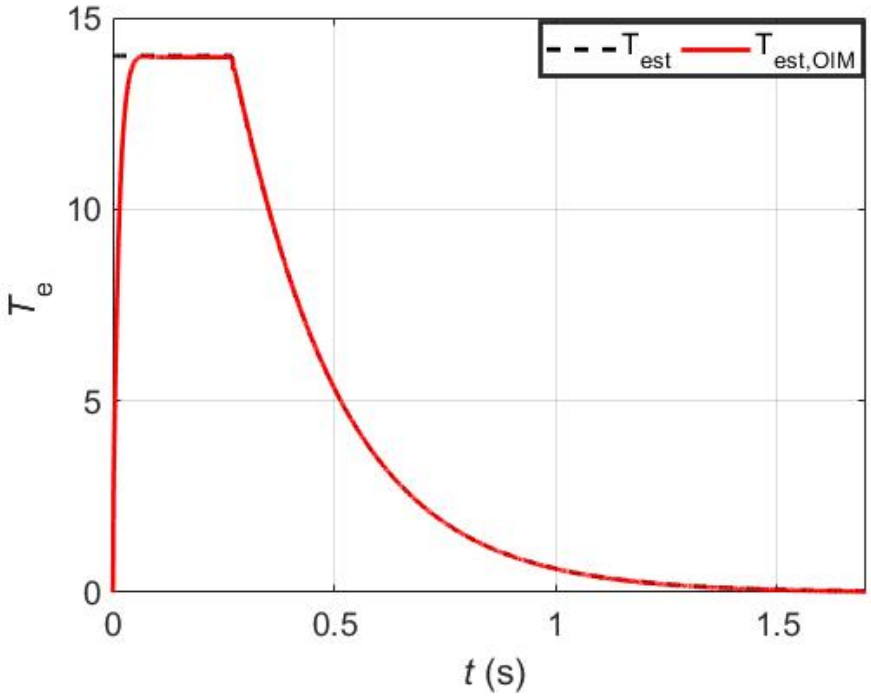

Figure 4.7: **Approach I** – *Simulated result*: Torque reference generated, i.e. $T_{c,ref}$ and estimated, i.e. T_{est} by the conrtollers upto 1500 rpm

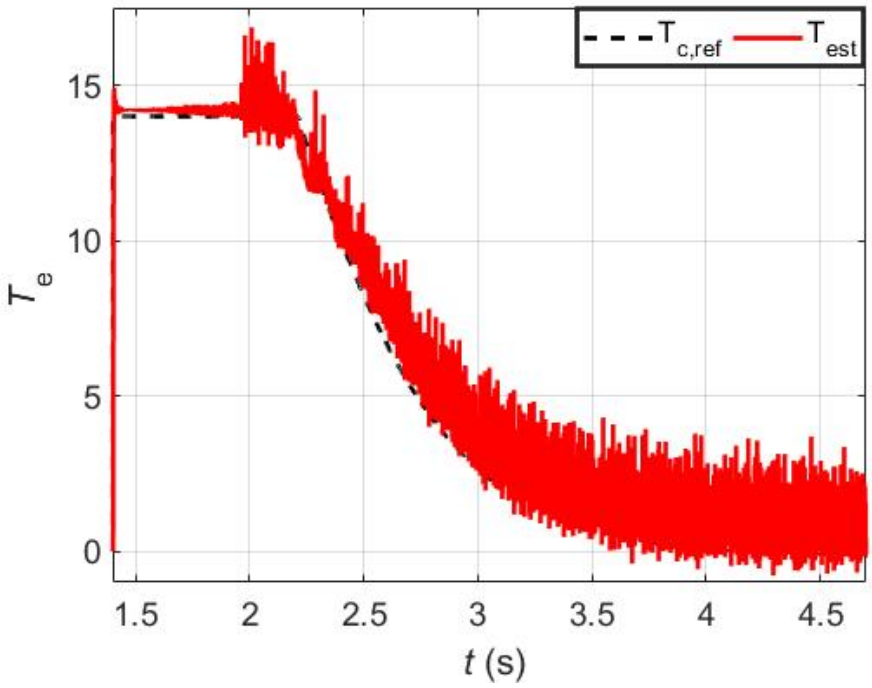

Figure 4.8: **Approach I** – *Experimental result*: Torque reference generated, i.e. $T_{c,ref}$ and estimated, i.e. T_{est} by the conrtollers upto 1500 rpm

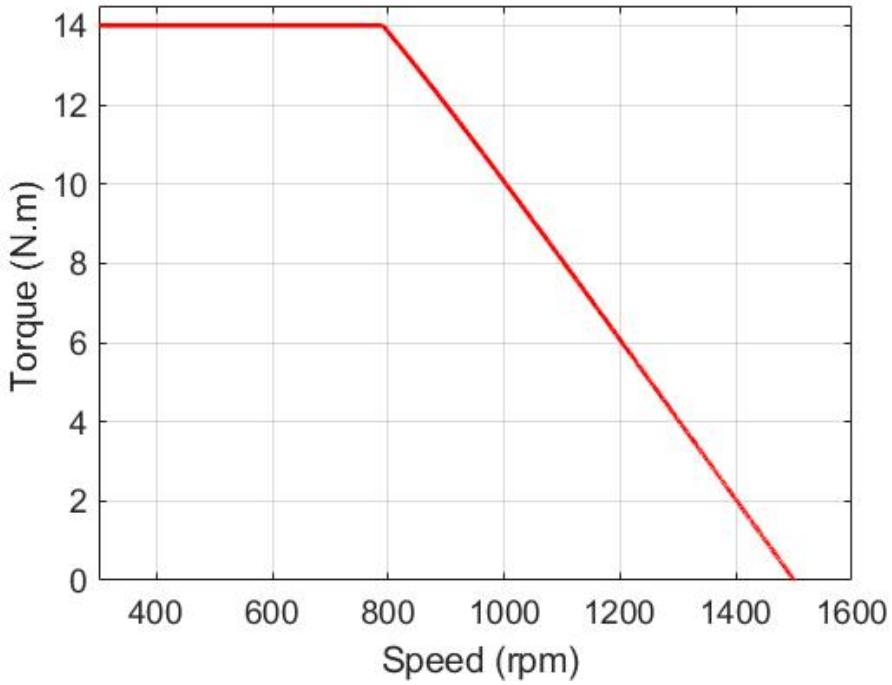

Figure 4.9: **Approach I** – *Simulated result*: Torque-speed curve upto 1500 rpm

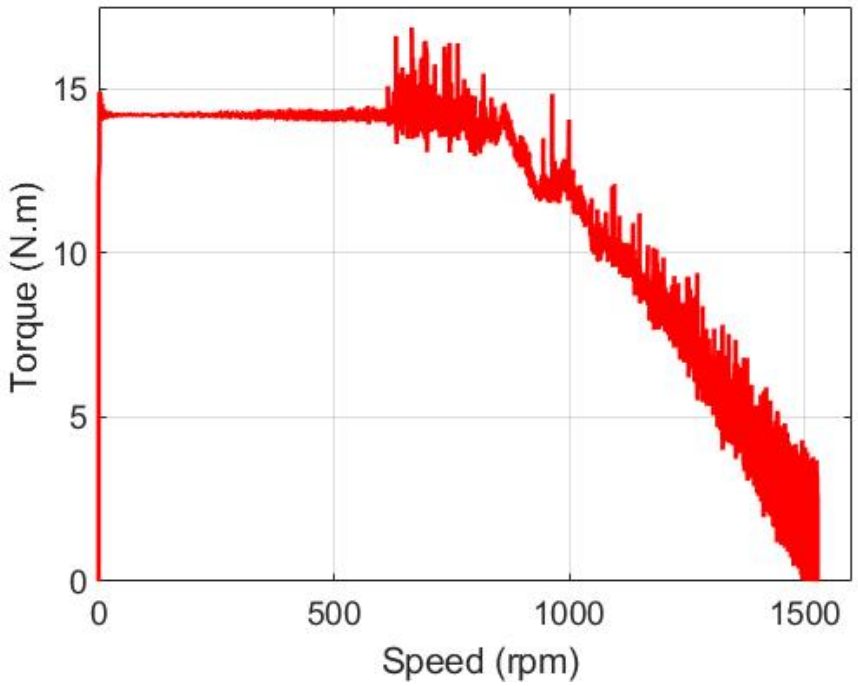

Figure 4.10: **Approach I** – *Experimental result*: Torque-speed curve upto 1500 rpm

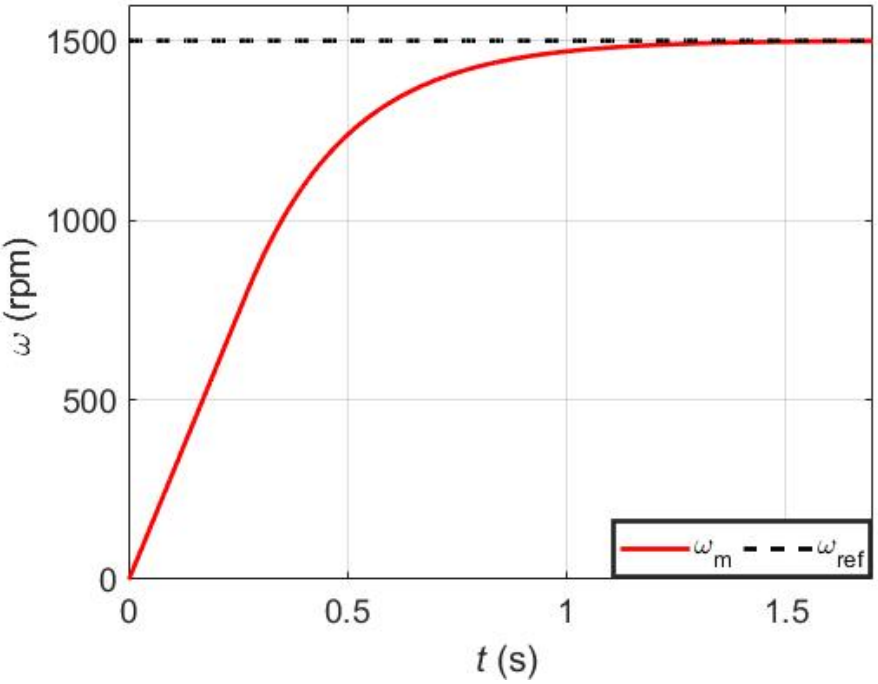

Figure 4.11: **Approach II** – *Simulated result*: Speed reference, i.e. ω_{ref} and speed measured, i.e. ω_m upto 1500 rpm

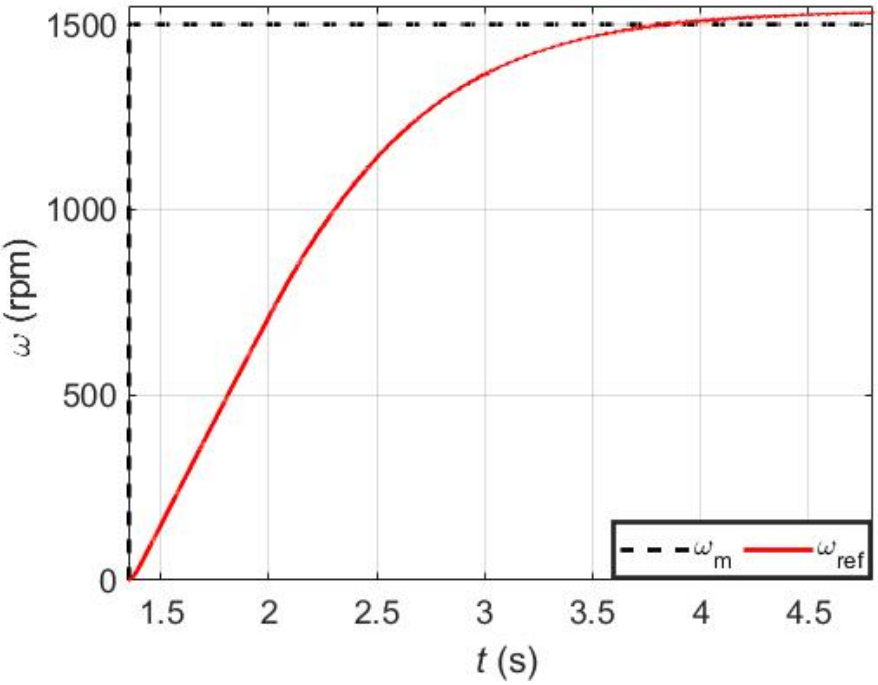

Figure 4.12: **Approach II** – *Experimental result*: Speed reference, i.e. ω_{ref} and speed measured, i.e. ω_m upto 1500 rpm

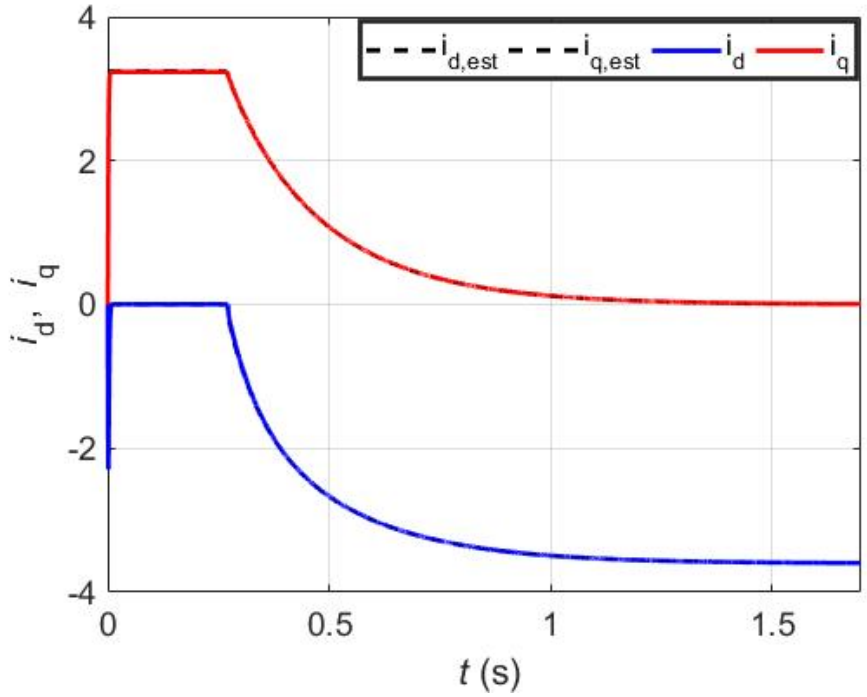

Figure 4.13: **Approach II** – *Simulated result*: Current components generated by the controller, i.e. $i_{d,cref}$, $i_{q,cref}$ and the actual ones, i.e. i_d and i_q upto 1500 rpm

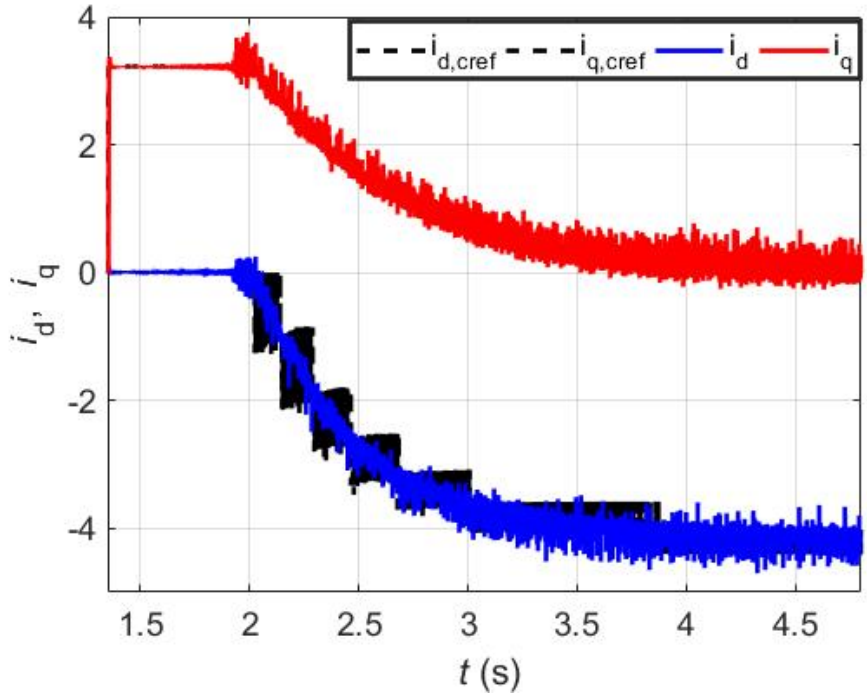

Figure 4.14: **Approach II** – *Experimental result*: Current components generated by the controller, i.e. $i_{d,cref}$, $i_{q,cref}$ and the actual ones, i.e. i_d and i_q upto 1500 rpm

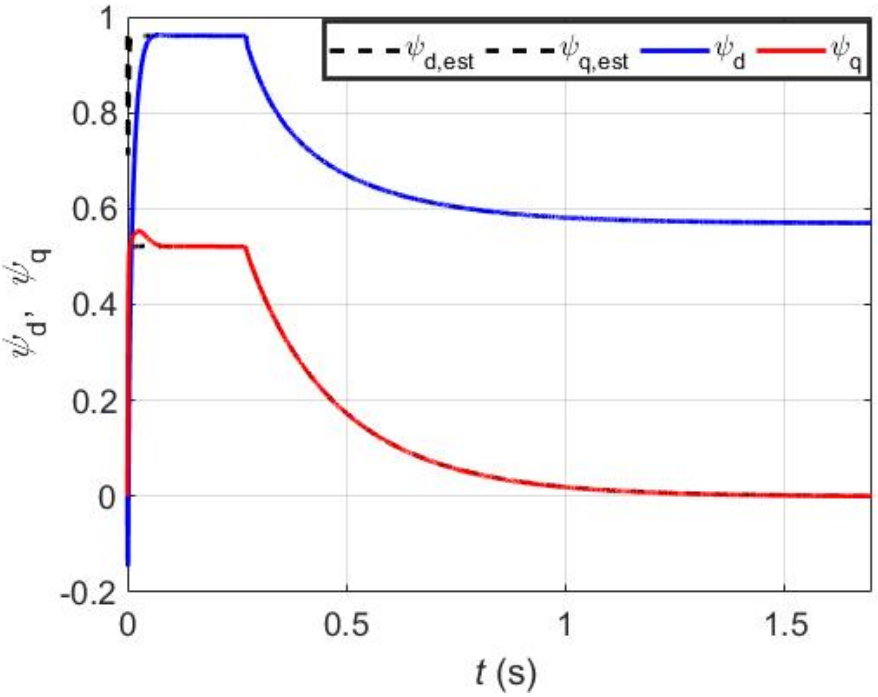

Figure 4.15: **Approach II** – *Simulated result*: Flux components generated, i.e. $\psi_{d,cref}$, $\psi_{q,cref}$ and estimated, i.e. $\psi_{d,est}$, $\psi_{q,est}$ by the controllers upto 1500 rpm

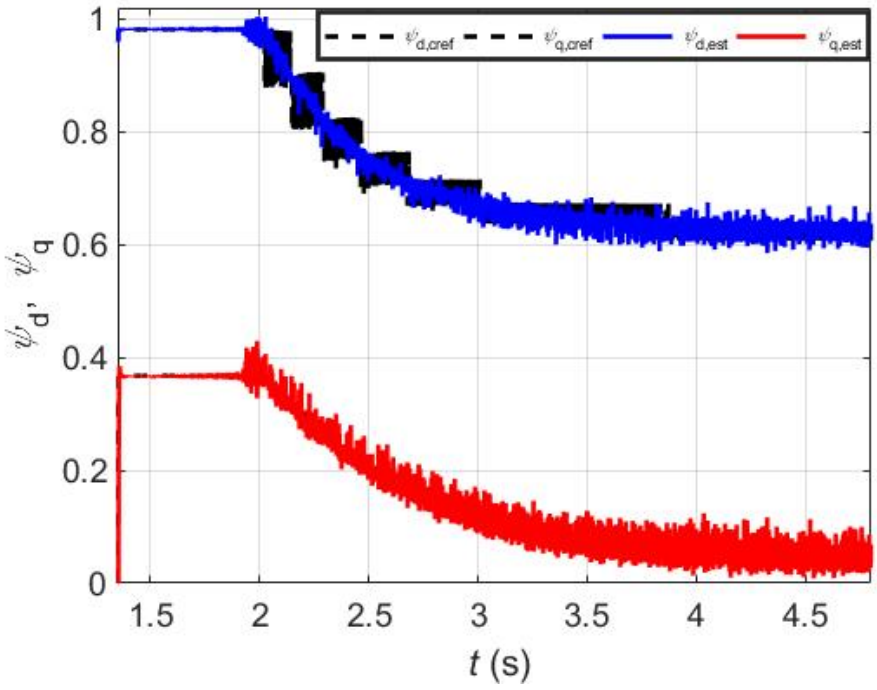

Figure 4.16: **Approach II** – *Experimental result*: Flux components, generated i.e. $\psi_{d,cref}$, $\psi_{q,cref}$ and estimated, i.e. $\psi_{d,est}$, $\psi_{q,est}$ by the controllers upto 1500 rpm

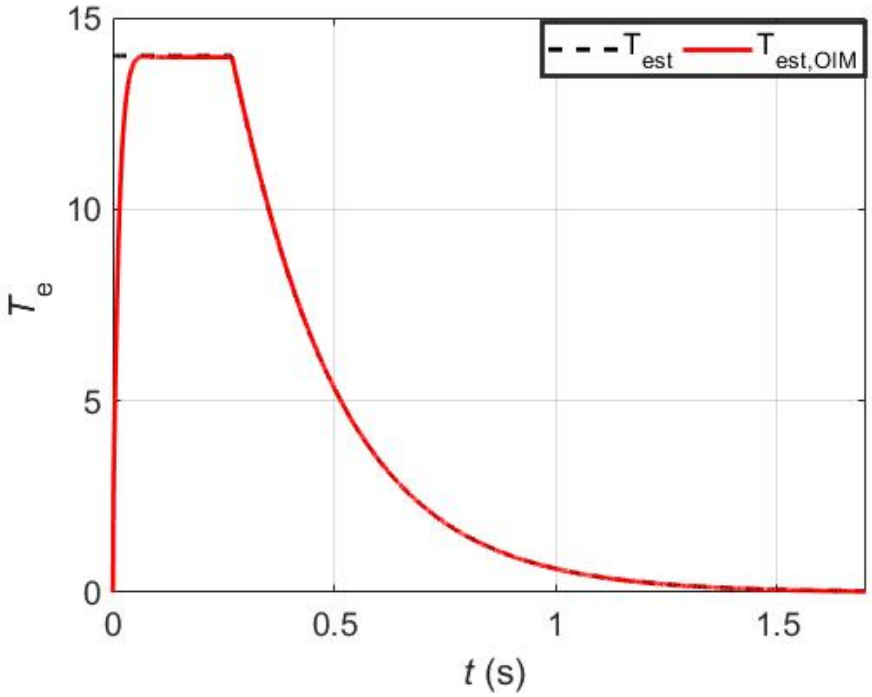

Figure 4.17: **Approach II** – *Simulated result*: Torque reference generated, i.e. $T_{c,ref}$ and estimated, i.e. T_{est} by the conrtollers upto 1500 rpm

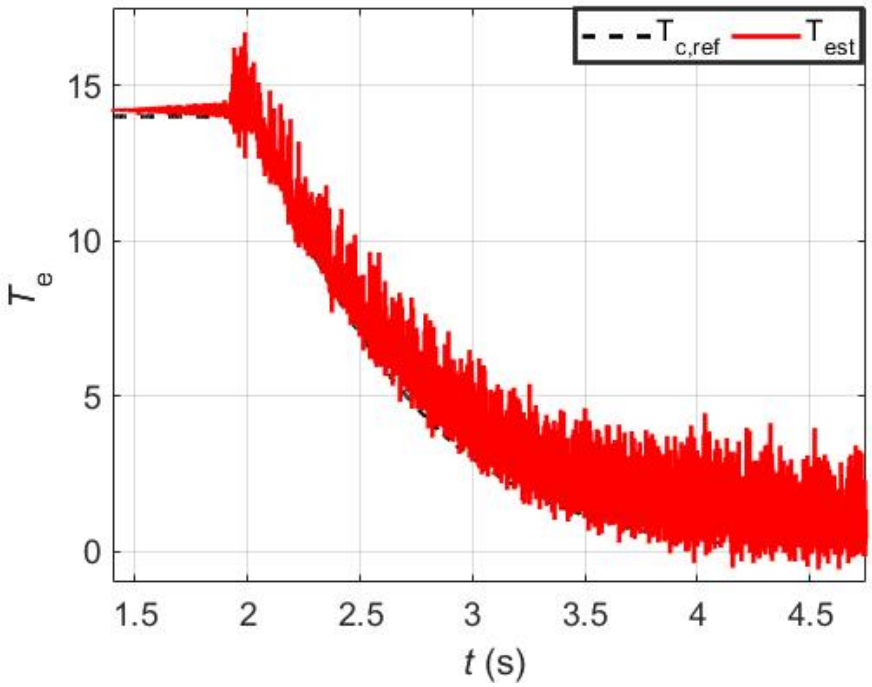

Figure 4.18: **Approach II** – *Experimental result*: Torque reference generated, i.e. $T_{c,ref}$ and estimated, i.e. T_{est} by the conrtollers upto 1500 rpm

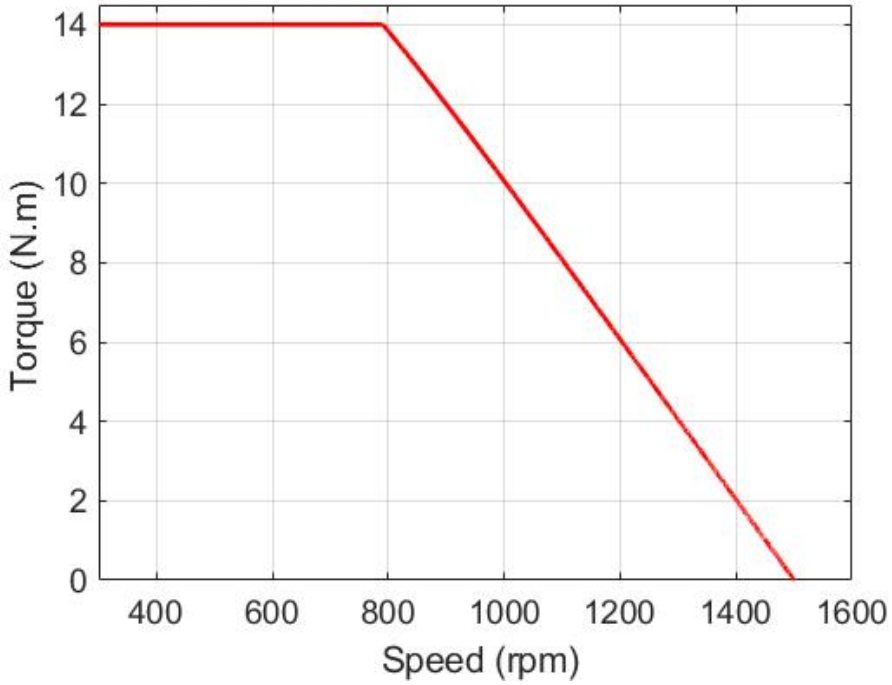

Figure 4.19: **Approach II** – *Simulated result*: Torque-speed curve upto 1500 rpm

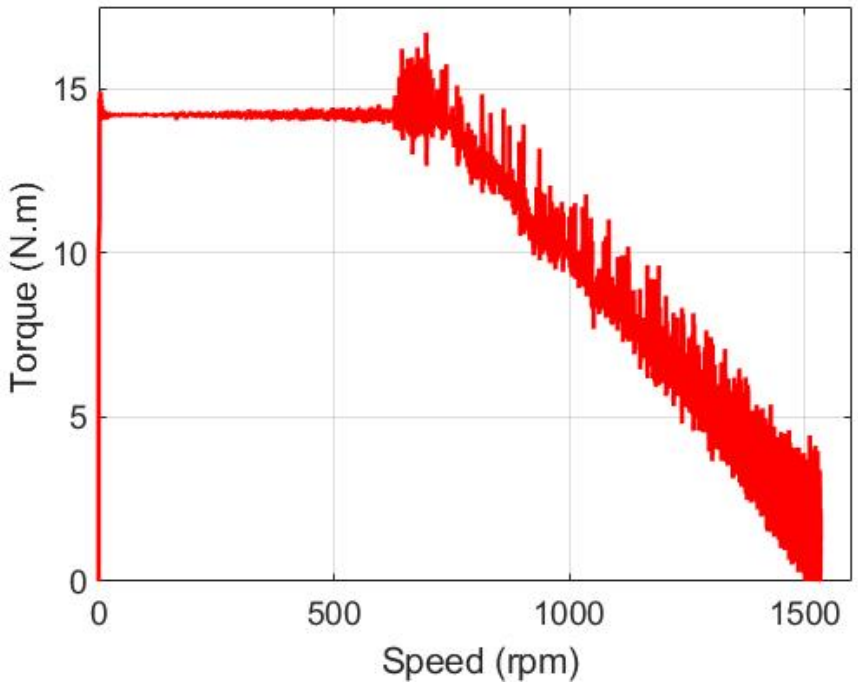

Figure 4.20: **Approach II** – *Experimental result*: Torque-speed curve upto 1500 rpm

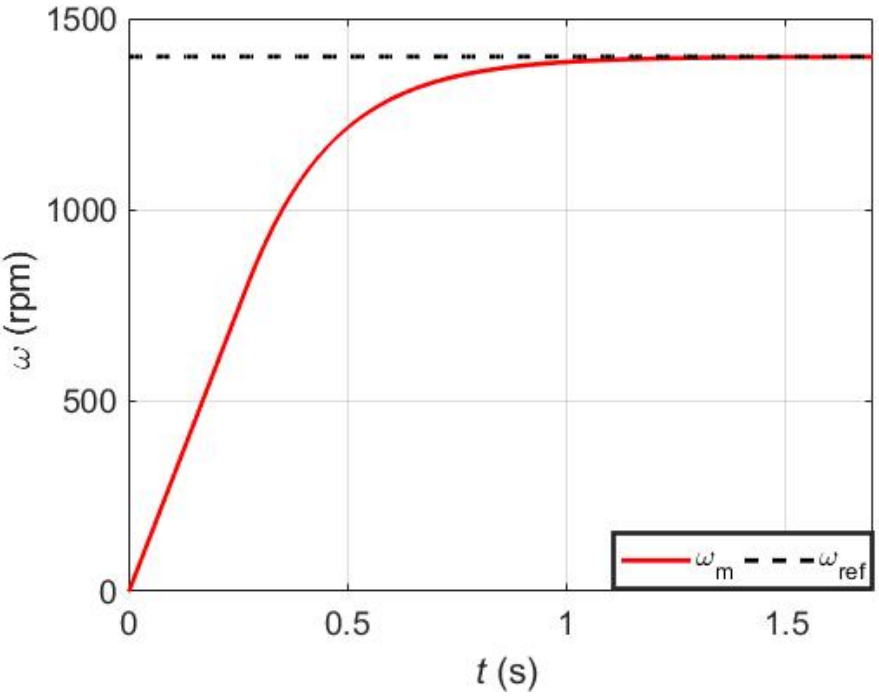

Figure 4.21: **Approach III** – *Simulated result*: Speed reference, i.e. ω_{ref} and speed measured, i.e. ω_m upto 1400 rpm

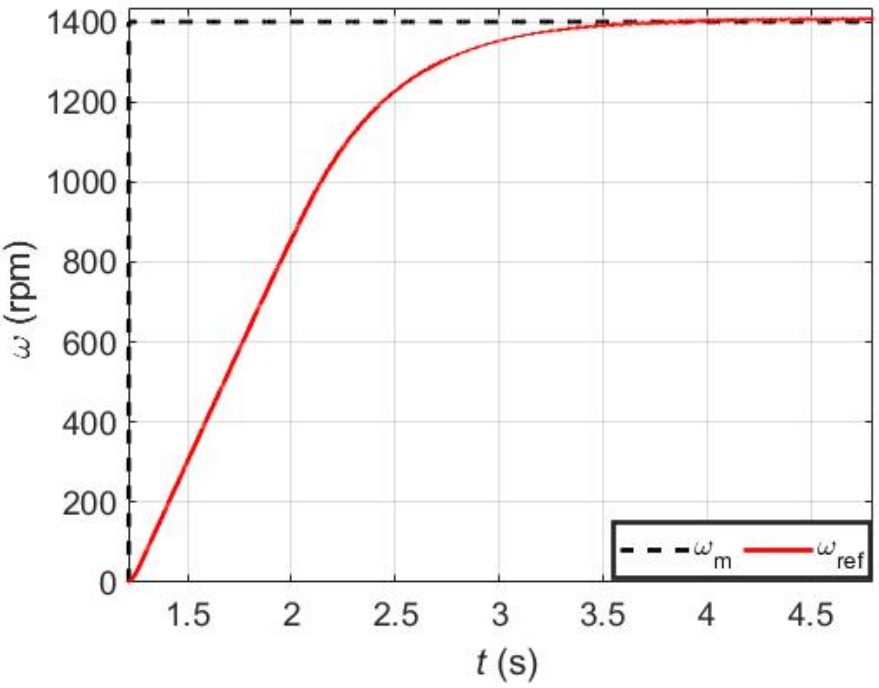

Figure 4.22: **Approach III** – *Experimental result*: Speed reference, i.e. ω_{ref} and speed measured, i.e. ω_m upto 1400 rpm

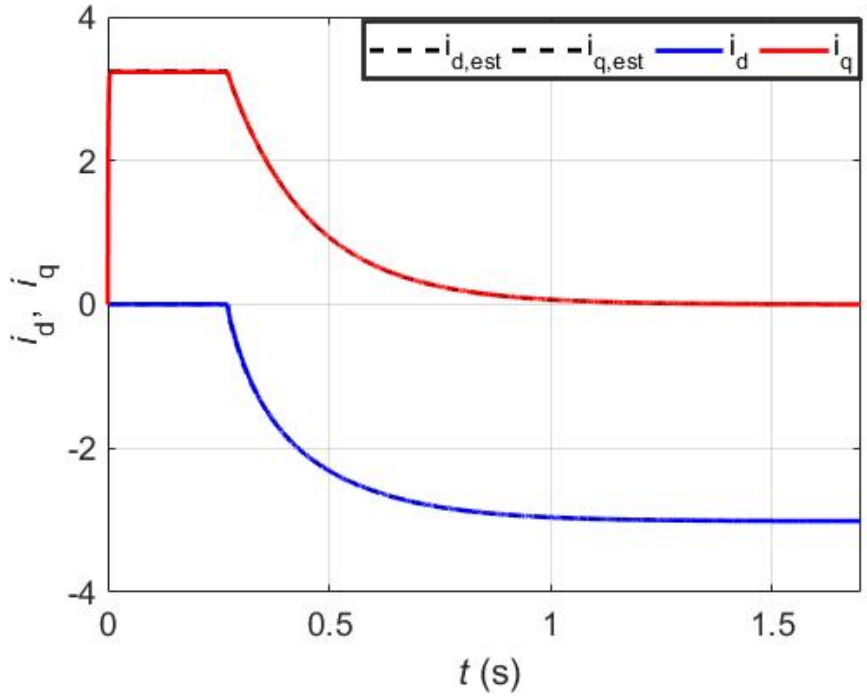

Figure 4.23: **Approach III** – *Simulated result*: Current components generated by the controller, i.e. $i_{d,cref}$, $i_{q,cref}$ and the actual ones, i.e. i_d and i_q upto 1400 rpm

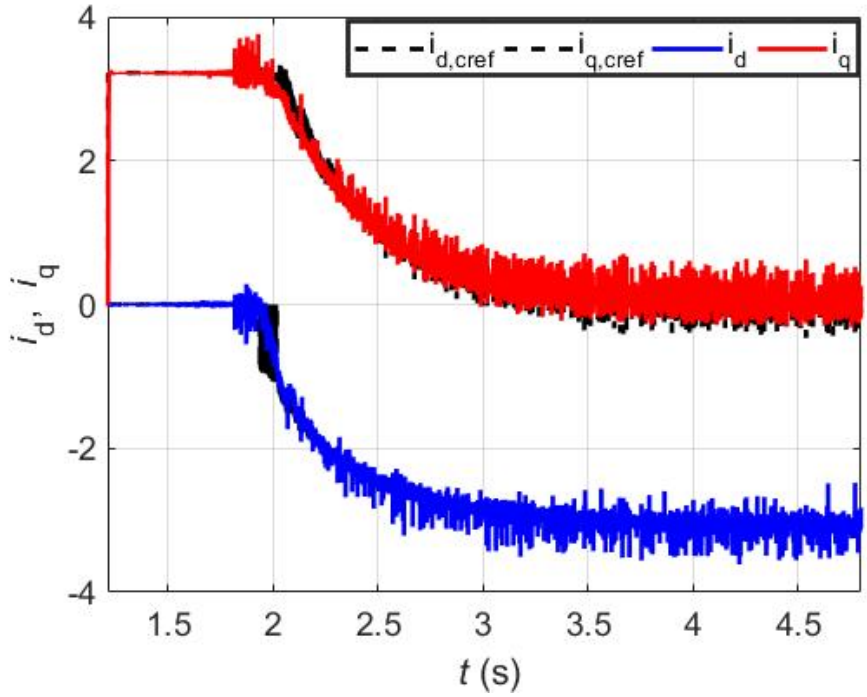

Figure 4.24: **Approach III** – *Experimental result*: Current components generated by the controller, i.e. $i_{d,cref}$, $i_{q,cref}$ and the actual ones, i.e. i_d and i_q upto 1400 rpm

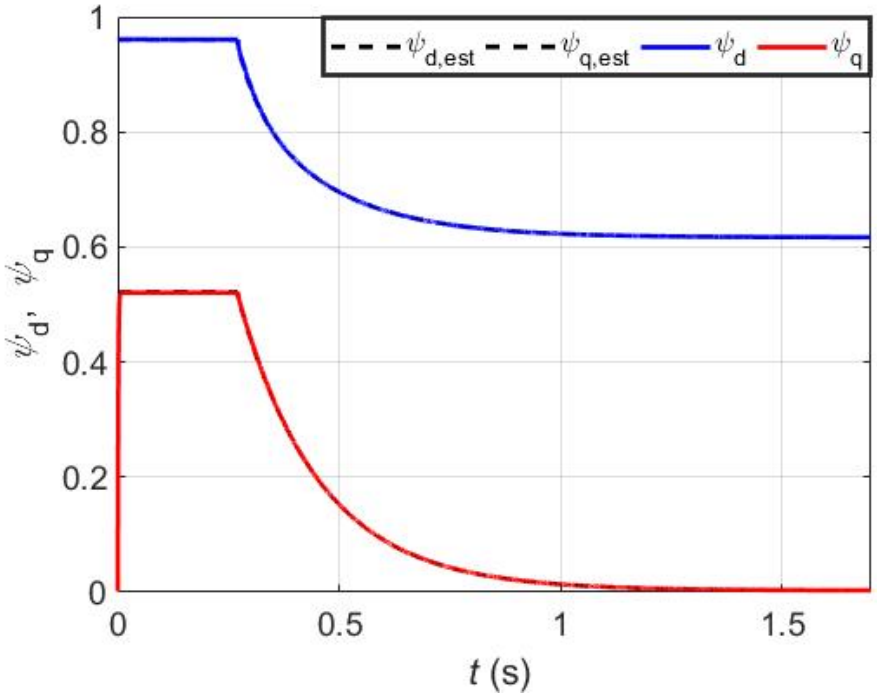

Figure 4.25: **Approach III** – *Simulated result*: Flux components generated, i.e. $\psi_{d,cref}$, $\psi_{q,cref}$ and estimated, i.e. $\psi_{d,est}$, $\psi_{q,est}$ by the controllers upto 1400 rpm

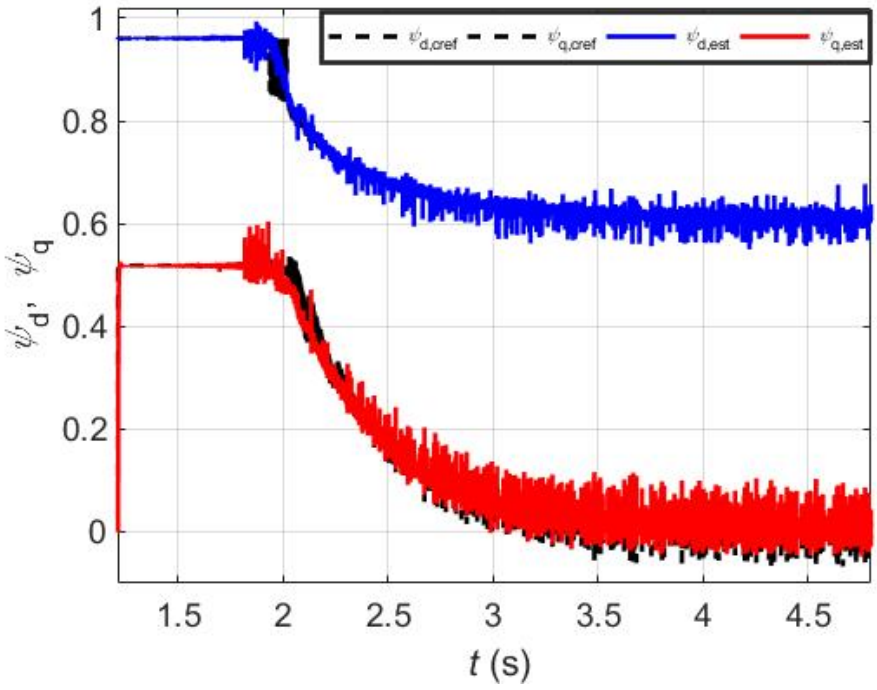

Figure 4.26: **Approach III** – *Experimental result*: Flux components generated, i.e. $\psi_{d,cref}$, $\psi_{q,cref}$ and estimated, i.e. $\psi_{d,est}$, $\psi_{q,est}$ by the controllers upto 1400 rpm

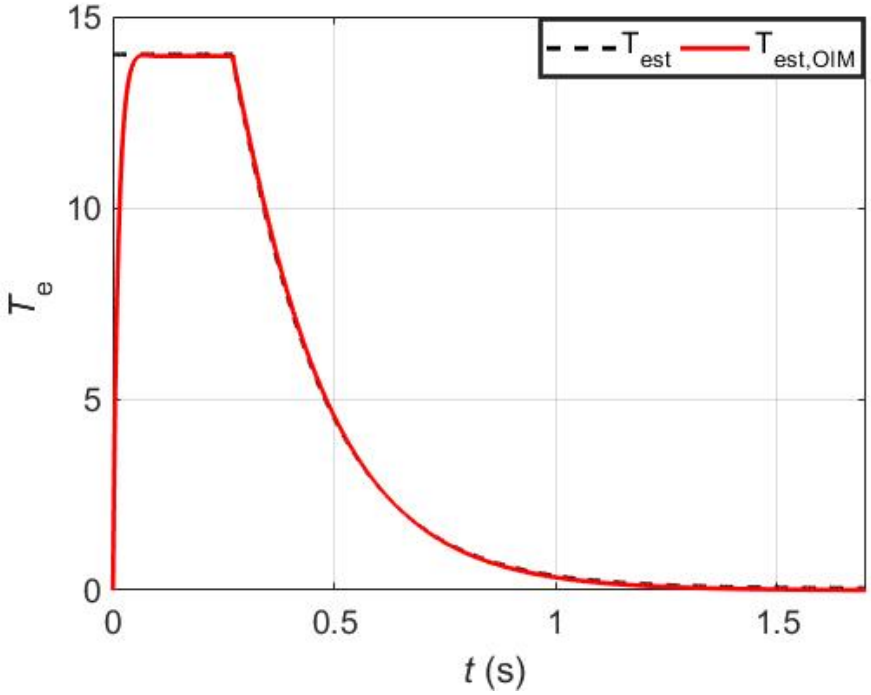

Figure 4.27: **Approach III** – *Simulated result*: Torque reference generated, i.e. $T_{c,ref}$ and estimated, i.e. T_{est} by the conrtollers upto 1400 rpm

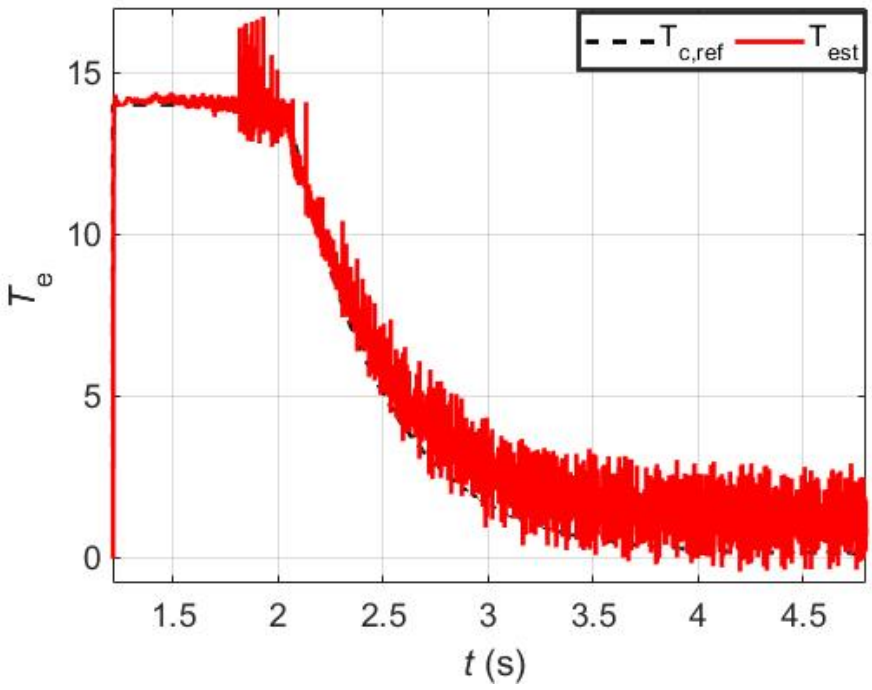

Figure 4.28: **Approach III** – *Experimental result*: Torque reference generated, i.e. $T_{c,ref}$ and estimated, i.e. T_{est} by the conrtollers upto 1400 rpm

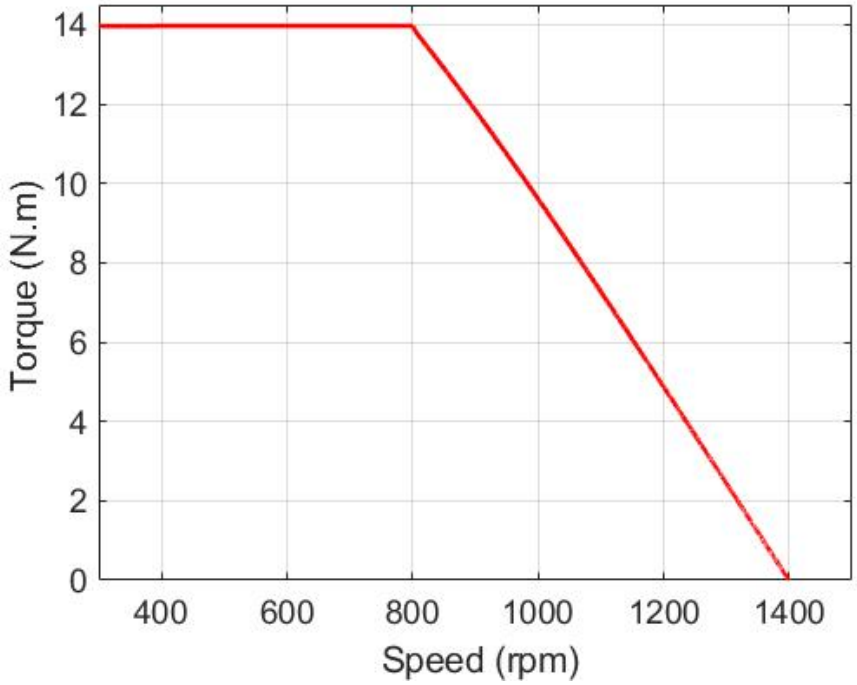

Figure 4.29: **Approach III** – *Simulated result*: Torque-speed curve upto 1400 rpm

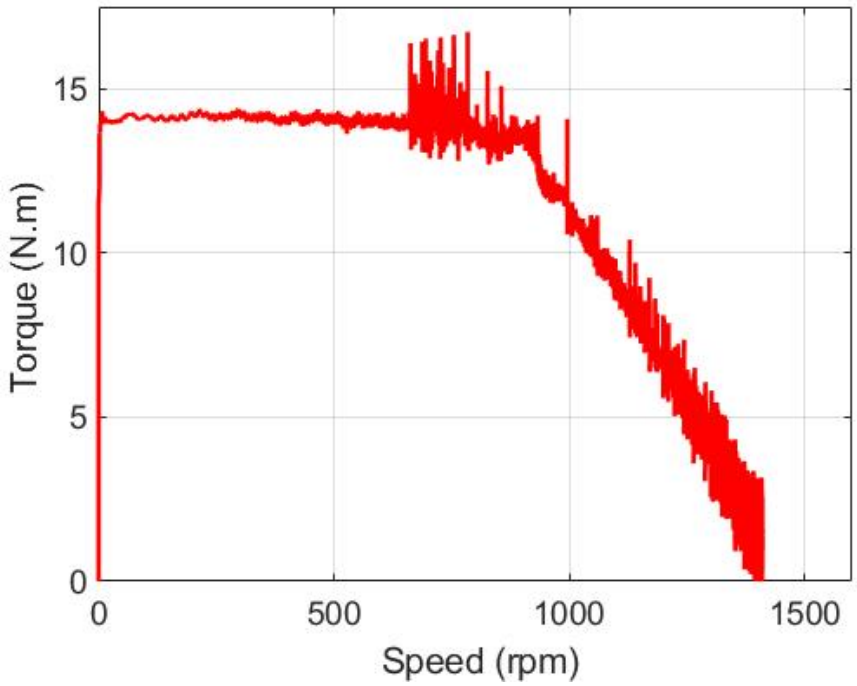

Figure 4.30: **Approach III** – *Experimental result*: Torque-speed curve upto 1400 rpm

4.2 Discussion

The figures above show both the simulated and experimental results for the three approaches followed in this thesis. The control methodology operates in a way that the reference is given for the speed. Depending upon the usage of the flux or current controller in Figure 2.11, the current or flux components are generated by the 'Reference generation' block. These components are produced according to the torque generated by the speed controller. 'Reference generation' block can be deemed as the component of the speed controller as well. To be precise, the names of all the quantities in these results is chosen specifically. For speed measurments, the ω_m and ω_{ref} correspond to the actual and reference speed respectively. The torque generated by the speed controller is named as $T_{c,ref}$. T_{est} represents the torque estimated by the flux or current controller used. The current components thus generated by the 'Reference generation' block according to the region of operation are represented by $i_{d,cref}$ and $i_{q,cref}$ for the d and q-components of current, respectively. Moreover, the i_d and i_q represent the actual current components. Similar to the current, the flux components from 'Reference generation' block are $\psi_{d,cref}$ and $\psi_{q,cref}$ whereas $\psi_{d,est}$ and $\psi_{q,est}$ refer to the flux components estimated by the controller. A good control designed operates in such a way that its all estimated values by the flux or current controller should match the corresponding components either produced by the speed controller or the 'Reference generation' block particularly.

Figure 4.1, Figure 4.11 and Figure 4.21 show the simulated results for the speed measured with the speed reference respectively. The speed exactly corresponds to its reference and there seems to be no overshoot in these results. The speed in the simulation reaches its reference at 1500 rpm for Approach I and II and 1400 rpm for Approach III. The base speed starts around 800 rpm that corresponds to around 0.3 s. After this point, the field weakening starts to play its role. The speed hence shown is almost 1.8 times of the base speed. Figure 4.2, Figure 4.12 and Figure 4.22 show the experimental results, the speed setpoint is set to be 1500 rpm or 1400 rpm for the three approaches. These experimental results are also performed such that the reference is set to be 1.8 times of the base speed that comes out to be around 800 rpm in this case. In the experimental results for the Approach I and Approach II, some overshoot can be seen in the Figure 4.2 and Figure 4.12. The error between the measured and reference speed comes out to be around 2 % in these cases that is quite close to the reference. In contrast, the Figure 4.22 showing the speed results for the Approach III presents that the measured speed is almost exactly corresponding to the reference speed. To be accurate, now the maximum difference is just 0.1 %. It is important to highlight the reasons for difference in the speed measurment error in Approaches I and II. There are some limitations that affect the results for the speed and other quantities as well discussed in subsection 4.3.

Figure 4.3, Figure 4.13 and Figure 4.23 show the simulated results for reference currents components $i_{d,cref}$ and $i_{q,cref}$ generated by the 'Reference generation' block and the actual current components, i_d and i_q. For all the three approaches, the FW operation starts at about 0.3 s. The d-component of the current goes negative

to approach the FW operation. Below the base speed, the i_d remains zero and i_q adjusts its value according to the torque. The greater torque demand will require more i_q current to flow. At 0.3 s, the operation moves towards the FW region and the negative i_d starts to increase. It is assured that the current remains within the limits and the negative i_d current should not exceed the current limit, otherwise it may damage the control system. Once the speed approaches its reference, the currents and other waveforms start to settle. As d-component of the current goes negative, the other q-component also decreases keeping in view the current limit. It settles to the zero since there is no torque required once the speed also settles down. Figure 4.4, Figure 4.14 and Figure 4.24 show the the experimental results for Approach I, II and III, respectively. It can be observed that the same phenomenon happens for the current components as in the simulations. The following of the measured and reference values can also be observed here.

One important point to be discussed here is that the reference currents components generated by the controller, $i_{d,cref}$ and $i_{q,cref}$, decrease in steps in Figure 4.4 and Figure 4.14. The variation of the machine parameters, especially L_d and L_q, in the calculation procedure of Approaches I and II is the main cause that produces unexpected changes in the reference current components. Moreover, it is also to be mentioned that there is a sudden dip happening in the $i_{d,cref}$ visible in Figure 4.24. It occurs in the transition region from base to the FW region because the current components immediately shift to the part operating for the FW region. However, the reference and actual currents follow each other smoothly and no steps can be observed now using Approach III. Another important factor that contribute to these steps and transition as well is the tuning of the controllers. If the controllers are not properly tuned, these affect the performance of the control system. The controllers needs to be more efficiently tuned for the better results.

Figure 4.5, Figure 4.15 and Figure 4.25 show similarly the simulated results for the d and q-flux components, $\psi_{d,cref}$, $\psi_{q,cref}$, $\psi_{d,est}$ and $\psi_{q,est}$. Here, again the d-component of flux plays the main role for the FW control. As we are operating keeping i_d zero before the nominal speed, the value of ψ_d starts from the PM flux value and no participation from the i_d can be seen. In the FW region, starting at 0.3 s, the negative current produced in the d-axis introduces a reducing flux that opposes the PM flux resulting in the overall decrease in the resultant flux. Similar to the i_q, the amount of the ψ_q changes according to the change in ψ_d as the maximum stator flux linkage available in the FW region decreases as well. Also, ψ_q tries to approach zero as the speed settles down. Figure 4.6, Figure 4.16 and Figure 4.26 show the experimental results. These provide the validation for the simulation results as well. Similar to the experimental results for $i_{d,cref}$ and $i_{q,cref}$, the $\psi_{d,cref}$, $\psi_{q,cref}$ also exhibit the similar steps and transition for the approaches I and II.

Figure 4.7, Figure 4.17 and Figure 4.27 refer to the simulated torque results, $T_{c,ref}$ and T_{est}. The operation of the machine can be categorized into two regions. Below the base speed, the torque remains constant, whereas, the torque drops in the field

weakening region. The prototype machine is operated at no load during the whole operation. Therefore, the machine operates at its nominal torque in the base region, 14 N.m. At 0.3 s, as the FW operation starts, the torque tends to fall causing the increase in speed and acting as the constant power region. The reduction in the torque is proportional to the increase in speed. The torque also tries to be zero in the later part of the operation since the torque production will only be the cause of losses, if not required for the speed here. However, the torque and other q-components do not exactly reach zero in practical due to the presence of friction, although these can be seen approaching zero in the simulations. Figure 4.8, Figure 4.18 and Figure 4.28 show the experimental results for the $T_{c,ref}$ and T_{est}. The transition effect for the torque can also be observed in these figures. Torque goes high momentarily but it remains under the maxium torque as controlled by the controller. As soon as the torque enters fully the FW region, both the $T_{c,ref}$ and T_{est} start to follow each other smoothly. Moreover, it is also to be highlighted that the exprimental results for Approach III exhibit less ripples in the torque waverform as compared to the other approaches.

Finally, Figure 4.9, Figure 4.19 and Figure 4.29 are the simulated results for the torque-speed curves. As mentioned earlier, the torque remains constant till the base speed, 800 rpm in the simulation results for all the three apporaches. The decrease of torque with further increase in the speed is quite visible in the later part as it enters the FW area. The torque continues to decrease until it approaches zero when the speed approaches its reference. The linearity in the decrease of torque can be understood from the Figure 2.4. As the prototype IPMSM exhibits low saliency, the reluctance torque would not have any additional torque effect for the machine. The only dominant part is from the magnetic torque term. Very similar effects can be seen in Figure 4.10, Figure 4.20 and Figure 4.30 for the experimental results. The experimental results show the decrease of torque for all the three approaches in the FW region as well.

For experimental results, it is quite visible that there are some oscillations in the current, flux and torque waverforms. This fluctuation is inexorable and happens due to the practical limitaions. One important source of these ripples in these experiments is that the encoder being used is only 600 pulses/revolution (PPR) that reduces its capacity to collect data, hence, it becomes the definite cause of noise. The other reason is the limited sampling frequency; the new state of the measured quantity cannot be exactly tracked by the previous state since there is only one sample in a particularly defined time period and the error remains there. The only way to eliminate this error is to make the sampling time period equal to zero that is not practically possible (Zhao, Qiao and Wu, 2012). Also, the physical capabilities of the inverter, losses and the switching noise cause this chattering to appear.

4.3 Limitations

As discussed in the section 3.2, the calculations for the references generation for Approaches I and II are based on the machine parameters. It can be seen that all the parameters like the inductances, the stator resistance and the PM flux were taken into account for these methods. These parameters exhibit variation during the operation of the machine, particularly the L_d and L_q. The magnetic saturation effect in IPMSM usually lead to the decrease in the L_d and L_q. Therefore, if these parameters are used in the calculation of any reference or estimated quantity, it may deteriorate the performance of the system. Another significant aspect that particularly affected the experimental results in this thesis is that L_d and L_q are not known exactly for the prototype machine, no experiments have been performed for that purpose. Rather, the FEM model results are assumed to be correct and its values are used in the real-time control as well. There might be some difference in actual and used values. This unknown difference will also certainly degrade the control performance. Furthermore, apart from the fact that no machine parameter is used in the calculation of reference or estimated quantity in Approach III, still there's some role of inductance variation there. It occurs as the flux or current controller being used contains the machine parameters, L_d, L_d and R_s as evdient from (2.65). Therefore, the parametric senstivity may also affect somewhat the control performance for Approach III as well, but its impact is much lower as compared to the other two Approaches I and II, as is also manifested in the results obtained. Lastly, the tuning of the controllers should also be considered. The more fine tuning of the controllers can produce even better results for all the approaches used.

Conclusion The results for the methodologies adopted in this thesis have been obtained. The behaviour of all the relevant quantities, the speed, current, flux and torque depict the good FW performance for all the approaches. The simulation results exactly correspond to the expected outcomes in the FW operation. The speed reaches its reference quite well and all the other reference components generated by the controller match the actual or the estimated values. In the real-time operation, it can be observed that the approach working independent of the machine parameters, 'algebraic constraint' approach, gives the superior results than the other two approaches, 'current approach' and 'flux-current approach'. The variation in the L_d and L_q affect the control performance. Some speed difference can be observed in the first two approaches while in the last approach, speed corresponds to its reference. Furthermore, the steps in the reference components of the current or flux are not experienced as well while operating with the algebraic constraint approach.

5 Conclusions and perspectives

This thesis aimed to implement the FW control for IPMSM utilizing a MOR technique, OIM. It was intended to exploit the OIM in the design of FW control such that the parametric sensitivity of the machine could be avoided. The effects of inductances variation, L_d and L_q, especially in the FW region can significantly degrade the performance of the system. In addition, the stator resistance and the PM flux deviate with the variation in the temperature. Hence, a model working independent of all the machine parameters could avoid all these effects and remain unaffected by the magnetic saturation and cross-coupling as well.

For this purpose, the OIM obtained by reducing the order of the FE model of the IPMSM, was included in the control design. The stator current components and the flux linkage components are the inputs and the outputs of the reduced model, respectively. There were three algorithms applied to accomplish the objective. The first two approaches, 'current approach' and 'flux-current approach' used the machine parameters, i.e. L_d, L_q, R_s and ψ_f in the calculations of the references generated by the controllers. The former approach takes into account the current and voltage limits that are definite constraints for the FW operation of the machine and derives for the current references. While the later exercises the idea of using the measured currents for the reference calculation. The final method i.e 'algebraic constraint' approach uses a simulink feature in conjunction with the OIM technique to produce the references. This approach does not need any machine parameter to be known for the references calculations that may degrade the control performance, especially at the high speeds. OIM was deployed in all the the three approaches for implementing the FW operation. The implementation of the overall control structure was obtained through the field oriented control scheme.

The control models for the developed approaches were validated through the simulations and then the experiments. The results in the section 4 show the feasibility for these methodologies. The results also show that the approach that works independent of any machine parameter could produce far better results as compared to the one that is affected by the paramteric senstivity in any way. The speed and other control quantities including the current and flux components can exhibit smooth and expected operation quite well. However, a few limitations in the used methodologies explained in the previous section need to be rectified and improved to achieve even superior results.

A good future work for this thesis is to improve the tuning of the speed and current controllers used in the FOC control scheme. A current controller needs to be implemented that works independent of the machine parameters as well. It would also be beneficial to have the accurate measurement of the L_d and L_q and other machine parameters.

References

Akin, B., M. Bhardwaj and J. Warriner (2013), 'Sensorless field oriented control of 3-phase permanent magnet synchronous motors', *Texas Instruments, Application Notes* .

Antoulas, A. C and D. C. Sorensen (2001), 'Approximation of large-scale dynamical systems: An overview', *International Journal of Applied Mathematics and Computer Science*, pp. 1093–1121.

Awan, H. A. A., Z. Song, S. E. Saarakkala and M. Hinkkanen (2017), 'Optimal torque control of synchronous motor drives: Plug-and-play method', *IEEE Energy Conversion Congress and Exposition (ECCE)*, pp. 334–341.

Awan, H. (2015), 'Discrete-time current control of synchronous motor drives', *Master's thesis*, Aalto University, Finland.

Belahcen, A., V. Mukherjee, M. Farzamfar, P. Rasilo and M. Hinkkanen (2016), 'Coupled field and space-vector equations of bearingless synchronous reluctance machine', *XXII International Conference on Electrical Machines (ICEM)*, pp. 2581–2587.

Blaschke, F. (1971), 'A new method for the structural decoupling of ac induction machines', *Conference Record in International Federation of Automatic Control*, Vol. 1, pp. 1–15.

Bose, B. K. (1988), 'A high-performance inverter-fed drive system of an interior permanent magnet synchronous machine', *IEEE Transactions on Industry Applications*, pp. 987–997.

Cheles, M. (2009), 'Sensorless field oriented control (foc) for a permanent magnet synchronous motor (pmsm) using a pll estimator and field weakening (fw)', *Microchip Technology Inc. Published Sep* .

Controls, Copley (2011), 'What is field oriented control and what good is it?', *Copley Controls Corp* .

Dutta, R. (2007), 'A segmented interior permanent magnet synchronous machine with wide field-weakening range', *Ph.D. dissertation*, The University of New South Wales, Australia.

Farzamfar, M. , F. Martin, A. Belahcen, L. Montier and T. Henneron (2018), 'Orthogonal interpolation method for order reduction of a synchronous machine model', *IEEE Transactions on Magnetics*, pp. 1–6.

Farzamfar, M., A. Belahcen, P. Rasilo, S. Clenet and A. Pierquin (2017), 'Model order reduction of electrical machines with multiple inputs', *IEEE Transactions on Industry Applications*, pp. 3355–3360.

Foo, G. H. B. and X. Zhang (2016), 'Robust constant switching frequency-based field-weakening algorithm for direct torque controlled reluctance synchronous motors', *IEEE Transactions on Industrial Informatics*, pp. 1462–1473.

Harnefors, L, M. Hinkkanen, O. Wallmark and A. G. Yepes (2014), 'Control of voltage-source converters and variable-speed drives', *Lecture notes, Västerås, Sweden* .

Hinkkanen, M., Z. Qu, H. A. A. Awan, T. Tuovinen and F. Briz (2015), 'Current control for ipmsm drives: Direct discrete-time pole-placement design', *IEEE Workshop on Electrical Machines Design, Control and Diagnosis (WEMDCD)*, pp. 156–164.

Jahns, T. M. (1987), 'Flux-weakening regime operation of an interior permanent-magnet synchronous motor drive', *IEEE Transactions on Industry Applications*, pp. 681–689.

Jahns, T. M., G. B. Kliman and T. W. Neumann (1986), 'Interior permanent-magnet synchronous motors for adjustable-speed drives', *IEEE Transactions on Industry Applications* (4), pp. 738–747.

Kataja, J., M. Antila, M. Sokolov, M. Hinkkanen, S. Saarakkala and K. Tammi (2016), 'Direct discrete-time flux-linkage control of bearingless synchronous reluctance motors', *IECON 2016 - 42nd Annual Conference of the IEEE Industrial Electronics Society*, pp. 2760–2765.

Kerschen, G., J.-C Golinval, A. F. Vakakis and L. A. Bergman (2005), 'The method of proper orthogonal decomposition for dynamical characterization and order reduction of mechanical systems: An overview', *Nonlinear Dynamics*, pp. 147–169.

Khan, W. (2016), 'Torque maximizing and flux weakening control of synchronous machines', *Master's thesis*, Aalto University, Finland.

Kim, H. and R. D. Lorenz (2002), 'Improved current regulators for ipm machine drives using on-line parameter estimation', *Conference Record of the 2002 IEEE Industry Applications Conference. 37th IAS Annual Meeting (Cat. No.02CH37344)*, Vol. 1, pp. 86–91.

Kim, J.M. and Seung K.S. (1997), 'Speed control of interior permanent magnet synchronous motor drive for the flux weakening operation', *IEEE Transactions on Industry Applications*, pp. 43–48.

Kumar, T. P. and P. Samyuktha (2013), 'Vector control drive of permanent magnet synchronous motor using resolver sensor'. *International Journal of Computer Science Engineering (IJCSE)*

Kwon, T. S., G. Y. Choi, M. S. Kwak and S. K. Sul (2008), 'Novel flux-weakening control of an ipmsm for quasi-six-step operation', *IEEE Transactions on Industry Applica*tions, pp. 1722–1731.

Li, Z. and H. Li (2012), 'Mtpa control of pmsm system considering saturation and cross-coupling', *15th International Conference on Electrical Machines and Systems (ICEMS)*, pp. 1–5.

Lindh, P., M. Rilla, H. Jussila, J. Nerg, J.A. Tapia and J. Pyrhönen (2011), 'Interior permanent magnet motors for traction application with non-overlapping concentrated windings and with integer slot windings', *International Review of Electrical Engineering* .

Lyshevski, S. E. (2018), 'Electromechanical systems, electric machines, and applied mechatronics', *CRC press.*, pp. 590–660.

Meyer, M. and J. Bocker (2006), 'Optimum control for interior permanent magnet synchronous motors (ipmsm) in constant torque and flux weakening range', *12th International Power Electronics and Motion Control Conference*, pp. 282–286.

Morimoto, S., M. Sanada and Y. Takeda (1994), 'Wide-speed operation of interior permanent magnet synchronous motors with high-performance current regulator', *IEEE Transactions on Industry Applications*, pp. 920–926.

Morimoto, S., Y. Takeda, T. Hirasa and K. Taniguchi (1990), 'Expansion of operating limits for permanent magnet motor by current vector control considering inverter capacity', *IEEE Transactions on Industry Applications*, pp. 866–871.

Moyer, E.T. and E.A. Schroeder (1991), 'Finite element formulations of maxwell's equations-advantages and comparisons between available approaches', *IEEE transactions on magnetics* , pp. 4217–4220.

Nalepa, R. and T. O. Kowalska (2012), 'Optimum trajectory control of the current vector of a nonsalient-pole pmsm in the field-weakening region', *IEEE Transactions on Industrial Electronics*, pp. 2867–2876.

Ni, R., X. Gui, G. Wang, G. Zhang and D. Xu (2014), ' Improvements in permanent magnet synchronous machines with delta-connected winding', *IECON 2014 - 40th Annual Conference of the IEEE Industrial Electronics Society*, pp. 3837–3842.

Perera, P.D. Chandana (2002), 'Sensorless control of permanent-magnet synchronous motor drives', *Ph.D. dissertation*, Institute of Energy Technology, Aalborg University, Denmark.

Piippo, A. et al. (2008), 'An adaptive observer with signal injection for interior permanent magnet synchronous motors', *Ph.D. dissertation*, Helsinki University of Technology, Finland.

Pillay, P. and R. Krishnan (1989), 'Modeling, simulation, and analysis of permanent-magnet motor drives. in the permanent-magnet synchronous motor drive', *IEEE Transactions on Industry Applications*, pp. 265–273.

Pyrhonen, J. , T. Jokinen and V. Hrabovcova (2009), 'Design of Rotating Electrical Machines', *Wiley*, pp. 201-210.

Ruoho, S. (2011), 'Modeling demagnetization of sintered ndfeb magnet material in time-discretized finite element analysis', *Ph.D. dissertation*, Aalto University, Finland.

Sarkar, P. and S. Bhunia (2017), ' Svpwm based vector control of pmsm drive in delta domain', *International Conference on Electrical, Computer and Communication Engineering (ECCE)*, pp. 5–10.

Schiferl, R. and T. A. Lipo (1988), ' Power capability of salient pole permanent magnet synchronous motors in variable speed drive applications', *Industry Applications Society Annual Meeting, 1988., Conference Record of the 1988*, pp. 23–31.

Sebastian, T., G. Slemon and M. Rahman (1986), 'Modelling of permanent magnet synchronous motors', *IEEE Transactions on Magnetics*, pp. 1069–1071.

Sirovich, L. (1987), 'Turbulence and the dynamics of coherent structures. i. coherent structures', *Quarterly of applied mathematics*, pp. 561–571.

Soong, W. L. and N. Ertugrul (2002), 'Field-weakening performance of interior permanent-magnet motors', *IEEE Transactions on Industry Applications*, pp. 1251–1258.

Soong, W. L. and T. J. E. Miller (1994), 'Field-weakening performance of brushless synchronous ac motor drives', *IEEE Proceedings - Electric Power Applications*, pp. 331–340.

Soong, W. L., S. Han and T. M. Jahns (2007), ' Design of interior pm machines for field-weakening applications', *Electrical Machines and Systems, 2007. ICEMS. International Conference on Electrical Machines*, pp. 654–664.

Zelaya De La Parra, H. (1999), 'Field-weakening control of an interior permanent magnet motor for application in electric vehicles', *European Power Electronics Conference (EPE), Laussane, 1999.*

Zhao, Y., W. Qiao and L. Wu (2012), 'Oscillation mitigation for sliding-mode observers in sensorless control of ipmsms', *IEEE Transportation Electrification Conference and Expo (ITEC)*, pp. 1–6.